PROCEEDINGS

Of

National Conference

On

DEVICE MODELING AND SOFT COMPUTING FOR REAL-TIME APPLICATIONS

(DMSC-2019)

13th & 14th September 2019

Organized by,

Dept. of Electronics & Communication Engineering

Mallabhum Institute of Technology, Bishnupur, India

In Collaboration with,

The Institution of Engineers India (IEI)

ABOUT
MALLABHUM INSTITUTE OF TECHNOLOGY, BISHNUPUR

With the mission, to develop the scenario of technical education in the backward region of West Bengal, a graduate engineering college namely Mallabhum Institute of Technology was setup in 2002 at Bishnupur. MIT has different streams (CSE, EE, ECE, ME & CE). The institute approved by AICTE and affiliated to MAKAUT.

In MIT, besides covering the course curriculum both in theory and practice, students are enabled to face cut-throat competition in this awesome competitive world to surge ahead. Our college is fully residential; hence the students reap special benefit to interact with teachers round the clock. Our rich central library with air conditioned reading room, book-bank facilities, reputed e-journals and internet facilities provide the students a congenial platform of convergent learning.

MIT is located amidst a tranquil terrain, having sprawling and eco-friendly campus, which offers a unique environment of study to the engineering students. Apart from academic exercises, wide scope of participation in different co-curricular activities helps our students to become healthy citizens in future years.

At MIT, we have redefined and redesigned our teaching-learning process as and when required to stay tuned and updated in the field of technical education. Continuous effort of our stake holders at MIT to achieve our goals deserves appreciation. We are sure that our proactive and able leadership will address all challenges to remain ahead of others amidst tough and volatile environment in the years to come.

ABOUT
THE INSTITUTION OF ENGINEERS INDIA (IEI)

The Institution of Engineers (India) or IEI is the largest multidisciplinary professional body that encompasses 15 engineering disciplines and gives engineers a global platform from which to share professional interest. IEI has membership strength of over 0.8 million. Established in 1920, with its headquarters at 8 Gokhale Road, Kolkata - 700020, IEI has served the engineering fraternity for over nine decades. In this period of time it has been inextricably linked with the history of modern-day engineering. In 1935, IEI was incorporated by Royal Charter and remains the only professional body in India to be accorded this honor. Today, its quest for professional excellence has given it a place of pride in almost every prestigious and relevant organization across the globe. IEI functions among professional engineers, academicians and research workers. It provides a vast array of technical, professional and supporting services to the Government, Industries, Academia and the Engineering fraternity, operating from 123 Centres located across the country. IEI provides grant-in-aid to its members to conduct research and development on engineering subjects. IEI, in collaboration with Springer, regularly publishes peer-reviewed international journals in five series, covering fifteen engineering disciplines.

OBJECTIVE OF THE CONFERENCE

Conference Theme: Two days National Conference on Device Modeling and Soft Computing for real-time applications (DMSC 2019) will basically focus on modeling of electronic devices and real-time applications of soft-computing. Semiconductor device modeling has developed in recent years from being solely the domain of device physicists to span broader technological disciplines involved in device and electronic circuit design and development. Traditional equivalent circuit models and closed-form analytical models cannot always provide consistently accurate results for all modes of operation of these very small devices. The desire to move towards computer aided design and expert systems have reinforced the need for models capable of representing device operation under DC, small-signal, large-signal and high frequency operation. It is also desirable to relate the physical structure of the device to the electrical performance. This demand for better models has led to the introduction of improved equivalent circuit models and an upsurge in interest in using physical models. Soft computing is based on natural as well as artificial ideas. Soft Computing is basically optimization technique to find solution of problems which are very hard to answer. Soft Computing techniques are Fuzzy Logic, Neural Network, Support Vector Machines, Evolutionary algorithms and Machine Learning, Probabilistic Reasoning etc. Moreover, Soft Computing techniques, which are based on the information processing of biological systems are now massively used in the area of pattern recognition, fuzzy logic, probabilistic reasoning, artificial neural network, making prediction, planning, as well as acting on the environment.

Sub-Theme: Semiconductor design, Device modeling, System optimization, Manufacturing systems, Process and System control, Signal & Image processing, Energy management, Solar Cell, Human Machine Interface, Robotics, Motion control, Power electronics, Green Computing, Biomedical Engg. and Industrial Electronics.

PATRONS

Chairperson, Mallabhum Institute of Technology, Bishnupur
Director, Mallabhum Institute of Technology, Bishnupur
Principal, Mallabhum Institute of Technology, Bishnupur
Advisor, Mallabhum Human Resource Development Trust, Bishnupur

ADVISORY COMMITTEE MEMBERS

Dr. Jatindra N. Roy, Adv. Technology Development Centre & School of Energy Science and Engineering, IIT Kharagpur
Dr. Smarajit Das, EEE Dept., IIT Guwahati
Dr. Anup K. Bhattacharjee, Dept. of ECE, NIT Durgapur
Dr. Ujjal Chakraborty, Dept. of ECE, NIT Silchar
Dr. Kaushik Mandal, Dept. of Radio Physics & Electronics, Calcutta University
Dr. Sujit Das, Dept. of CSE, NIT Warangal
Dr. Joydeep Sengupta, Dept. of ECE, VNIT Nagpur
Dr. Sougata Kumar Kar, Dept. of ECE, NIT Rourkela
Dr. Saikat Ranjan Maity, Dept. of ME, NIT Silchar
Dr. Subhas Ganguly, Dept. of Met. Engineering, NIT Raipur
Dr. Rajendra P. Ghosh, Dept. of Electronics, Vidyasagar University
Dr. Partha Pratim Sarkar, Department of Engineering and Technological Studies (DETS), University of Kalyani, Kalyani
Dr. Durbadal Mandal, Dept. of ECE, NIT Durgapur
Dr. Indrajit Saha, Dept. of CSE, NITTTR Kolkata
Dr. Debasish Nandi, Dept. of ME, MIT Bishnupur
Dr. Indrani Chakraborty, Dept. of EE, MIT Bishnupur
Dr. Bappadittya Roy, Dept. of ECE, Madanapalle Institute of Technology & Science, Andhra Pradesh
Mr. Buddhadeb Ghosh, Dept. of S & SS, MIT Bishnupur

ORGANIZING COMMITTEE MEMBERS

Dr. Khanindra Pathak, Chaiman, IEI, Kharagpur Local Centre

Dr. Pavuluri Srinivasa Rao, Honorary Secretary, IEI, Kharagpur Local Centre

Mrs. Manira Khatun, Dept. of ECE, MIT Bishnupur

Mr. Supratim S. Das, Dept. of ECE, MIT Bishnupur

Mr. Avijit Paul, Dept. of ECE, MIT Bishnupur

Miss. Debashree P. Karmakar, Dept. of ECE, MIT Bishnupur

Mr. Subhajit Bhattacharyya , Dept. of ECE, MIT Bishnupur

Mr. Kausik Chakraborty, Dept. of ECE, MIT Bishnupur

Mrs. Mayumi Mukherjee, Dept. of ECE, MIT Bishnupur

Mr. Suvajit Giri, Dept. of ECE, MIT Bishnupur

CONVENER

Ms. Mousumi Karmakar, HOD, ECE Dept., MIT Bishnupur

PROGRAM CO-ORDINATOR

Mr. Ankan Bhattacharya, ECE Dept., MIT Bishnupur

LIST OF CONTENTS

Invited Abstracts

Technical Papers

INVITED ABSTRACTS

HIGHLY SENSITIVE AND SELECTIVE RESISTIVE GAS SENSORS ON MEMS--CMOS PLATFORM

Dr. Prasanta Kumar Guha,

Associate Professor, Department of Electrical & Electronics Communication Engineering, Indian Institute of Technology Kharagpur, Kharagpur, India

Abstract

There has been increasing interest to develop new low cost, low power gas sensors for various application-specific areas. This includes air pollution monitoring of both indoor and outdoor spaces, near industrial premises and also sensors for biomedical applications. There has been a rapid rise in levels of toxic gases and volatile organic compounds (VOCs) in air in recent years; particularly in urban spaces. This is mostly true for many cities in under-developed or developing countries, e.g. 2018World Health Organization (WHO) report shows that fifteen Indian cities are amongst the fifty most polluted cities in the world. The major sources of polluted air are fuelwood and biomass burning, burning of large scale crop residue, fuel adulteration, uncontrolled emission from vehicles and factories, traffic congestion and rapid construction.

Resistive gas sensors are simple, low cost and CMOS compatible. The sensor/circuit integration on the same silicon die makes them cheap and reliable. Such sensors contain highly sensitive nano metal oxide sensing layer, micro-heaters and interdigitated electrodes (IDEs). Metal oxide sense various gases at elevated temperature (200-450C). These make them power hungry and less selective. Thus, power efficient selective sensor fabrication for electronic gadgets has always been a challenge. These drawbacks can be improved through fabrication of sensors on MEMS-CMOS platform and pattern recognition.

INTRODUCTION OF GENETIC ALGORITHM IN SOLVING OPTIMIZATION PROBLEMS: APPLICATION IN EV ENERGY MANAGEMENT

Dr. Arup Kumar Nandi,

Principal Scientist, CSIR-Central Mechanical Engineering Research Institute, Durgapur, India

Abstract

Optimization is one of the most common and pervasive issues in real-world systems including engineering. It is a technique to arrive at one or more solutions, which correspond to either minimum or maximum values of one or more objectives (in the form of objective/subjective functions or performance indices) satisfying certain conditions. Real world problems commonly involve more than one objective, and many times that are contradictory in nature. Unlike to a single objective optimization, the motivation of finding a preferred solution for implementation is different in multi-objective optimization. The extreme value principle is not applicable in situations where all the objectives are equally significant. In this case, a number of solutions may be produced to create a compromise among different objectives. A solution that is extreme with respect to one objective requires a compromise with other objective(s). This restricts the choice of a solution which is optimal with respect to only one objective. Therefore, a number of sets of solutions are obtained and then the designer has to select a set from these sets of solutions, which will serve the purpose originally intended. In the present lecture, the working principle of a simple genetic algorithm (GA) is introduced in solving single objective optimization problem. Then, the basic concept of solving multi-objective optimization problem is presented. In order to solve multi-objective optimization problem using GA will be described subsequently. Finally the methodology of solving an engineering problem using multi-objective genetic algorithm is demonstrated consider the problem of electric vehicle (EV) energy management.

SCOPE, OPPORTUNITIES AND CHALLENGES OF COPPER (Cu) BASED SEMICONDUCTING DEVICE IN OPTOELECTRONIC APPLICATIONS

Dr. Ratan Mandal,

Associate Professor, School of Energy Studies, Jadavpur University, Kolkata, India

Abstract

The factors that have been taken into account in developing new photovoltaic materials with improved efficiency and reduced cost include: a suitable energy band gap, the possibility of depositing the material using low cost deposition methods, abundance of the elements and low environmental costs with respect to the synthesis of the elements, production, operation and disposal of modules. Among the common p-type semiconductors, copper sulphide [$Cu_{(2-x)}$ S] based device, $2 \geq x \geq 1$, stands out mainly because of its excellent p-type conductivity, its low cost and non-toxicity. The material Cu_XS [X= (2-x)] is a narrow-band-gap semiconductor material with a visible optical transmittance of about 60% for a 50 nm thick film. Copper sulphide is known to exist in several crystallographic and stoichiometric forms. It is found in two forms at room temperature as 'copper-rich' and 'copper- poor'. The copper rich phases exist as Chalcocite, Djurlite, Digenite and Anilite and on the other hand the copper poor phase exists as Covellite. Researchers discussed that the copper sulphides are recognized as promising materials; thus recent investigations have evoked considerable interest because of their extensive potential applications in solar cells, photo-thermal conversions of solar energy as solar absorber coating, electro-conductive coatings, solar control coatings, and microwave shielding coatings as well as sensors.

The Cu_2S thin films are efficiently used in solid junction solar cells that have many applications as it is a direct conversion device. Moreover, the Cu_2S is known to be excellent heterojunction partner with CdS. Much attention has been focused on thin film CdS / Cu_2S heterojunction due to their great promise as a low cost solar power converter owing to their high efficiency with improved stability. Very recently Cu_XS thin films have also been paid special attention to be a promising candidate for gas sensor material in room temperature, such as solid-state gas sensors for ammonia. The most attractive advantage obtained by utilizing Cu_XS as sensor material is the low working temperature. Most sensor materials are mainly based on oxides that typically demand temperatures of at least a few hundred degrees to achieve good gas sensing properties, while a gas sensor based on Cu_XS is effective already at room temperature.

For successful commercial applications thrust require to be given on the fabrication techniques of the compound for having it in appropriate phase. Researchers reported about several techniques for Cu_XS thin film deposition on basic substrates as reported elsewhere.

In present study we have taken $Cu_{2-x}S$ as a suitable p-type absorber layer material but the formation of stable $Cu_{2-x}S$ film was being difficult task. We have found the elemental stacked layer deposition method is one of the promising techniques. Further we have tried to optimize the thickness and layer no's for developing multilayer $Cu_{2-x}S$ thin film on the glass substrate by physical vapour deposition technique. The results obtained in this method shows that the optimum numbers of layer is 10 ensures formation of crystalline Cu_2S structure with optical band gap is around 1.65 eV to 1.85 eV by different characterization technique like XRD, EDX, SEM, Spectrophotometry and PL. The I-V characteristic of Schottky junction using silver and bulk resistance (ρ_b)with the sample shows semiconductor behavior of the same.

NANOTECHNOLOGY FOR DEVICE MODELING AND PHOTONICS APPLICATIONS

Dr. Arindam Biswas,

Assistant Professor, School of Mines & Metallurgy, Kazi Nazrul University, Asansol, India

Abstract

Nanotechnology is concerned with materials, structures and systems whose components exhibit novel and significantly modified physical, chemical and biological properties due to their nanoscale sizes. A principal goal of Nanotechnology is to control and exploit these properties in structures and devices. Revolutionary changes in the ability to measure, organize and manipulate matter on the nanoscale are highly beneficial for electronics with its persistent trend of downscaling devices, components and integrated systems. Practical implementations of nanoscience and nanotechnology have great importance and they depend critically on training people in these fields. Thus modern education needs to address the rapidly evolving facets of nanoscience and nanotechnology. A new generation of researchers, technologists and engineers has to be trained in the emerging nanodisciplines. Miniaturization required by electronics is one of the major driving forces for nanoscience and nanotechnology. The seminar will provide the basic ideas and understanding on the recent developments in nanoscience and nanotechnology as applied to electronics and photonics device modeling.

BIOMEDICAL SENSORDEVICES FOR POINT-OF-CARE DISEASE DIAGNOSIS

Dr. Gorachand Dutta,

Assistant Professor, School of Medical Science and Technology (SMST), Indian Institute of Technology Kharagpur, Kharagpur, India

Abstract

Over the years, there are increasing needs for the development of simple, cost-effective, portable, integrated biosensors that can be operated outside the laboratory by untrained personnel. However, to reach this goal a reliable sensor technology based on printed electronics has to be developed. Our research aims to develop and establish the field of Biosensor and Electrochemistry for Bench to Bedside diagnosis. Our goal will be the use of redox cycling-based wash-free electrochemical technique in a portable electronic device that can be operated outside the laboratory for simple and effective point-or-care testing in India for early stage disease diagnosis (i.e. cancer, malaria, dengue, tuberculosis, HIV/AIDS etc.). The main challenges of point-of-care testing require to implement complex analytical methods into low-cost technologies. This is particularly true for countries with less developed health care infrastructure. Our washing-free technique is very simple and innovative. We can develop a low-cost disposable wash-free chip and our approach will make it possible to perform highly sensitive detection of biomarkers with printed electronics. The redox cycling technology will detect several interesting targets at the same time on a printed chip. The proposed research projects are inherently cross-disciplinary, combining expertise in biosensing, electrochemistry, electronics & electrical engineering, healthcare and manufacturing, entailing close collaboration and knowledge exchange among the different labs. Also our focused areas: (1) integration of biosensors with fuel cell for self-powered biodevices, (2) low-cost, fully integrated biosensor devices using Lab-on-Printed Circuit Board (PCB) approach, (3) enzyme based immunosensor (ELISA), (4) ultra-sensitive biosensors using magnetic bead assays, nanoparticles, CNT, dendrimer, (5) Lab-on-a-Chip devices for biomedical diagnostics, (6) bio-nanotechnology for drug delivery, (7) microfluidics.

Proceedings of National Conference on Device Modeling and Soft Computing for real time applications (DMSC-2019)
Organized by Dept. of ECE, MIT Bishnupur in collaboration with The Institution of Engineers India (IEI)

ANALYTICAL MODEL FOR A DOPED DOUBLE GATE MOSFET DEVICE BASED ON CONFORMAL MAPPING TECHNIQUE

Supratim Subhra Das*
Dept. of Electronics & Communication Engineering, Mallabhum Institute of Technology, Bishnupur, India
*supratimsubhradas@gmail.com

Abstract: *In this paper, an analytical two dimensional model for channel potential within ultra scaled DG MOSFET has been developed which is valid in sub threshold regime. The potential model is derived by applying Schwarz-Christoffel transformation method and conformal mapping techniques. From that, the threshold voltage model of the device is also evaluated. To validate our model, the result has been compared with numerical simulation data from 3D TCAD Sentaurus which shows good accuracy for channel length as short as 25 nm considered for our device.*

Keywords: *Doped Double Gate MOSFET, Conformal Mapping Technique*

I. INTRODUCTION

With continuous downscaling of the conventional MOSFET in nano scale regime, the device faces lot of challenges including some physical effects known as short channel effects (SCEs). Some important SCEs which immensely affects electrostatic behavior of the device are subthreshold slope degradation due to punch through effect, threshold voltage roll-off and drain-induced barrier lowering effect resulting from close proximity of source and drain region [1]. To mitigate these problems, multi-gate structures such as double gate (DG) MOSFET, triple gate (TG) MOSFET or FinFET and gate all around (GAA) MOSFET have been proposed [2] over the past few years. These new devices have proved to show improved electrical characteristics as compared to a conventional single gate MOSFET structure. Therefore in this paper we focus on the DG MOSFET structure having an ultra thin channel as shown in Fig 1.

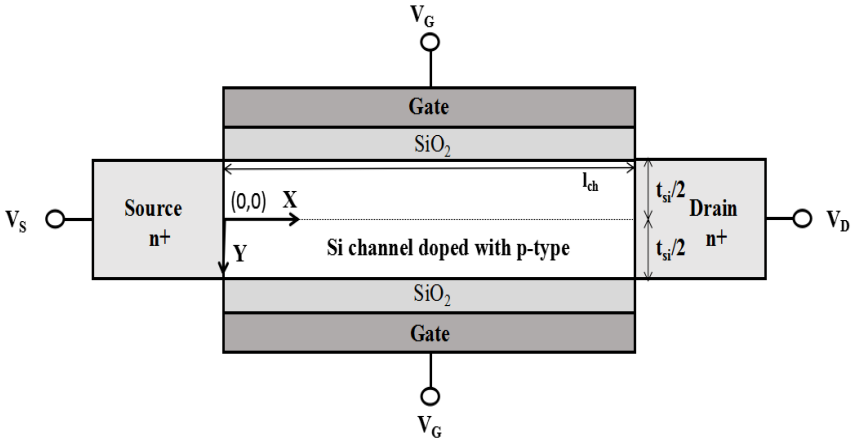

Figure 1. Schematic of cross-sectional view of symmetric DG MOSFET device

A two dimensional (2D) potential model in the entire channel region has been derived by using Schwarz-Christoffel transformation method [3]. The model is analytical and does not include any fitting parameters. An expression for threshold voltage of the device is also obtained from the model. The remaining paper has been organized as : Section II represents the detailed method of modeling, Section III describes the validation of the model with numerical simulation using TCAD Sentaurus and finally Section IV concludes the paper.

II. MODELING

In this section, the electrosttic potential of the device is derived in sub threshold region. The calculation starts with solving 2D Poisson's equation [4] in channel region given as

$$\Delta\phi(x,y) = -\frac{\rho}{\varepsilon_{si}} = \frac{qN_a}{\varepsilon_{si}} \tag{1}$$

Where q is the charge of an electron, N_a is the doping concentration, ε_{si} is the permittivity of silicon. As the device is operated in sub threshold region, we neglect mobile charge term in eq. (1). The solution of the Poisson's equation is considered to be composed of a 1D particular solution $\phi_p(y)$ and a 2D solution $\varphi(x,y)$ obtained from Laplacian differential equation. Finally potential solution can be expressed by

$$\Delta\phi(x,y) = \Delta\varphi(x,y) + \Delta\phi_p(y) \tag{2}$$

Where $\Delta\varphi(x,y) = 0$ (3)

and hence $\Delta\phi_p(y) = \dfrac{qN_a}{\varepsilon_{si}}$ (4)

Next we apply conformal mapping technique on laplace part only to find $\varphi(x,y)$.

- **Assumptions and Simplification**

As the channel thickness considered for our device is not less than 10 nm, we neglect quantum mechanical effects in the device [5]. Parasitic source/drain resistances are also neglected for sake of simplicity. To avoid electric field discontinuity due to different permittivity of silicon and oxide at Si-SiO_2 interfaces, the concept of scaled oxide thickness has been applied [6] following the condition $t_{ox} << t_{si}$. The scaled oxide thickness $\tilde{t}_{ox}$ is given by

$$\tilde{t}_{ox} = \frac{\varepsilon_{si}}{\varepsilon_{ox}} \cdot t_{ox} \tag{5}$$

The four corner device structure under study is decomposed into two corner structure as shown in Fig. 2 for ease of calculation.

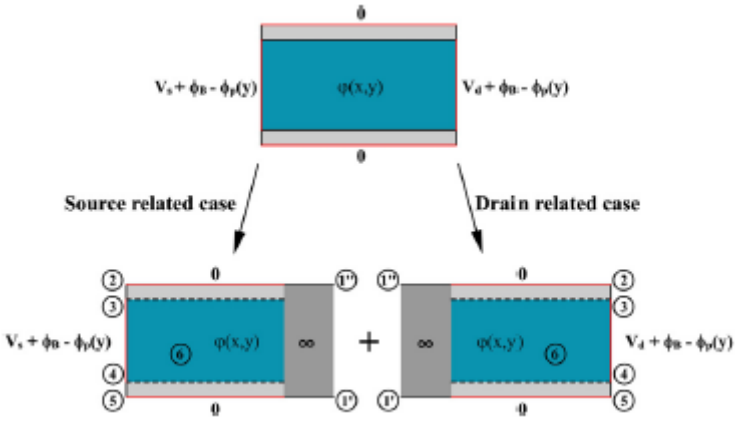

Figure 2. Decomposition of 4 corner DG MOSFET structure into 2 corner problem

This is a valid approximation as long as $l_{ch} > t_{si}$. In decomposed two corner structure two corner problems are obtained. One problem is called as source related case and other as drain related case as illustrated in with proper transformed boundary condition. In this approach short channel effects are taken into account [7].

- **Conformal mapping**

Using this approach, co-ordinates of a complex z plane is mapped to a less complex w plane by means of analytical function $z = f(w)$. Schwarz-Christoffel transformation [3] is a special technique of solving 2D potential problem analytically in transformed w plane. By applying this method, the entire structure in z plane has been conformally mapped into complex w plane in which device boundaries are located on the real axis and inner region is located onto upper half of the w plane. The following inverse function [6] determines the transformation

$$w = f^{-1}(z) = u + iv = \cosh\left(\frac{\pi z}{\Delta y}\right) = \cosh\left(\frac{\pi(x+iy)}{\Delta y}\right) \tag{6}$$

Where $\Delta y = 2\tilde{t}_{ox} + t_{si}$ (7)

- **Single vertex approach**

Single vertex approach [7,8] is an existing method of solving potential in upper half of the w plane which follows the equation

$$P = \Phi + i\Xi = d\varphi + i\frac{d\varphi}{\pi}\ln\left(w - \bar{u}\right) \tag{8}$$

- **Electrostatic potential modeling**

Electrostatic potential of DG MOSFET device can be obtained by superposing the laplacian solution with the aprroximated particular solution as given by eq. (2). Here the calculations have been done for source related case and for drain related case similar calculations can be done only with some changing boundary condition. At first we approximate the particular solution of the potential as given by

$$\phi_p(y) = \frac{qN_a}{\varepsilon_{si}}y^2 + \phi_{0p} \tag{9}$$

Where ϕ_{0p} is the potential solution at the center of the silicon channel. The potentials from eq. (2) for the decomposed structure at source boundary are depicted in Fig. 3.

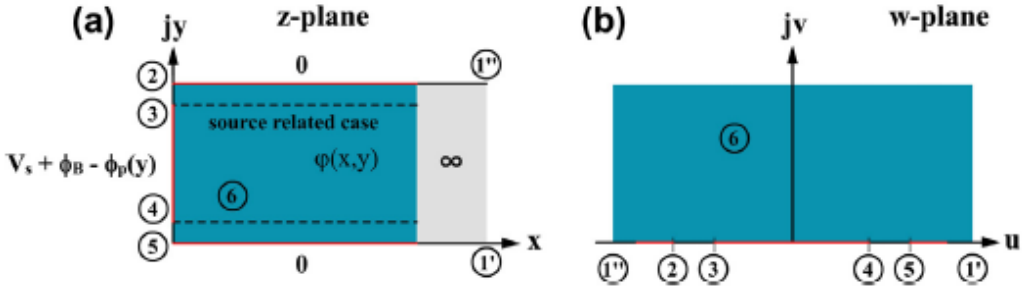

Figure 3. Conformal mapping of DG MOSFET structure from z plane a) onto the upper half of a w plane b) mapping by using analytical function. The source related case is taken as example in this figure.

The particular potential solution at the surface and center of the silicon channel are analytically obtained from eq. (9) and given by

$$\phi_{sp} = V_g - V_{fb} - V_{ox} \quad \text{with } V_{ox} = \frac{qN_a t_{si}}{2C_{ox}} \tag{10}$$

$$\phi_{0p} = V_g - V_{fb} - V_{ox} - \frac{qN_a t_{si}^2}{8\varepsilon_{si}} \tag{11}$$

After obtaining particular solution, two dimensional laplace solution is analytically obtained using Schwarz-Christoffel transformation. With the help of this approach, the parameters w and $\bar{u}$ from eq. (8) can be obtained. Some important points for conformal mapping technique are shown in Fig. 4.

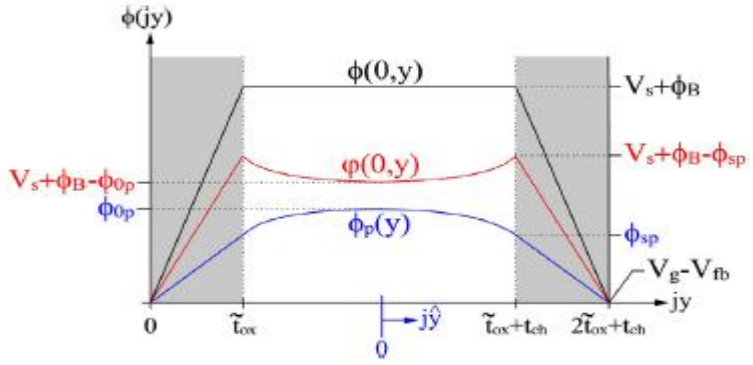

Figure 4. Curves of all potentials in eq. (2) along the source boundary of the device.

The expression for parameter $\bar{u}$ as derived from eq. (6) while moving from one point to another in the real axis of the conformal map (Fig. 3) are obtained as

$$②\rightarrow③: \bar{u}_i = u + iv = \cosh\left(\frac{\pi\left(0 + iy_{i,top}\right)}{2\tilde{t}_{ox} + t_{ch}}\right) \tag{12}$$

$$③\rightarrow④: \bar{u}_i = u + iv = \cosh\left(\frac{\pi\left(0 + iy_{i,middle}\right)}{2\tilde{t}_{ox} + t_{ch}}\right) \tag{13}$$

$$⑤\rightarrow④:: \bar{u}_i = u + iv = \cosh\left(\frac{\pi\left(0 + iy_{i,bottom}\right)}{2\tilde{t}_{ox} + t_{ch}}\right) \tag{14}$$

Where y_i represents the following moving co-ordinates

$$y_{i,top} = 2\tilde{t}_{ox} + t_{ch}, ..., \tilde{t}_{ox} + t_{ch} \tag{15}$$

$$y_{i,top} = \tilde{t}_{ox} + t_{ch}, ..., \tilde{t}_{ox} \tag{16}$$

$$y_{i,bottom} = \tilde{t}_{ox}, ...,0 \tag{17}$$

Where index $i = 1,2,...,n$ indicates the number of steps required to predict the given boundary condition in oxide and channel region. An arbitrary point in the channel region is represented by

$$w = u + iv = \cosh\left(\frac{\pi\left(\sigma + i\left(t_{ox} + \Delta t_{ch}\right)\right)}{2\tilde{t}_{ox} + t_{ch}}\right) \tag{18}$$

Where $\sigma = 0$ for source and $\sigma = l_{ch}$ for drain related case respectively. The boundary potential is assumed to be linear in the oxide and parabolic in the channel region with step function involved along the boundaries. For source related case, the following expressions are obtained.

$$\varphi_{\text{source\_2}\gg3} = \sum_{i=1}^{n}\left[\frac{\left(V_s + \phi_B - \phi_{sp}\right)}{n} + i\frac{\left(V_s + \phi_B - \phi_{sp}\right)}{\pi n}\cdot\ln\left(w - \bar{u}_i\right)\right] \tag{19}$$

$$\varphi_{\text{source\_3}\gg4} = \sum_{i=1}^{n}\left[d\varphi + i\frac{d\varphi}{\pi}\cdot\ln\left(w - \bar{u}_i\right)\right] \tag{20}$$

$$\varphi_{\text{source\_5}\gg4} = \sum_{i=1}^{n}\left[\frac{-\left(V_s + \phi_B - \phi_{sp}\right)}{n} + i\frac{-\left(V_s + \phi_B - \phi_{sp}\right)}{\pi n}\cdot\ln\left(w - \bar{u}_i\right)\right] \tag{21}$$

For drain related case, similar expressions can be used with replacing the term V_s with V_d in eq. (19) and eq. (20) and also putting $\sigma = l_{ch}$ while obtaining w from eq. (18). Finally 2D laplace solution of potential for DG MOSFET is given by

$$\varphi(x,y) = \varphi_{source\_2->3} + \varphi_{source\_3->4} + \varphi_{source\_5->4} + \varphi_{drain\_2->3} + \varphi_{drain\_3->4} + \varphi_{drain\_5->4} \quad (22)$$

Now complete potential solution can be evaluated by superposing particular solution with laplace solution as given by

$$\phi(x,y) = \varphi(x,y) + \phi_p(y) \quad (23)$$

- **Threshold voltage modeling**

The threshold voltage for the device is estimated by the gate voltage at which the minimum potential $\phi_{\min}$ ocuurs at $x_{\min}$ equals the value of ϕ_T [9] which are given by

$$x_{\min} = \frac{l_{ch}}{\pi} \arccos\left(\frac{V_d}{V_d + 2\phi_B}\right) \quad (24)$$

$$\phi_T = V_{th} \ln\left(\frac{N_a}{n_i}\right) \quad (25)$$

Where ϕ_B is expressed by

$$\phi_B = V_{th} \ln\left(\frac{N_{SD}}{n_i}\right) \quad (26)$$

Where N_{SD} is the source/drain doping concentration.

According to [9], the expression for threshold voltage is

$$V_T = V_g + \Delta V_g \left(\frac{\phi_T - \phi_{\min(V_{g1})}}{\phi_{\min(V_{g2})} - \phi_{\min(V_{g1})}}\right) \quad (27)$$

III. MODEL VALIDATION

The analytical model derived in section are verified with the numerical simulation using 3D TCAD Sentaurus tool. Table I depicts the list of device parameters used for simulation.

TABLE I: Device parameters

SYMBOL	NAME	VALUE
l_{ch}	Channel length of the device	30 nm
t_{si}	Channel thickness	10 nm
t_{ox}	Gate oxide thickness	2.3 nm
H	Channel Height	35 nm

It is found from Fig. 5 that surface potential model for DG MOSFET is in good agreement with simulation result when V_g ranges from 0.1 V to 0.3 V. As the model is valid in sub threshold region, we neglect mobile charges in our approach. Our model covers all 2D effects associated with source or drain side of the device. The variation of threshold voltage with respect to channel length is also plotted in Fig. 6. It has been observed from Fig. 6 that threshold voltage increases as channel length decreases. Threshold voltage decreases even further if drain voltage V_d is increased depicting the effect of DIBL. For such a shorter channel length device as considered in our study, the increase of V_{ds} has more influence on V_T compared to a longer channel device as observed in Fig. 6.

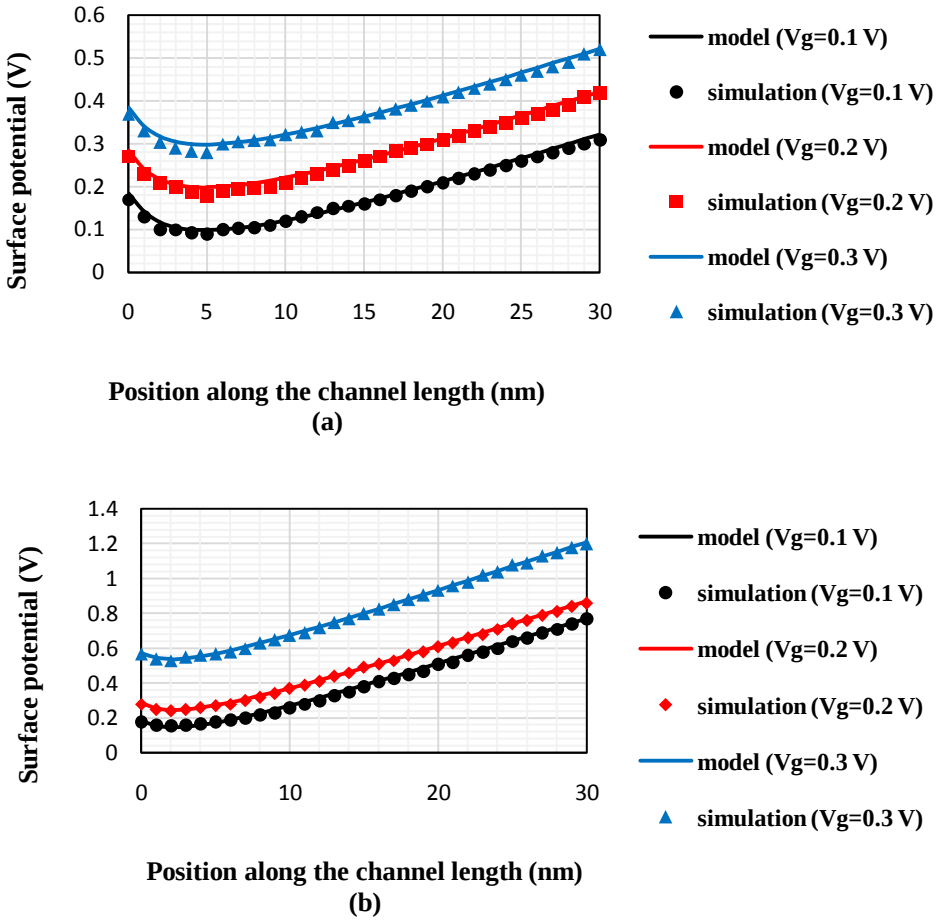

Figure 5. Variation of surface potential along the channel length direction of the device for a) V_d=0.05 V and b) V_d=0.5 V

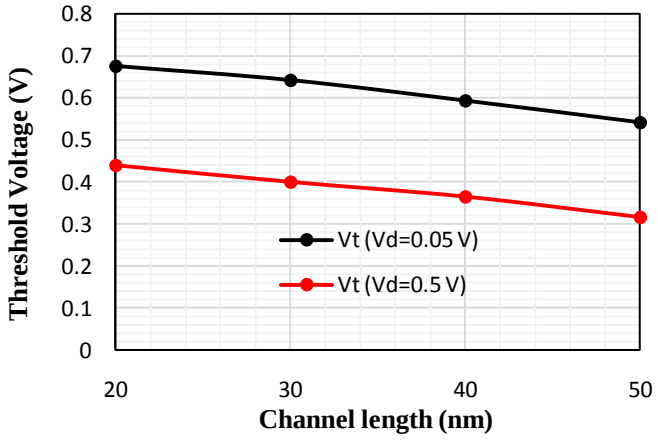

Figure 6. Variation of threshold voltage at different channel length values of the device.

IV. CONCLUSION

In this work, a 2D analytical model for electrostatic potential in the channel region of a DG MOSFET is developed. The potential at the surface along the channel length direction is plotted and verified with numerical simulation results. It has been shown that model establishes good match with simulation data. By using the results obtained from model, a threshold voltage model is also derived which shows a strong dependence on channel length of the device and its drain voltage. In future we may extend the model by including mobile charge term in the model in order to apply it in saturation region. The expressions for electric field and hence current equation can also be derived subsequently for our ongoing work.

REFERENCES

[1] Arora N. MOSFET models for VLSI circuit simulation. Wien: Springe-Verlag;1993.
[2] Colinge J-P. FinFETs and other multi-gate transistors. Springer; 2007.
[3] Weber. Electromagnetic fields. 3rd ed. Wiley; 1950.
[4] Holtij T, Schwarz M, Kloes A, Iniguez B. 2D analytical modeling of the potentialwithin junctionless DG MOSFETs in thesubthreshold regime. EuroSOI,Montpellier; 2012.
[5] Omura Y, Horiguchi S, Tabe M, Kishi K. Quantum-mechanical effects on thethreshold voltage of ultrathin-SOI nMOSFETs. IEEE Electron Dev Lett1993;14(12):569–71. http://dx.doi.org/10.1109/55.260792.
[6] Kloes A, Kostka A. A new analytical method of solving 2D Poisson's equation inMOS devices applied to threshold voltage and subthreshold modeling. Solid-State Electron 1996;39(12):1761–75. http://dx.doi.org/10.1016/S0038-1101(96)00122-0.
[7] Schwarz M, Weidemann M, Kloes A, Iniguez B. 2D analytical calculation of theelectrostatic potential in lightly doped Schottky barrier Double-Gate MOSFET.Solid-State Electron 2010;54(11).
[8] Holtij T, Schwarz M, Kloes A, Iniguez B. 2D analytical modeling of the potentialin doped multiple-gate-FETs including inversion charge. Fringe Poster Sessionat ESSDERC/ESSCIRC, Helsinki; 2011.
[9] Holtij T, Schwarz M, Kloes A, Iniguez B. 2D analytical potential modeling ofjunctionless DG MOSFETs in subthreshold region including proposal forcalculating the threshold voltage. ULIS2012, Grenoble; 2012.

STUDY OF THE PERFORMANCE OF DRIVING ASSISTANCE SYSTEM FOR COMPLEX TRIP PLANNING OF ELECTRIC VEHICLES USING EVOLUTIONARY ALGORITHM

Mousumi Khanra (Karmakar)*[1] and Arup Kr Nandi [2,3]
[1]*Dept. of Electronics & Communication Engineering, Mallabhum Institute of Technology, Bishnupur, India*
[2]*CSIR-Central Mechanical Engineering Research Institute, Durgapur, India*
[3]*Academy of Scientific and Innovative Research (AcSIR), Ghaziabad, India*
*mkmit2008@gmail.com

Abstract: *In order to tackle the various drawbacks of electric vehicle, a Driving Assistance System (DAS) was developed in the recent past for properly manage the energy consumption through optimal driving during performing a trip. In the present paper, the DAS performance is analyzed towards planning a trip of typical configuration. Three driving cycles (neighborhood, urban and highway) are considered for making various complexities of the trip for this investigation. The effect of driving cycle lengths in a given trip on DAS results is demonstrated here. Moreover, effectiveness of DAS towards energy saving is analyzed for a typical complex trip planning.*

Keywords: *Driving Assistance System, trip planning, electric vehicle, micro-trip, optimal driving strategy, trip complexity, multi-objective optimization, driving cycle*

I. INTRODUCTION

Day by day vehicular sectors are improving to increase the acceptance of Electric vehicles (EVs) for personal transportation. To plan a trip using electric vehicle (EV) drivers need to carefully plan the trip in order to ensure that they will reach their destination. There are many factors that drive this important consideration such as limited battery storage, insufficient charging stations, and high charging time when compared to conventional internal combustion vehicles. To overcome such EV related drawbacks, an optimal driving based Energy Management System (so called DAEM) was introduced in [1]. The DAEM system works based on multi-objective optimization problem (MOOP), MOOP of minimizing energy, E, minimizing trip time, T_{Trip}, and minimizing average jerk, J_{Avg} were considered simultaneously. In [2], authors analyzed the influence of initial battery charge and route characteristics on DAEM results. Depending upon the quality of road and other reasons (not overtaking zone, hospital, school, high traffic, narrow road, bridge, etc.), the speed limits of a road are restricted [3] [4]. Such speed limit variations create the trip complexity. In [5], the influence of trip complexity on DAEM results was investigated.
In the present paper, the performance of DAS and its working principle were studied by analyzing the its results in terms of the battery state-of-charge after trip completion (SOC_{Trip_end}) with total trip time (T_{Trip}) in different complex trip planning [6-14]. Furthermore, an investigation on the amount of energy saving through adopting DAS during trip performing was carried out.
In Section 2, the architecture of DAS and its working principle are briefly described and the definition of a micro-trip is presented in Section 3. In section 4, results and discussion are presented. Finally, concluding remarks are stated in Section 6.

II. OPTIMAL DRIVING BASED DAS

Fig. 1 demonstrates the architecture of the optimal driving based energy management system (DAEM) [1] which comprises two primary modules HMI (Human machine interface) and OTP optimal trip planning. HMI is used as a platform to collect information from various sources (such as driver, GPS/Internet, etc.) and feed to OTP. Based on this information, OTP determines a set of optimal driving strategies (multiple output information on trip planning). In addition, various other information corresponding to the optimal driving strategies, namely range, trip end *SOC* and total trip time are also determined by OTP. Determination of optimal driving strategies is made by solving a multi-objective optimization problem that considers three conflicting objectives as follows.

$$\text{Minimization of trip time}(T_{Trip}) = f_T\left(v_{ref}, a_{ref}, k_p, k_i\right) \tag{1}$$

$$\text{Minimization of Energy consumsion}(E) = f_B\left(v_{ref}, a_{ref}, k_p, k_i\right) \tag{2}$$

$$\text{Minimization of average jerk}(J_{Avg}) = f_{J_{Total}}\left(a_{ref}^{1,2,\ldots,K},\ t_{1,2,3,\ldots K-1}, k_p,\ k_i\right) \tag{3}$$

subject to

$$v_{\min}^{dc} \le v_{ref} \le v_{\max}^{dc} \tag{4}$$

$$a_{\min} \le a_{ref}^{1,2,\ldots,K} \le a_{\max} \tag{5}$$

$$0.01 \le k_p \le 0.3 \quad (6)$$

$$0.01 \le k_i \le 3.0 \quad (7)$$

Where v_{ref}, a_{ref} and t are the reference velocity, acceleration/deceleration and corresponding durations [17], respectively, *kp* and *ki* are the controller gains.

After each execution of OTP, a set of solutions (ODS) and corresponding various predicted information (such as range, trip end *SOC*, and trip time) are presented to the driver for making a suitable trip planning [16]. Driver may choose an appropriate ODS from the solution set based on the present circumstances or his desire. Otherwise, any decision making technique may be adopted to select a preferred one [15]. The driver is recommended to follow the preferred ODS for driving till the further ODS as evaluated in the subsequent OTP execution. The subsequent execution of OTP is performed on the basis of current route data corresponding to the original or updated trip start/end location (destination) and battery *SOC*.

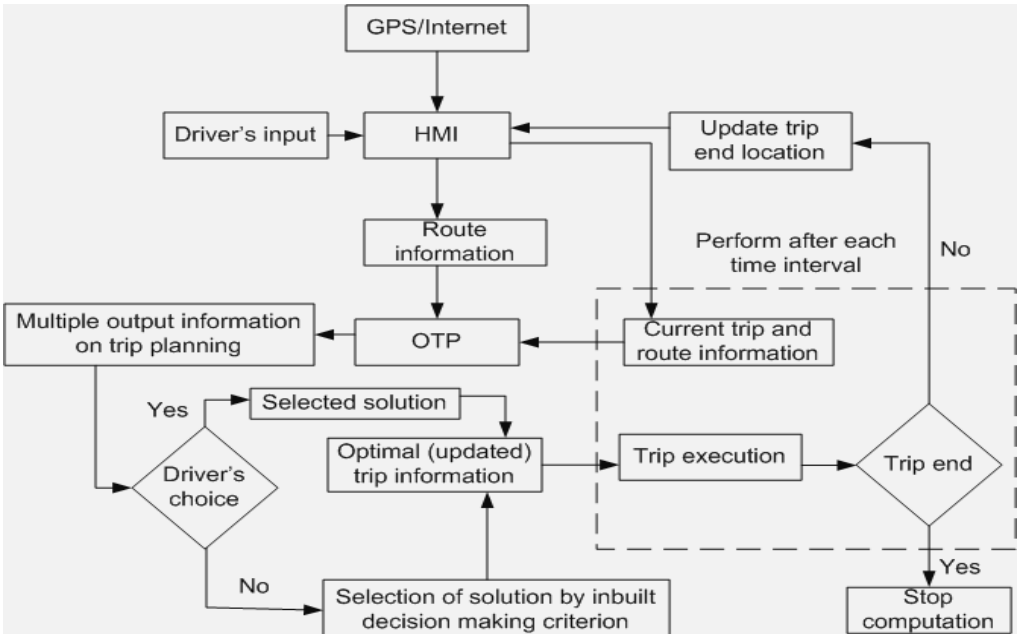

Fig. 1. Schematic layout of DAEM architecture

III. CONCEPT OF MICRO-TRIP

A micro-trip may be defined as an excursion between two successive locations of travel route at which the vehicle is definitely stopped [18] [19]. In general, an entire trip comprises several micro-trips. The length (range) of a micro-trip is defined by the distance covered the two stop points of vehicle and may be called start and end points of that micro-trip, respectively. A typical simple micro-trip consists of the following modes: acceleration mode, constant speed mode and deceleration mode.

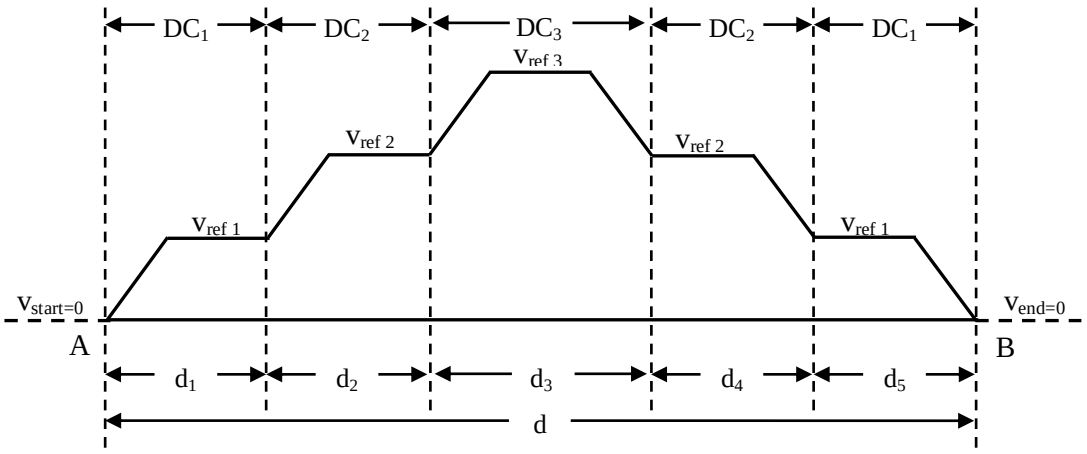

Fig. 2. The velocity profile of a typical complex micro-trip

According to safety and differentiation of type of road, a micro-trip may face four category of road type based on maximum and minimum speed limits [20] [21] such as neighborhood (speed range 8 km/h - 40 km/h), urban (speed range 40 km/h - 56 km/h), highway (speed range 56 km/h - 88.5 km/h), interstate (speed range 88.5 km/h - 112.6 km/h).
The minimum and maximum speed limits of each driving cycle need to be strictly followed by driver according to the rules and regulation. Thus, the proposed DAS must be valid for each driving cycle. Accordingly, its performance for each driving cycle is required to be studied independently for a complex trip planning using EV.
In real life journey, when we plan a trip at first we start the journey from a neighborhood driving zone and then after few kilometers of journey reach to urban driving zone. Generally, after the completion of urban driving zone, we follow highway driving zone. Before reach to final destination the trip again covers urban and neighborhood zones, respectively. In the present paper, such type of trip is considered for DAS analysis shown in Fig. 2. In Fig. 2, d_1 and d_5 represents neighborhood driving cycle (DC_1), d_2 and d_4 represents urban driving cycle (DC_2) and d_3 represents highway driving cycle (DC_3).
Fig. 2 demonstrates the velocity profile of a typical complex micro-trip that consists of three driving cycles with five parts. The first and fifth part of the micro-trip corresponds to neighborhood driving cycle, the 2nd and 4th part corresponds to urban driving cycle and 3rd part corresponds to highway driving cycle. The vehicle reference speeds, v_{ref1}, v_{ref2} and v_{ref3} belong to 1st, 2nd and 3rd part of the micro-trip. The 5th part of micro-trip, the vehicle reference speed is same as 1st part and 2nd part of micro-trip, the vehicle reference speed is same as 4th part. According to the definition of micro-trip, v_{start} and v_{end} in Fig. 2 both are zero. According to rule of traffic signal, at each signal normally the vehicle has to stop at a red signal light until the signal becomes green. Locations, A and B (in Fig. 2) are considered as two successive red signals.

IV. RESULTS AND DISCUSSION

Fig. 3 demonstrates the Pareto front of DAS results obtained through solving the MOOP using a non-dominated sorting genetic algorithm (NSGA II) [22] for the typical complex micro-trip of length 20 km and 50 km. Optimization results obtained by varying length of three driving cycles for the same MT (micro-trip) and analyzed the performance in order to understand the effect of complexity due to the driving cycle length. The Fig. 3a and Fig. 3b shows the Pareto-optimal solutions of SOC_{Trip_end} with T_{Trip} for the complex micro-trips (as shown in Fig. 2) for different values of urban and highway driving cycle length. The total trip length for both cases was considered as 20 km.
From Fig. 3a, it was found that the Pareto fronts are overlapping for different urban driving cycle length for 20 km trip length with fixed length of highway driving cycle (10 km). With increasing the urban driving cycle length, the characteristics of SOC_{Trip_end} and T_{Trip} is not significantly changed. In Fig. 3b, with increasing the highway driving cycle length for fixed urban driving cycle length, the Pareto fronts are not overlapping. Moreover, it was found that the Pareto front width is stretched with increasing the highway driving cycle length and also improves the value of SOC_{Trip_end}. Similar observation studies for 50 km trip length for the same complex micro-trip as shown in Fig. 4.
From Fig. 4a and Fig. 4b, it was observed that with the increase of total trip length, Pareto front are not overlapped for different length of urban and highway driving length. Moreover, from Fig. 4a and Fig. 4b, it was noticed that the SOC_{Trip_end} value is increased with the increase of urban and highway driving cycle length for fixed trip length (50km). The rate of increase of SOC_{Trip_end} with respect to T_{Trip} was found more when the highway driving cycle length is high (as shown in Fig. 4b). But when the urban driving cycle length is high, rate of SOC increase with respect to time is not so high (as shown in Fig. 4a) compare to high highway driving cycle length for same micro-trip, as shown in Fig. 4(b). Therefore, from the plot of Pareto-optimal solutions of SOC_{Trip_end} with T_{Trip} for the typical complex micro-trip, we see that with the increase of length of urban and highway driving cycle energy consumption is reduced and finally at the end of trip we get high SOC_{Trip_end} with the use of DAS. Moreover, the rate of trip end SOC_{Trip_end} improvement is higher in high length of highway driving cycle than urban driving cycle.

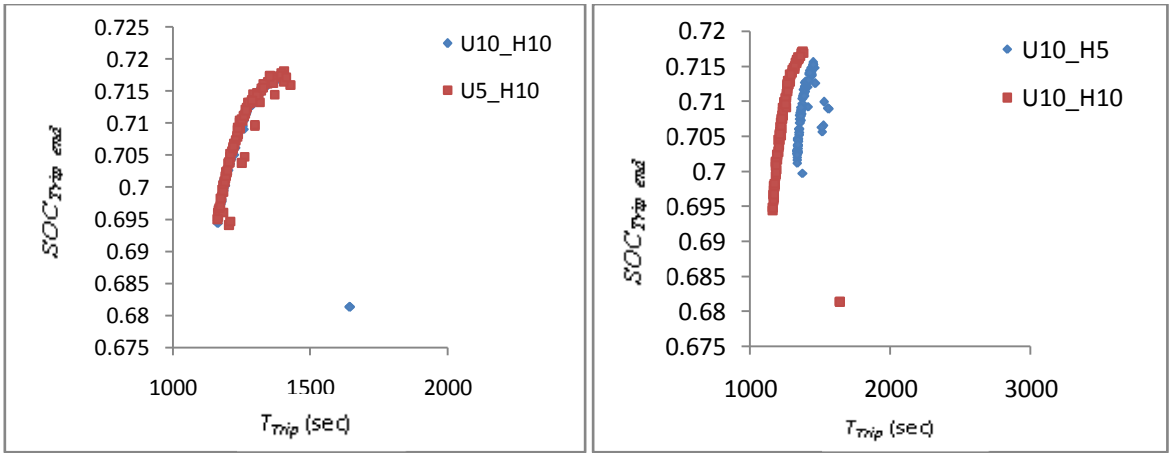

Fig. 3. Comparative results of a typical complex micro-trip (20 km trip length) with different lengths of urban and highway driving cycle (a) Highway length=10 km (b) Urban length=10km

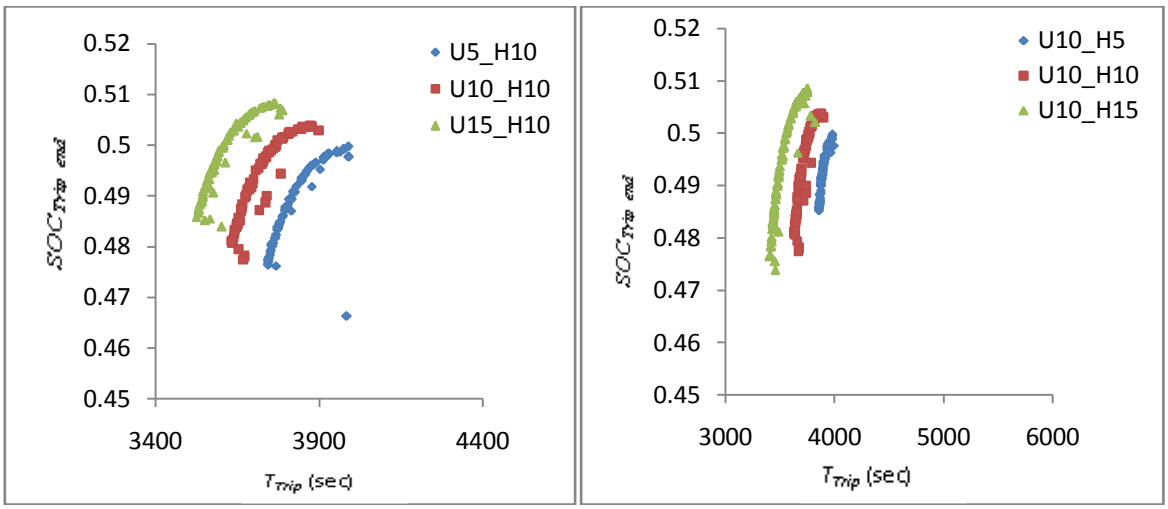

Fig. 4. Comparative results of a typical complex micro-trip (50 km trip length) with different lengths of urban and highway driving cycle (a) Highway length=10 km (b) Urban length=10km

The effectiveness of DAS is analyzed by comparing the energy consumptions with and without using DAS during trip performing. Table 1 presents the amount of energy saving can be obtained for different driving cycle lengths of the same micro-trip as presented in Fig. 2. Based on energy saving for different driving cycle length of a complex micro-trip are analyzed and listed in Table 1.

Table 1: Energy saving for different driving length of a complex micro-trip with the use of DAS

Trip Length (Km)	**Driving cycle Length (Km)**		**Energy Consumption (J)**		**Energy Saving (%)**
	Urban	**Highway**	**With DAS**	**Without DAS**	
20	5	10	739481	856610	13.6736
	10	10	745500	858730	13.1858
	10	5	785603	825032	4.77909
50	5	10	194051	205237	5.45028
	10	10	191810	203070	5.54489
	15	10	189754	200194	5.21494
	10	5	193975	200412	3.21188
	10	15	189092	204704	7.62662

From Table 1, it was observed that there is always energy saving with adopting DAS but is varies with the driving cycle length. For a 20 km trip length, a maximum of 13.67% energy saving is found with 10 km highway length, 5 km urban length and remaining is neighborhood. If we decrease the highway length from 10 km to 5 km, the energy saving is reduced from 13.18% to 4.779%. On the other hand, the speed limits of highway driving cycle are higher than urban or neighborhood. Thus, the above finding indicates that selection of optimal speed in higher driving cycle is important.
On the other hand, variation of urban length, the energy saving (%) is not found to be significantly changed. Similar observation is also noticed for other trip lengths, and it was noticed that energy saving increasing with increasing the highway driving cycle length provided that the speed should be optimum.

V. CONCLUSIONS

In this paper, the performance of DAS is analyzed for a typical complex trip planning. The above observations draws the following conclusions-

- For low trip length, variation of urban driving length is not significantly changes the trip end SOC_{Trip_end} rather variation of highway driving length.
- For high trip length, with the increase of urban and highway driving length trip end SOC_{Trip_end} improved.
- Percentage of energy saving is found in any trip length with the use of DAS in a complex trip planning.
- Maximum energy saving is found in high value of highway length and minimum energy saving is found in low value of highway length.

ACKNOWLEDGMENT

First author is thankful to Principal of Mallabhum Institute of Technology, Bankura, West Bengal, India to provide the necessary support for her research work at CSIR-CMERI, Durgapur, India.

REFERENCES

[1] M. Karmakar, A.K. Nandi, "Trip Planning for Electric Vehicle through optimal driving using Genetic Algorithm, International Conference on Power Electronics," Intelligent Control and Energy Systems (IEEE ICPEICES), Delhi, India , 2016.
[2] M. Karmakar, A.K. Nandi, "Driving Assistance for Energy Management in Electric Vehicle, International Conference on Power Electronics," Drives and Energy Systems (IEEE PEDES), Trivandrum, Kerala, India, 2016, .
[3] S. Tsugawa, Super smart vehicle system: Future intelligent driving and the measures for the materialization, in Proceeding of Surface Transportation: Mobility, Technology, and Society. Proceedings of the IVHS AMERICA 1993 Annual Meeting,Washington, D.C., pp. 192–198,1993.
[4] H. Fujii, O. Hayashi, N. Nakagata, Experimental research on intervehicle communication using infrared rays, in Proc. IEEE Intelligent Vehicles Symposium, Tokyo, Japan, pp. 266–271, 1996.
[5] M. Khanra, A.K. Nandi, "Influence of trip complexity on optimal driving based Energy Management System of Electric Vehicle", International Conference on Communication and Electronics Systems (ICCES 2019), Coimbatore, India , 2019.
[6] Feng, L., Ge, S., Liu, H., Electric Vehicle Charging Station Planning Based on Weighted Voronoi Diagram. Proceedings of Power and Energy Engineering Conference (APPEEC), Asia-Pacific, published by IEEE, pp. 1-5, 2012.
[7] E. Gilman, A. Keskinarkaus, S. Tamminen, S. Pirttikangas, J. Röning, and J. Riekki, "Personalised assistance for fuel-efficient driving," Transportation Research Part C: Emerging Technologies, 58D, pp. 681-705, 2015.
[8] M. Ceraolo, G. Pede, Techniques for estimating the residual range of an electric vehicle. IEEE Transactions on Vehicular Technology 50 (1) 109-115, 2001.
[9] E.J. Yao, M.Y. Wang, Y.Y. Song, T. Zuo, Estimating the cruising range of electric vehicle based on instantaneous speed and acceleration, Applied Mechanics and Materials 361-363, 2104-2108, 2013.
[10] A. Szumanowski, Y. Chang, Battery management system based on battery nonlinear dynamics modeling, IEEE Transactions on Vehicular Technology 57(3), 1425-1432, 2008.
[11] K.A. Smith, C.D. Rahn, C.Y. Wang, Model-based electrochemical estimation and constraint management for pulse operation of lithium ion batteries, IEEE Transactions on Control Systems Technology 18(3), 654-663, 2010.
[12] W.X. Shen, K.T. Chau, C.C, Chan, E.W.C. Lo, Neural network-based residual capacity indicator for nickel-metal hydride batteries in electric vehicles, IEEE Transactions on Vehicular Technology 54(5), 1705-1712, 2005.
[13] F. Baronti, W. Zamboni, N. Femia, R. Saletti, M.Y. Chow, Parameter identification of Li-Po batteries in electric vehicles: A comparative study. IEEE International Symposium on Industrial Electronics, Taipei, Taiwan, doi:10.1109/ISIE.2013.6563887 , pp. 1-7, 2013.
[14] L.L. Du, B. Li, H.D. Zhang, Estimation on state of charge of power battery based on the grey neural network model, Applied Mechanics and Materials 427-429, 1158-1162, 2013.
[15] K. Miettinen, Nonlinear multiobjective optimization. Kluwer, Boston, 1999.
[16] A.K. Nandi, D. Chakraborty, and W. Vaz, "Design of a comfortable optimal driving strategy for electric vehicles using multi-objective optimization," Journal of Power Sources, vol. 283, pp. 1-18, 2015.
[17] W. Vaz, A.K. Nandi, U.O. Koylu, "A multi-objective approach to find optimal electric vehicle acceleration: simultaneous minimization of acceleration duration and energy consumption," IEEE Transactions on Vehicular Technology, (DOI 10.1109/TVT.2015.2497246), 2015.
[18] Haan, M. Keller, Real-world driving cycles for emission measurement: ARTEMIS and Swiss cycles, Final Report, 2001.
[19] M. Andre, Real-world driving cycles for measuring cars pollutant emissions – Part A: The ARTEMIS European driving cycles, Institut National de Recherche sur les Transports et leur Securite (INRETS), Report INRETS-LTE 0411, 2004.

[20] A. G. Ostensen , Effects of Raising and Lowering Speed Limits on Selected Roadway Sections, U.S. Department of Transportation, Federal Highway Administration, Publication No. FHWA-RD-97-084, 1997.
[21] M.I. Berry,The effects of driving style and vehicle performance on the real-world fuel consumption of US light-duty vehicles. Master's Thesis, Massachusetts Institute of Technology, available at http://web.mit.edu/sloan-auto-lab/research/beforeh2/files/IreneBerry_Thesis_February2010.pdf, 2010.
[22] Deb, K., Pratap, A., Agarwal, S. and Meyarivan, T., A fast elitist non-dominated sorting genetic algorithm for multi-objective optimisation: NSGA-II. IEEE Transactions on Evolutionary Computation 6 (2), 2002. .

SOLVING TRAVELLING SALESMAN PROBLEM USING INTUITIONISTIC FUZZY SET BASED GENETIC ALGORITHM

Amalendu Si* [1] and Sujit Das [2]
[1]*Dept. of CSE, Mallabhum Institute of Technology, Bishnupur-722122, India*
[2]*Dept. of Computer Science and Engineering, NIT Warangal, Warangal 506004, India*
*amalendu.si@gmail.com

Abstract: *The purpose of the travelling salesman problem is to find the optimal path for visiting all cities in each set of cities and finally return to the stating city. Finding the optimal path is often critical due to the presence of some contradictory parameters. In this article, we present an approach to solve travelling salesman problem (TSP) using intuitionistic fuzzy set (IFS) based genetic algorithm (GA), where the travelling cost between cities is considered as benefits and expenditures which are represented using IFSs. Total cost of the path is estimated using intuitionist fuzzy aggregation operator (IFAO). Then GA is used to reduce the searching complexities and to find the optimal solution.*

Keywords: *Genetic Algorithm, Intuitionistic Fuzzy Sets, Intuitionistic Fuzzy Aggregation Operator, Travelling Salesman Problem.*

I. INTRODUCTION

Travelling salesman problem (TSP) [2] is a well-known, popular and extensively studied problem in the field of conditional optimization. The definition of TSP is that there are number of cities of which, the salesman start his journey from his home city to visit all cities exactly once and then return to the home city again and find the order of the cities in such a way, so that the cost of the tour is minimum. The cost is calculated on the basis of distance between cities, travelling time, security during travel, loss of energy etc. The TSP is easy to describe but too difficult to solve. Initially, the TSP is solved by using the different mathematical techniques like random searching, dynamic programming, branch and bound method, greedy procedure and so on, to reduce the time complexity. Then the TSP is modified in various ways depending on the application type, varieties of purposes and requirements of the users and current situations. After the modification of the TSP, the simple mathematical procedure is not appropriate to get optimal or suitable solutions in the reasonable time. Then, many researchers have proposed different modified methods to solve the problem. Among them, some researchers have changed the constraints of the problem and some researchers have introduced new parameters which are directly related with problem. Author [4] has proposed a fuzzy multi-objective linear programming problem solving technique and explored the aspiration parameter for choosing the route. Here, the decision variables are defined with the three parameters which are related to travelling cost, time and distance. Then the three LP problems are considered for the said parameters for the optimization and after that, based on those optimized solutions, the authors have created another simple LP problem for calculating the aspiration level 'L' of the route. In this article, three LP problems have been considered to optimize three parameters. An 'n' parameter problem is needed to solve an 'n' number of LP problems which is time consuming. A new technique is introduced by S. Dhanasekar and others [3] to solve the TSP in fuzzy environment by ranking the fuzzy numbers. A. Kumar and A. Gupta [7] have proposed two methods of fuzzy assignment problems and fuzzy travelling salesman problems with LR parameters to solve the TSP easily. So, most of the researchers consider either maximizing the cost of the tour or minimizing the loss. When an expert considers the maximization side then, the minimization side is in dark position and alternatively when he considers the minimization side then maximization side in dark position. In this article, we consider both the maximization and minimization side of the tour. Intuitionist Fuzzy Sets (IFS) is a suitable technique to represent both of them within a single quantizer and Intuitionist Fuzzy Aggregation Operator (IFAO) is applied to merge them. Then we use Genetic Algorithm (GA) to choose the best alternative among the available solutions.

II. CLASSICAL TSP AND SOLVING TECHNIQUE

The mathematical notation of the Travelling Salesman Problem can be represented with a graph, where a city is represented with a point or node and the link between two nodes is called edge or arc. A distance is associated with each edge which is considered as the cost of edge. The cost of the edge is fixed and static. If a node of the graph is connected with all other nodes of the graph, it is called a complete graph. A round trip of all the cities corresponds to a special subset of the edges. When each city is visited exactly once and returned to the staring city again, it is called a tour or Hamiltonian cycle (h) of the graph. The h_i is the combination of $city_i$, $city_{k1}$, $city_{k2}$,.... $city_{km}$, $city_i$, where k_1, k_2...k_m ϵ(n-i). The total cost (c) of the tour denotes round trip distance

of the cycle. The cost of the Hamiltonian cycle h_i is denoted as c_i and calculated using (1). Then, among the Hamiltonian cycles, the minimum cost ($c_{optimal}$) cycle is chosen and considered as final or optimal solution. The TSP is symmetric or asymmetric, depending on the direction of the edge. When the edges are bidirectional, then the problem becomes symmetric, otherwise the problem is considered as an asymmetric problem. If the travelling cost from the *city*$_i$ to *city*$_j$ is denoted with c_{ij} if $c_{ij}=c_{ji}$ then the problem is symmetric. We introduce a variable x_{ij} of each arc with the value of either 0 or 1 for the representation of the problem. When x_{ij} is 1 (i=1,2,3…n and j=1,2,3….n) it means that the arc is connected from city$_i$ to city$_j$. Let $x_{ii}=0$ (i=1, 2, 3…n) which means that no tour is considered from a city to itself.

$$c_i = \sum_{k=1}^{n-1} c_{ik} + c_{ki} \qquad (1)$$

$$c_{optimal} = \min_i (c_i) \qquad (2)$$

III. INTUITONISTIC FUZZY SET

In this section, we briefly review about IFS, its operation and comparison.

Definition of IFS and IFV with necessary conditions

Atanassov [8] defined the concept of intuitionistic fuzzy sets in 1989. Consider a set E be a universal set. An intuitionistic fuzzy sets or IFS in $\mathbf{Z}$ is an element having the form $A' = \{\langle z, \mu_{A'}(z), \nu_{A'}(z)\rangle | x \in \mathbf{Z}\}$ where the function $\mu_{A'} : \mathbf{Z} \to [0,1]$ and $\nu_{A'} : \mathbf{Z} \to [0,1]$ denoted the degree of membership and the degree of non membership respectively of the element z from $\mathbf{Z}$ to set A'. For any element zϵ $\mathbf{Z}$ satisfy the condition $z \in \mathbf{Z}, 0 \le \mu_{A'}(z) + \nu_{A'}(z) \le 1$.

The function $\pi_{A'} : \mathbf{Z} \to [0,1]$ specified by $\pi_{A'}(z) = 1 - \mu_{A'}(z) - \nu_{A'}(z), z \in \mathbf{Z}$ defines the degree of uncertainty of membership of the element z to set A` called hesitant function. For a fixed zϵ $\mathbf{Z}$, an object $\{\mu_{A'}(z), \nu_{A'}(z)\}$ is usually called intuitionistic fuzzy value (IFV) or intuitionist fuzzy number (IFN).

Basic Operation On Intuitionistic Fuzzy Sets

Addition $\oplus$ and Multiplication $\otimes$ of IFSs

The operation of addition $\oplus$ and multiplication $\otimes$ on intuitionistic fuzzy values are defined by Atanassov [8] as follows: Let $A' = (\mu_{A'}(z), \nu_{A'}(z))$ and $B' = (\mu_{B'}(z), \nu_{B'}(z))$ be two IFVs, then

$$A' \oplus B' = (\mu_{A'} + \mu_{B'} - \mu_{A'}.\mu_{B'}, \nu_{A'}.\nu_{B'}) \qquad (3)$$

$$A' \otimes B' = (\mu_{A'}.\mu_{B'}, \nu_{A'} + \nu_{B'} - \nu_{A'}.\nu_{B'}) \qquad (4)$$

These operations are constructed in such a way that they generate IFV, since it is proved that $0 \le \mu_{A'} + \mu_{B'} - \mu_{A'}.\mu_{B'} + \nu_{A'}.\nu_{B'} \le 1$ and $0 \le \mu_{A'}.\mu_{B'} + \nu_{A'} + \nu_{B'} - \nu_{A'}.\nu_{B'} \le 1$.

Each ordinary fuzzy set A may be written as:

A`$= \{< z, \mu_{A'}(z), 1 - \mu_{A'}(z) > | z \in \mathbf{Z}\}$.

If $A', B' \in IFSs$, then the following operations can be found in

1) $A' \subseteq B'$ iff $(\forall z \in \mathbf{Z})(\mu_{A'}(z) \le \mu_{B'}(z) \& \nu_{A'}(z) \ge \nu_{B'}(z))$;

2) $A' = B'$ iff $(\forall z \in \mathbf{Z})(\mu_{A'}(z) = \mu_{B'}(z) \& \nu_{A'}(z) = \nu_{B'}(z))$;

3) $A'^C = \{\langle z, \nu_{A'}(z), \mu_{A'}(z)\rangle \mid z \in \mathbf{Z}\}$.

Multiplication ⊗ of IFS with real values

The addition and multiplication of IFSs with real values are evaluated using (3) and (4) in [8].

$nA' = \left\{1-\left(1-\mu_{A'}\right)^n, \nu_{A'}^n\right\}$ & $A'^n = \left\{\mu_{A'}^n, 1-\left(1-\nu_{A'}\right)^n\right\}$, where n is any integer.

These aforementioned operations produce IFVs which depends not only for integer n but also for all real value $\lambda > 0$ i.e.,

$$\lambda A' = \left\{1-\left(1-\mu_{A'}\right)^{\lambda}, \nu_{A'}^{\lambda}\right\} \qquad (5)$$

$$A'^{\lambda} = \left\{\mu_{A'}^{\lambda}, 1-\left(1-\nu_{A'}\right)^{\lambda}\right\} \qquad (6)$$

Intuitionistic weighted arithmetic mean: the IWAM can be found using expression (3) and (6) as follows:

$$IWAM = w_i A_i \oplus w_2 A_2 \oplus ..... \oplus w_n A_n = \left\{1-\prod_{i=1}^{n}\left(1-\mu_{A_i}\right)^{w_i}, \prod_{i=1}^{n}\nu_{A_i}^{w_i}\right\} \qquad (7)$$

Where $0 \le w`_i \le 1$ and $\sum_{i=1}^{n} w`_i = 1$.

IFNs is determined using this aggregating operator which is the most accepted in the solution of MCDM problem in the intuitionistic fuzzy setting.

Comparison of IFSs

The comparison of IFVs is important problem in this paper. The $S(z) = \mu(z) - \nu(z)$, where *z* is an IFV, is used as a score function in Chen and Tan [3]. In addition to the above score function, the accuracy function as $H(z) = \mu(z) + \nu(z)$ is introduced in Hong and Choi [6]. In Xu [9], the function S and H is used to construct order relation between any combinations of two intuitionistic fuzzy values (c` and d`) as follows:

If $(S(c') > S(d'))$, then $c' > d'$;

$(S(c') == S(d'))$, then

(1) If $(H(c') == H(d'))$ then $c' = d'$

(2) If $(H(c') < H(d'))$, then $c' < d'$

IV. GENETIC ALGORITHM

GAs [7] are very much practical methods of robust optimisation. The general idea is the replication of natural evolution in the search for finding the most favourable solution of a given problem. In nature, individuals compete to survive in unfit environment. In this competition, only the fittest individuals survive and reproduce the next generation. Therefore, the genes of the fittest survive while the genes of weaker individuals die out. Genetic material is saved into the chromosomes. Parents' genetic materials are mixed during reproduction and the offspring has genes of both parents. Also, an individual's genetic material can be transformed by crossover and mutation operations. Mutation operation can randomly change single or multiple instance of genes of the chromosome and avoid local optimization. Whereas crossover operation rapidly changes the genes of chromosome internally (intra) or with the interaction with other chromosome (inter) to improve the standard quality of the chromosome. When we simulate the natural genetic algorithm, each individual (chromosome) represents a potential solution of a given problem. The GA expends most of the time on evaluating population. Therefore, the representation of chromosome is very important; it could be an array of bits, a number, an array of numbers, a matrix, a string of characters or any other data structure. A chromosome must gratify given precision and constraints and of course, it must be suitable for the implementation of genetic operators. Fig. 1 shows the common structure of GA.

Algorithm: Genetic Algorithm
Begin
Generate population
Do
Begin
Evaluate population
Choose specific for succeeding population
Execute crossover and mutation
While upto set condition
End
End

Fig. 1 Pseudo Code of basic genetic algorithms

V. THE MODIFIED TSP AND REPRESENTATION IN IFS AND GA

There are several ways to represent the TSP for solving the problem using genetic algorithm. In this article, we use two matrices for this purpose, one is called binary matrix, and another is cost matrix. The size of the matrices is n*x*n, where n denote the number of cities considered in the problem. Binary matrix is used to indicate the links among the cities with the help of elements x_{ij}, where $x_{ij}=1$, if there is a link between $city_i$ to $city_j$, otherwise the value of x_{ij} is 0. The binary matrix is symmetric. The cost matrix highlights the travelling cost between two cities with the help of cost element f_{ij}, where $f_{ij}= (\mu_{ij}, \nu_{ij})$ which is an intuitionistic fuzzy number (IFN). IFN consists of two parameters, μ_{ij} and ν_{ij} where μ_{ij} indicates the benefit criteria and ν_{ij} indicates the cost criteria of the link. The benefit criteria can reduce the travelling cost like shortest distance, high speed roadway, consumption of low energy etc. whereas the cost criteria of the link can increase the travelling cost of the link like high traffic, low security, high toll fees or service tax etc. between the $city_i$ to $city_j$. The basic condition of the two variables μ_{ij} and ν_{ij} is that $0\leq \mu_{ij}+\nu_{ij}\leq 1$ because the values of μ_{ij} increase if the values of ν_{ij} decrease or vice versa. The binary matric of the problem is symmetric whereas the cost matrix of the same problem may not be symmetric as the value of μ_{ij} and μ_{ji} or ν_{ij} and ν_{ji} are not same. Because the traffic of the road in all directions is not same; in forward direction of the road there may not be any traffic whereas in the backward direction there may be heavy traffic. The values of parameter, μ_{ij} and ν_{ij} change from time to time or season to season or occasion to occasion. The speed of vehicles depends on weather; the speed is affected during rainy and winter season due to heavy rain and fog respectively. The links between the cities are classified into two types: symmetric link and asymmetric link. For the symmetric link, the travelling cost f_{ij} between the $city_i$ to $city_j$ and travelling cost f_{ji} between the $city_j$ to $city_i$ are the same; whereas in the asymmetric link the travelling cost f_{ij} between the $city_i$ to $city_j$ and travelling cost f_{ji} between the $city_j$ to $city_i$ are not the same. The asymmetric links play an important role to create the optimal route because changing the direction of link can increase the cost of the route.

At first, we generate the chromosomes for the implementation of GA in TSP problem. The chromosomes consist of a sequence of integers. This sequence of integers indicates the sequence of nodes which are visited by the salesman to complete a round trip tour. So, the number of genes of the chromosome depends on the number of nodes present in the problem. If the problem holds 'n' number of nodes, the length of the chromosome of the problem is 'n+1'. During the generation or after the reproduction of the chromosome, it surely follows the binary matrix. According to the constrains of the TSP problem, the chromosome must hold all the genes with single instance and the sequence of the genes of the chromosome depends on the link between the nodes of the problem that is presented in binary matrix. If the chromosome holds multiple instances of genes or if any gene remains absent in the chromosome and if there's no link between the two nodes based on genes sequence within the chromosome, then the chromosome will be defective. If the chromosome is correct, we process it further otherwise discard. According to Fig 3, we consider the chromosome [1,6,2,3,4,7,5,8,9,1] as defective because this chromosome represents the tour 1-6-2-3-4-7-5-8-9-1. This tour is discontinuous due to the absence of the link between the nodes 4 and 7. We consider another chromosome [1,9,7,8,5,4,3,2,6,1] of the same figure which represents the route 1-9-7-8-5-4-3-2-6-1. This route visits all the nodes at one time which are present in the problem and the tour ends at the starting point. If the links between the nodes of the tour are present in the defined binary matrix of the problem, the chromosome is correct. After generating the correct chromosome, we calculate the fitness value of the chromosome. The fitness value indicates the travelling cost of the round-trip tour. Each link has a travelling cost in the form of IFN. A tour consists of a number of IFN. The IFAO operator is used to merge all the IFNs of the tour. The resultant IFN is considered as the travelling cost of the tour.
Correct chromosomes [1,9,7,8,5,4,3,2,6,1], [1,6,2,3,4,5,8,7,9,1], [1,6,2,3,4,5,7,8,9,1].

Defective chromosomes [1,6,2,3,4,7,5,8,9,1], [1,6,2,3,4,6,7,5,8,9,1], [1,2,3,4,5,6,7,8,9,1].
The correct chromosomes are considered as initial solutions. Then, we apply GA based crossover and mutation operators to modify the initial chromosome and create the new chromosome which is better than the parent chromosome by decreasing the travelling cost of the tour.
Here we use the reverse crossover operation for avoiding premature convergence and rapid change. We use the exchange mutation operation for randomly choosing and exchanging the genes of the chromosome to explore the search space. Both the mutation and crossover operations play an important role to converge the optimal or acceptable solution.
In reverse crossover [7] operation, we randomly choose a set of sequence cities in the tour and arrange them in reverse order. Let's consider the tour [1,9,7,8,5,4,3,2,6,1] and Choose the sequence of cities (4,3,2,6) and arrange them in reverse order like (6,2,3,4) so the resultant tour after the crossover operation is [1,9,7,8,5,6,2,3,4,1].
Exchange mutation [8] operation was projected by Banzhaf in 1990. In the exchange mutation operation, we haphazardly choose two cities from the tour and replace them. If we think the tour represented by [1, 3, 4, 5, 2, 1] and choose the city3 and city2 and exchange them, then the resultant chromosome will be [1, 2, 4, 5, 3, 1].

VI. PROPOSED ALGORITHM

Fig.2 explains the extended version of GA. We consider P(c) and C(c) as the parent and child in current generation c respectively. Fitness value FP(c) and FC(c) of parent and child is computed by the IFAO operator correspondingly**.** We choose the next generation P(c1) from P(c) and C(c) according to their fitness values. The general representation of GA is described as follows:

Algorithm: Evolution of Genetic Algorithm
Input: data sets of the problem, GA constrains
Output: Optimal solution

```
Begin
    Initialize population P(c)by encoding
    If P(c)is defective
        Discard and reinitialize P(c)
    Do
    Begin
        Evaluate P(c) by decoding
        Calculate fitness value FP(c)of P(c)using IFAO operator
        Create C(c)from P(c)by reverse crossover and exchange mutation
        If C(c)is defective
            Discard and regenerate C(c)
        Evaluate C(c) by decoding
        Calculate fitness value FC(c) of C(c) using IFAO operator
        Select P(c1)from P(c)and C(c)base of minimum value of FP(c)and FC(c)
        P(c) = P(c1)
        While (FP(c) ≠ FC(c))
    End
End
```

Fig. 2 Pseudo Code of modified genetic algorithms

VII. CASE STUDY

We consider the following asymmetric travelling salesman problem with nine cities and connection among those cities is shown in fig.3. The connectivity and cost of the connection are represented with the help of binary matrix and cost matrix respectively. The salesmen start the journey from his home city and visit all the cities exactly once and finally return to the home city again by the minimum travelling cost of the tour. Here, the travelling cost between two cities is represented by the fuzzy quantifier which highlights the cost or profit and loss or expenditure in the form of IFN. This problem is solved by our proposed method.
Initially, the generated chromosome with route map is 1-2-6-3-4-5-7-8-9-1. The travelling cost from city to city of the route is (1.0, 0.0), (0.2, 0.75), (0.3, 0.6), (0.7, 0.25), (0.3, 0.65), (0.5, 0.5), (0.6, 0.25), (0.8, 0.1) and (0.2, 0.8) respectively according to the sequence. Then, the total calculated travelling cost with the help of eq. (7) is (0.46, 0.57). After that, the created route will be

modified iteratively and finally get the tentative optimal route map, 1-9-7-8-5-4-6-3-2-1 in which the travelling cost is (0.75, 0.12).

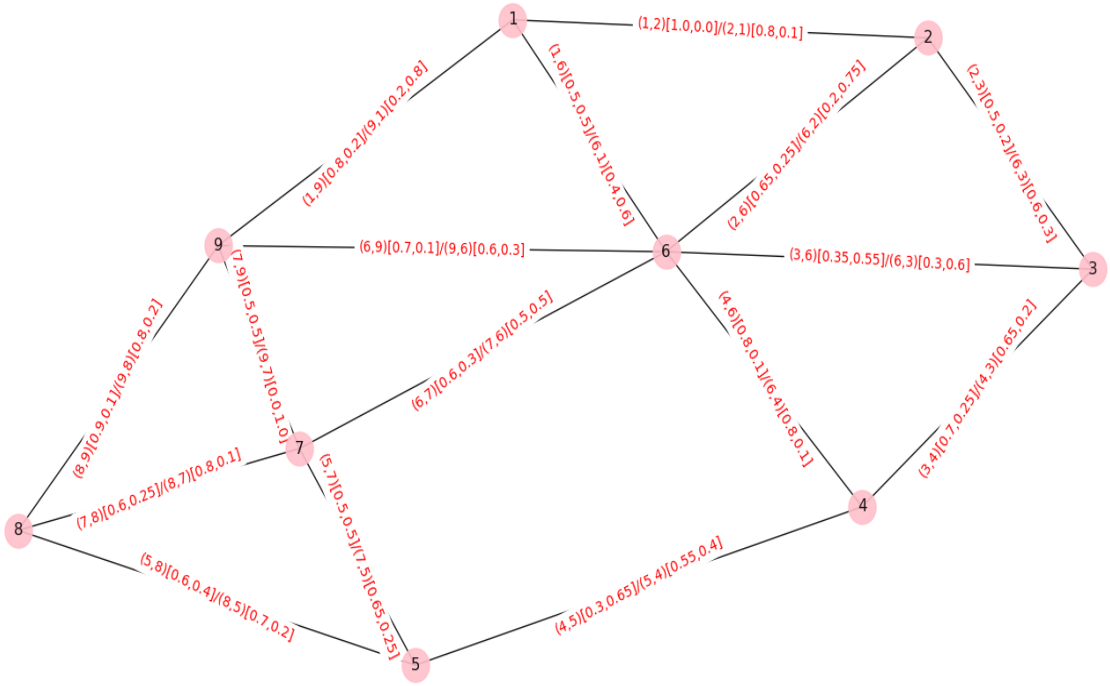

Fig 3 (a). A graph representation of a network of cities.

$$\begin{bmatrix} - & 1 & 0 & 0 & 0 & 1 & 0 & 0 & 1 \\ 1 & - & 1 & 0 & 0 & 1 & 0 & 0 & 0 \\ 0 & 1 & - & 1 & 0 & 1 & 0 & 0 & 0 \\ 0 & 0 & 1 & - & 1 & 1 & 0 & 0 & 0 \\ 0 & 0 & 0 & 1 & - & 0 & 1 & 1 & 0 \\ 1 & 1 & 1 & 1 & 0 & - & 1 & 0 & 1 \\ 0 & 0 & 0 & 0 & 1 & 1 & - & 1 & 1 \\ 0 & 0 & 0 & 0 & 1 & 0 & 1 & - & 1 \\ 1 & 0 & 0 & 0 & 0 & 0 & 1 & 1 & - \end{bmatrix}$$

Fig. 3 (b) Binary Matrix of the Fig: 3

$$\begin{bmatrix} - & (1.0,0.0) & (0.0,0.0) & (0.0,0.0) & (0.0,0.0) & (0.5,0.5) & (0.0,0.0) & (0.0,0.0) & (0.8,0.2) \\ (0.8,0.1) & - & (0.5,0.2) & (0.0,0.0) & (0.0,0.0) & (0.65,0.25) & (0.0,0.0) & (0.0,0.0) & (0.0,0.0) \\ (0.0,0.0) & (0.6,0.3) & - & (0.7,0.25) & (0.0,0.0) & (0.35,0.55) & (0.0,0.0) & (0.0,0.0) & (0.0,0.0) \\ (0.0,0.0) & (0.0,0.0) & (0.65,0.2) & - & (0.3,0.65) & (0.8,0.1) & (0.0,0.0) & (0.0,0.0) & (0.0,0.0) \\ (0.0,0.0) & (0.0,0.0) & (0.0,0.0) & (0.3,0.65) & - & (0.0,0.0) & (0.5,0.5) & (0.6,0.4) & (0.0,0.0) \\ (0.4,0.6) & (0.2,0.75) & (0.3,0.6) & (0.8,0.1) & (0.0,0.0) & - & (0.6,0.3) & (0.0,0.0) & (0.7,0.1) \\ (0.0,0.0) & (0.0,0.0) & (0.0,0.0) & (0.0,0.0) & (0.65,0.25) & (0.5,0.5) & - & (0.8,0.1) & (0.0,1.0) \\ (0.0,0.0) & (0.0,0.0) & (0.0,0.0) & (0.0,0.0) & (0.7,0.2) & (0.0,0.0) & (0.6,0.25) & - & (0.9,0.1) \\ (0.2,0.8) & (0.0,0.0) & (0.0,0.0) & (0.0,0.0) & (0.0,0.0) & (0.6,0.3) & (0.5,0.5) & (0.8,0.2) & - \end{bmatrix}$$

Fig. 3 (c) Cost matrix of Fig. 3

VIII. CONCLUSION

In this article, we solve the TSP with the help of GA in intuitionistic fuzzy environment. This hybrid implementing technique handles both the uncertainty and ambiguity related to the problem and also manages profit as well as loss of the tour. This is different from the other conventional TSP solving methods. Random searching of GA can reduce the time complexity of the problem which is efficient from the traditional searching method. This is very important for the large size of chromosome and high density connectivity of the problem. Generation of the correct chromosome and maintaining the correctness of the chromosome after reproduction are considered as significant concerns in the proposed approach. Future scope of this research work can be enhanced by considering the robustness nature of GA.

REFERENCES

[1] J. Botzheim, P. Foldesi, L. T. Koczy: Solution for Fuzzy Road Transport Traveling Salesman Problem Using Eugenic Bacterial Memetic Algorithm, IFSA-EUSFLAT 2009.

[2] A. Kumar, A. Gupta: Assignment and Travelling Salesman Problems with Coefficients as LR Fuzzy Parameters, International Journal of Applied Science and Engineering, 10, 3: 155-170.2012.

[3] S. Dhanasekar, S. Hariharan, P. Sekar: Classical Travelling Salesman Problem (TSP) based Approach to Solve Fuzzy TSP using Yager's Ranking, International Journal of Computer Applications (0975 – 8887) Volume 74– No.13, July 2013.

[4] S. Fereidouni: Solving traveling salesman problem by using a fuzzy multi-objective linear programming, African Journal of Mathematics and Computer Science Research Vol. 4(11), pp. 339-349, October 2011.

[5] B. Hu, G. R. Raidl: Solving the Railway Traveling Salesman Problem via a Transformation into the Classical Traveling Salesman Problem. https://www.ac.tuwien.ac.at/files/pub/hu-08a.pdf

[6] D. H. Hong, C. H. Choi: Multicriteria fuzzy decision making problems based on vague set theory. Fuzzy Sets and Systems, 114, 2000, 103–113.

[7] P. Larranaga, C.M.H. Kuijpers, R.H. Murga, I. Inza, S. Dizdarevic: Genetic Algorithms for the Travelling Salesman Problem: A Review of Representations and Operators, Artificial Intelligence Review 13: 129–170, 1999.

[8] K.T. Atanassov, C. Georgiev: Intuitionistic fuzzy prolog, Fuzzy Sets and Systems, 53, 1993, 121-128.

[9] Z.S. Xu, J. Chen, J.J. Wu: Clustering algorithm for intuitionistic fuzzy sets, Information Sciences, 178, 2008, 3775-3790.

MODELING AND SIMULATION OF A LOW-PROFILE MICROSTRIP PATCH ANTENNA OPERATING AT 2.45 GHZ

Ankan Bhattacharya*
Dept. of Electronics and Communication Engineering, Mallabhum Institute of Technology, Bishnupur, India
*bhattacharya.ankan1987@gmail.com

Abstract: *This paper focuses on modeling and simulation of a compact microstrip patch antenna. The dimensions of the antenna are optimized to operate at 2.45 GHz frequency range. The antenna is 27.72 x 27.72 x 1.8 mm^3 in dimension. Rogers TMM 4, having an electrical permittivity of 4.5 is used as the substrate material. The Return Loss $|S_{11}|$ is ≥ 30 dB at 2.45 GHz. The antenna shows a realized gain of 6.28 dB and directivity of 6.5 dBi at the resonant frequency.*

Keywords: *Microstrip Patch Antenna, Resonant Frequency, Return Loss, Gain, Directivity*

I. INTRODUCTION

Introduction of microstrip patch antennas was a revolutionary step in the evolution of wireless communication technology. This technology was described in detail by Carver and Mink in 1981 [1]. It is an integral part of any communicating device and is used for transmission and reception of microwave signals. It can be of shapes and sizes e.g. rectangular, triangular, circular etc. [2-4]. Various other theories related to design techniques is presented in [5] by Chang. In this paper, a simple square patch antenna operating at 2.45 GHz frequency band is modeled and simulated in electromagnetic simulation software and the results are presented.

II. ANTENNA DESIGN

The proposed antenna has a compact dimension of 55.45 x 55.45 mm^2. The patch is placed on the top of the substrate. The size of the patch is 27.73 x 27.73 mm^2. The ground plane lies below the substrate. The patch is feed by a discrete port as shown in Fig. 1. FR-4 having an electrical permittivity of 4.4 has been used as the substrate material. The substrate lies between the patch and the ground plane. The dimensions of the antenna are obtained using the analytical formulae provided in [6].

Considering the resonant frequency, f_r the effective length is given as,

$$L_{eff} = \frac{c}{2f_r\sqrt{\varepsilon_{eff}}} \quad (1)$$

The resonant freq. of TM mode of rectangular patch is given as,

$$f_r = \frac{c}{2\sqrt{\varepsilon_{eff}}} \left(\frac{m}{L}\right)^2 + \left(\frac{n}{W}\right)^2 ^{1/2} \quad (2)$$

where, *n* and *m* are modes along the width W and length L respectively.

The patch's width, W is now given as,

$$W = \frac{c}{2f_r\sqrt{\frac{\varepsilon_r+1}{2}}} \quad (3)$$

where, *c* denotes light wave's velocity.

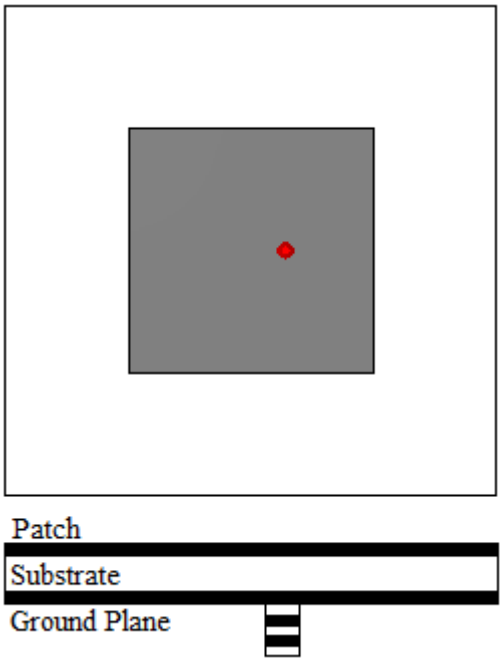

Fig. 1. Proposed microstrip patch antenna.

III. ANALYSIS OF ANTENNA RESPONSES

Fig. 2 shows the S_{11} vs. Frequency plot of the proposed patch antenna. The resonant frequency is exactly centered at 2.45 GHz. The return loss obtained i.e. $|S_{11}| \geq 33$ dB. The VSWR is ≤ 2 at 2.45 GHz as is observed from Fig. 3.

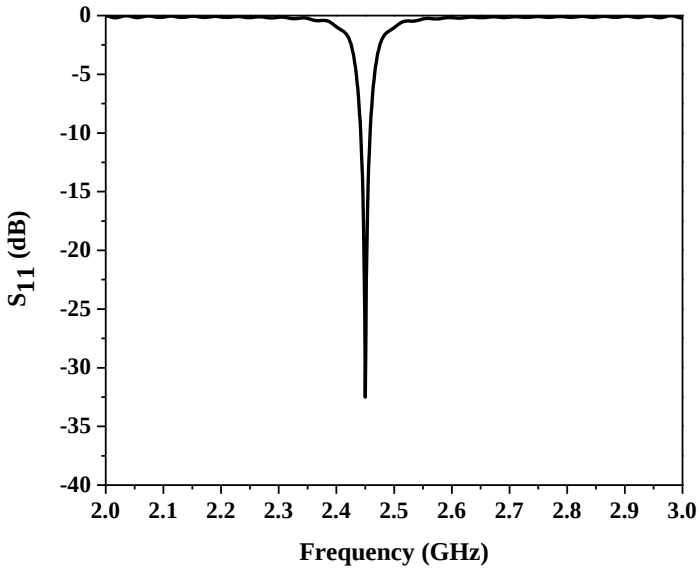

Fig. 2. Return Loss of proposed patch antenna.

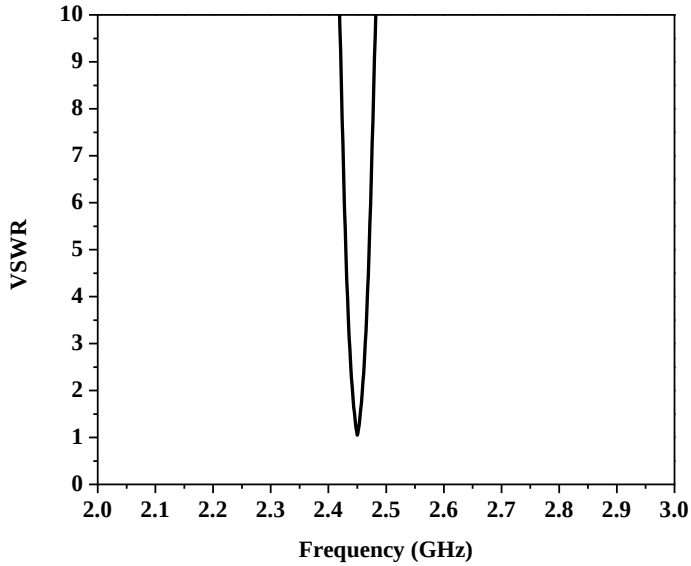

Fig. 3. VSWR of proposed patch antenna.

The 3D radiation pattern of the proposed antenna is shown in Fig. 4. As observed from the scale, the antenna has achieved a peak gain of 6.28 dB.

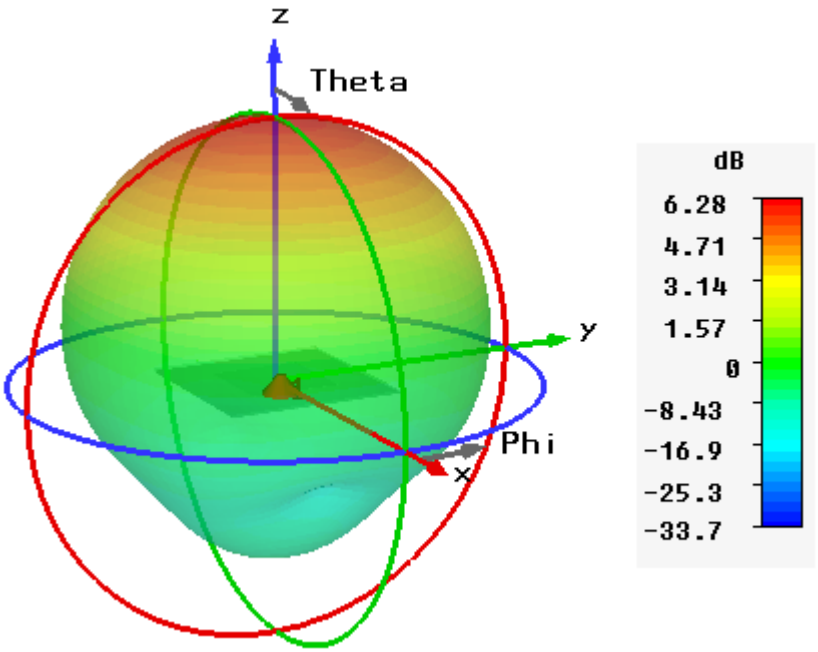

Fig. 4. 3D radiation pattern of the proposed antenna.

IV. CONCLUSION

A simple, discrete port fed, square shaped microstrip patch antenna has been modeled and simulated in this paper. The antenna resonates exactly at 2.45 GHz. It has achieved a realized gain of 6.28 dB and directivity of 6.5 dBi. The antenna VSWR is

less than 2 at the resonant frequency. The planar design makes it suitable to be incorporated in devices supporting wireless communications.

REFERENCES

[1] K. Carver and J. Mink, "Microstrip antenna technology," in IEEE Transactions on Antennas and Propagation, vol. 29, no. 1, pp. 2-24, January 1981.
[2] C. Krowne, "Cylindrical-rectangular microstrip antenna," in IEEE Transactions on Antennas and Propagation, vol. 31, no. 1, pp. 194-199, January 1983.
[3] E. Kuester and D. Chang, "A geometrical theory for the resonant frequencies and Q-factors of some triangular microstrip patch antennas," in IEEE Transactions on Antennas and Propagation, vol. 31, no. 1, pp. 27-34, January 1983.
[4] C. Wood, "Analysis of microstrip circular patch antennas," in IEE Proceedings H - Microwaves, Optics and Antennas, vol. 128, no. 2, pp. 69-76, April 1981.
[5] D. Chang, "Analytical theory of an unloaded rectangular microstrip patch," in IEEE Transactions on Antennas and Propagation, vol. 29, no. 1, pp. 54-62, January 1981.
[6] David M. Pozar; Daniel H. Schaubert, "Basic Microstrip Antenna Elements and Feeding Techniques," in Microstrip Antennas: The Analysis and Design of Microstrip Antennas and Arrays , pp. 57-104, IEEE, 1995.

Proceedings of National Conference on Device Modeling and Soft Computing for real time applications (DMSC-2019)
Organized by Dept. of ECE, MIT Bishnupur in collaboration with The Institution of Engineers India (IEI)

MODELING AND OPTIMIZATION OF A CMPA USING GENETIC ALGORITHM

Arnab De*[1], Bappadittya Roy[2], Ankan Bhattacharya[3] and Anup K. Bhattacharjee[1]
[1]*Dept. of Electronics and Communication Engineering, National Institute of Technology, Durgapur, India*
[2]*Dept. of Electronics and Communication Engineering, Madanapalle Institute of Technology & Science, Madanapalle, India*
[3]*Dept. of Electronics and Communication Engineering, Mallabhum Institute of Technology, Bishnupur, India*
*ade.ece1990@gmail.com

Abstract: *In this paper we have modeled a compact multiband patch antenna for wireless communications. Genetic Algorithm (GA) has been applied for optimization of the antenna dimensions. Three antennas have been designed and simulated in IE3D Software and the parametric dimensions of the proposed antenna have been optimized using GA for supporting multiband operation.*

Keywords*: Microstrip Patch Antenna, Multiband operation, Genetic Algorithm*

I. INTRODUCTION

Compared to conventional antennas, microstrip patch antennas have many advantages. The main advantages are (i) They are having very less weight and possess a planar architecture (ii) They conform to the host surface (iii) Printed-circuit technology is used for mass production at low cost (iv) They can be easily integrated with other components (v) They support both Linear Pol. and Circular Pol. (vi) They are applicable for personal wireless communications (vi) They allow multiband frequency operations. Microstrip patch antennas have huge popularity due to their compact nature and planar architecture. They are useful for all portable wireless devices like all modern wireless gadgets. They are even used for satellite and TTCM operations. Several multiband/wideband antennas have been studied in [1-10], but there exists an issue regarding compactness in every case. In this paper we have presented a compact, multiband patch antenna for wireless communications. Genetic Algorithm (GA) has been applied for optimization of the antenna dimensions.

II. GENETIC ALGORITHM

Genetic Algorithm or popularly GA has been extremely popular in optimization of designs. The optimization process is based on the popular concept of 'Natural Selection' and 'Survival of the Fittest'. 'Gene' is the unit of a Chromosome. In the process of optimization the Genes are treated as Parameters and the fittest or in other words an optimum dimension of a parameter is selected to obtain the 'fittest' or the 'best result' from the parameters provided [11].

III. ANTENNA DESIGN

The antenna evolution process is shown in Figs. 1, 2 and 3 respectively. In the first step, antenna 1 is considered as a reference antenna, which consists of a simple rectangular patch and a ground plane. The reference patch has an width of 'W' = 26 mm and length of 'L' =18 mm . The ground plane has a width of W and length of L. The patch size contributes to the obtained resonant frequency while the ground size gives the overall gain and the frequency of operation of the reference antenna. In antenna 1, the gap between patch and ground plane is taken as w1 and l with measurements of 4.4322 mm and 5.614 mm respectively.
This gap ensures the obtained results from the reference antenna. In the second step, a geometrical semi-circular elongated U shaped structure is used as a slot on the patch in antenna 2, the width and length of the patch and ground plane is also modified to get the resonant frequency at 56.2 & 7.8 GHz with a return loss of -16dB. The practice of using slot on the patch is a common method to reduce the patch size and thereby make the antenna resonate at desired frequencies by determining the radiation distribution pattern.
The main advantage of slotted antenna lies in the fact of its design simplicity, robustness and using it in PCB board. Here, the bandwidth of the structure is better than the reference antenna 1 with an increase.
The gap between the patch and ground plane is different on the sides. The gap w1 and l is considered as 4.432 mm and 5.614 mm respectively. In the proposed model i.e. in antenna 3, two geometrical elongated U shaped structures are used as slots on the patch. The proposed antenna (Antenna 3) is nested on FR- 4 substrate having dielectric constant $\varepsilon_r = 4.4$ and loss tangent, $\delta=0.02$ with a substrate height of 1.6 mm. The length and width of the model is well chosen as W=8.6000 mm and L=6.5503 mm.

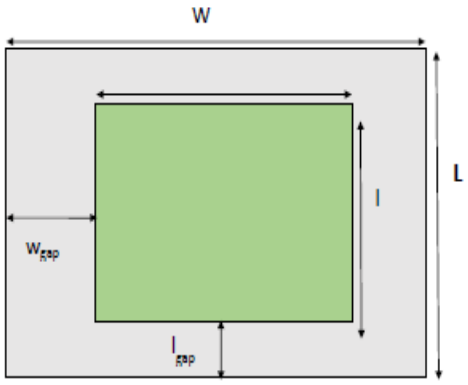

Fig. 1. Patch antenna (Antenna 1).

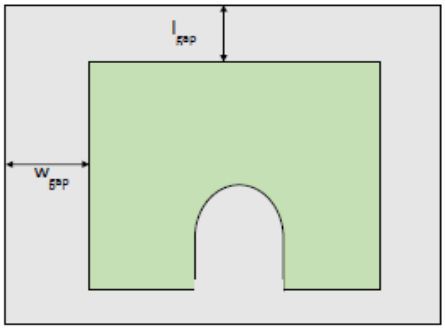

Fig. 2. Etched antenna (Antenna 2).

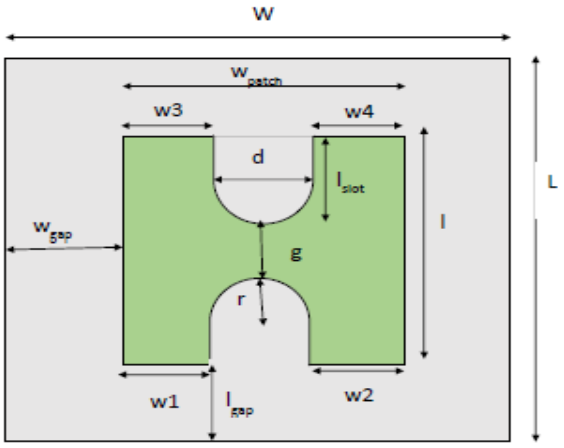

Fig. 3. Dual etched antenna (Antenna 3).

The patch has the U-shaped slots in the middle and so its width would be calculated as W_{patch} = 'w3+d+w4'. The radius of U-shaped slot is chosen to be r =0.6703 mm. The depth or length of the U-shaped structure is optimized through multiple simulations and finally chosen as l_{slot} = 1.1874 mm. One of the important parameter in this proposed model is the gap 'g' between the two slots. This gap g = 2.4315 mm. The other parameters such as w1, w2, w3, w4, w_{gap}, l_{gap} can be seen from the table of parameters. All the parameters are collectively optimized (one at a time) to get the desired result. The feeding point of the antenna is chosen to be at the middle of gap 'g'. The feeding technique here is coaxial feed.. The dimensions of Antenna 3 i.e. proposed antenna were optimized using Genetic Algorithm (GA). The optimized dimensions of Antenna 3 are W = 25.32 mm, L = 17.84 mm, w_{gap} = 7.75 mm, l_{gap} = 5.25 mm, w1 = w2 = w3 = w4 = 5.75 mm, d = 6.25 mm, r = 3 mm and g = 4.25 mm.

Another advantage of this type of feed is that it eliminates the feed radiation because it is directly connected to the patch. In the proposed model, the feed point is experimented at different locations and finally chosen at the aforementioned point in order to match the resonant frequency.

Difficulty in fabricating can be counted as a disadvantage for this kind of feeding. The diameter and depth of the slot affects the resonant frequency and the gap between the patch and the ground affects the impedance bandwidth of the proposed model of antenna.

IV. RESULTS AND DISCUSSION

Three antennas have been modeled in IE3D Software and simulated. Antenna 1 exhibits two resonant frequency bands (Fig. 4). In Antenna 2 the resonating bands are shifted (Fig. 5). The resonating bands of the final antenna i.e. Antenna 3 are obtained at (5.15-5.25) GHz and (7.22-7.3) GHz respectively (Fig. 6). Fig. 7 shows the comparison plot of return losses of Antenna 1, 2 and 3.

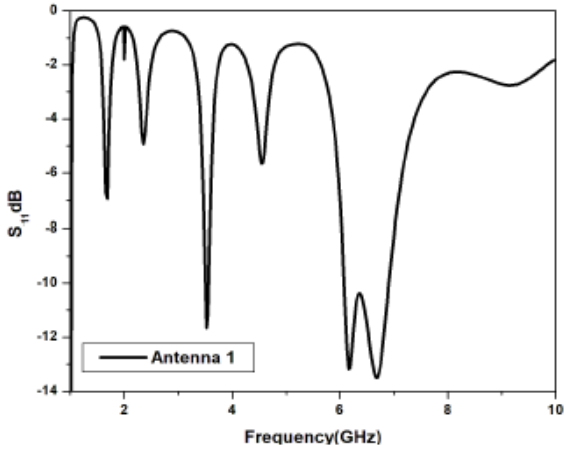

Fig. 4. Return loss of Antenna 1.

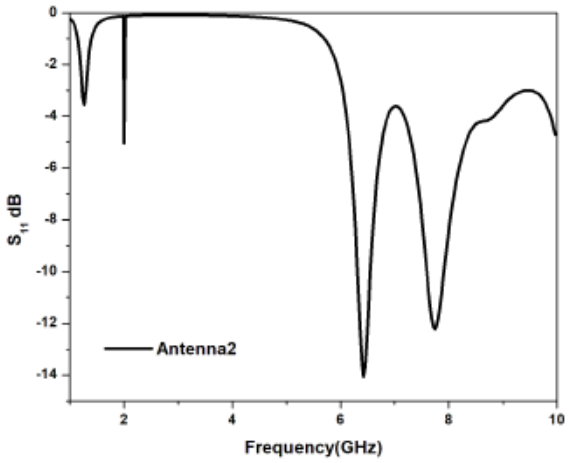

Fig. 5. Return loss of Antenna 2.

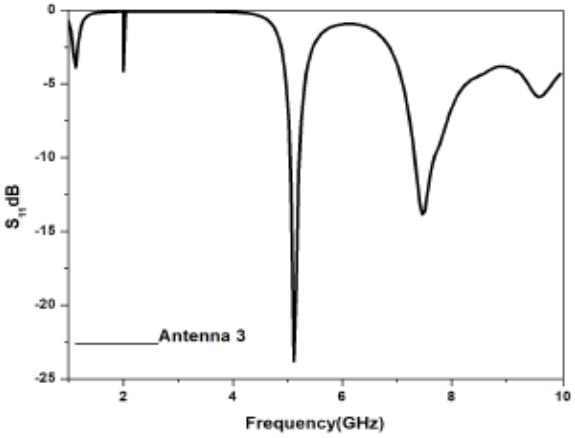

Fig. 6. Return loss of Antenna 3.

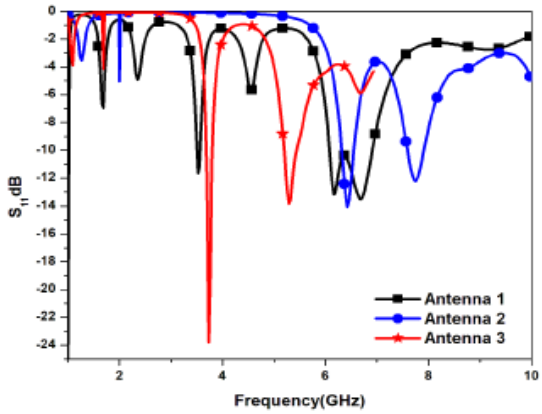

Fig. 7. Return losses of Antenna 1,2 and 3.

It can be clearly be observed that after optimization, the return loss of Antenna 3 has improved, which is ≥ 24 dB at around 4 GHz. An average gain ~ 3 dBi has been realized at the frequency bands of interest (Fig. 8).

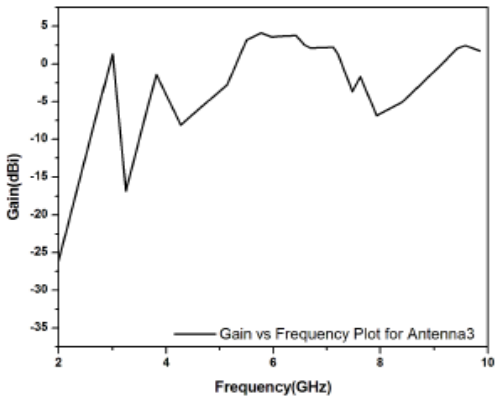

Fig. 8. Realized gain of Antenna 3.

V. CONCLUSION

The receiving wire has a U space fix settled inside a rectangular ground plane opening alongside a coaxial feed. The proposed receiving wire additionally great reradiated over a wide range. For accomplishing better execution and to expand the increase of the receiving wire two U spaces are utilized both side of the reradiating patch. Further streamlining of the thickness of the substrate and other parameter of the proposed radio wire recurrence may add to more extensive transfer speed and increase likewise control the bordering impact of the receiving wire. The receiving wire will be appropriate for remote broadband, therapeutic imaging, radar applications, and other convenient remote applications.

REFERENCES

[1] Girish Kumar and K. P. Ray, Broadband Microstrip Antennas, Revised edition, Artech House, 2003.
[2] Tapan Mandal and Santanu Das, “Microstrip feed Spanner Shape Monopole Antennas for Ultra Wide Band Applications”, Journal of Microwaves, Optoelectronics and Electromagnetic Applications, Vol. 12, No. 1, June 2013.
[3] Abdo Abdel Monem Shaalan and M. I. Ramadan, “Design of a Compact Hexagonal Monopole Antenna for Ultra-Wideband Applications”, J Infrared Milli Terahz Waves, vol. 31, pp. 958–968, 2010.
[4] K.P.Roy and S.Tiwari, “Ultra Wide Band Printed Hexagonal Monopole Antennas” IET Microwaves, Antenna and Propagation, vol. 4, Iss. 4, pp. 437-445, 2010.
[5] C. Zhang and A. E. Fathy, “Development of an Ultra – Wide Band Elliptical Disk Planar Monopole Antennas with Improved Omni-directional Performance using a Modified Ground”, IEEE Int. Antenna Propagation Symp Dig., Alburqueque, NM. pp. 1689 – 1692, 2006.
[6] Z. N. Chen, T.SP. See, and X. M. Qing, “Small Printed Ultra Wide Band with Reduced Ground Plane Effect,”IEEE Trans. Antenna Propag., vol. 55, no.2, pp.383-388, Feb.2007.
[7] Hosseini, S. A., Z. Atlasbaf, and K. Forooraghi, “Two New Loaded Compact Planar Ultra-Wideband Antennas Using Defected Ground Structures”, Progress In Electromagnetic Research B, Vol. 2, 165–176, 2008.
[8] T.Yang and W. A. Davis, "Planar half-disk antenna structures for ultrawideband communications," in Proc. IEEE Int. Symp. Antennas Propagation, Jun. 2004, vol. 3, pp. 2508-2511.
[9] D. H. Kwon and Y. Kim, "CPW-fed planar ultrawideband antenna with hexagonal radiating elements," in Proc. IEEE Int. Symp. Antennas Propagation, Jun. 2004, voL 3, pp. 2947-2950.
[10] Hosseini, S. A., Z. Atlasbaf, and K. Forooraghi, “Two New Loaded Compact Planar Ultra-Wideband Antennas Using Defected Ground Structures”, Progress In Electromagnetic Research B, Vol. 2, 165–176, 2008.
[11] Srinivas, M. And Patnaik, L. M., 1994. Genetic algorithms: a survey, in Computer, vol. 27, no. 6, pp. 17-26.

MODELING AND TESTING OF A PRINTED MONOPOLE ANTENNA FOR VARIOUS WIRELESS APPLICATIONS

Susmita Bala*[1], Partha Pratim Sarkar[2], Sushanta Sarkar[3] and Rajendra Prosad Ghosh[4]
[1]*Dept. of Electronics, Vidyasagar University, Midnapore, India,*
[2]*Dept. of USIC, University of Kalyani, Kalyani, India*
[3]*Dept. of USIC, University of Kalyani, Kalyani, India*
[4]*Dept. of Electronics, Vidyasagar University, Midnapore, India*
*susmitabala@mail.vidyasagar.ac.in

Abstract: *A monopole antenna with E shaped radiating patch is designed for multiband operations. Initially a simple E shaped patch with partial ground plane of dimension 23mm×35mm is designed. This provides only one resonant frequency at 7.84 GHz. Introducing a thin metallic strip in the ground plane, two additional resonances occur at 6.78 GHz and 9.22 GHz with the previous resonance. The proposed antenna is fabricated using low cost FR4 substrate of dimension 42 mm×35mm×1.6mm. The antenna offers gain of 4 dBi, 2 dBi and 3 dBi at three resonant frequencies of 6.78 GHz, 7.84 GHz and 9.22 GHz respectively.*

Keywords*: E-shaped antenna, multiband operation, wireless applications*

I. INTRODUCTION

With the rapid development of the wireless communication systems, the role of antennas with multiband operations has greatly increased because of combining numerous communication tasks in a single compact wireless system. To satisfy multiband operation, these types of antennas should have important features like simple in structure, compact in size, easy of fabrication and easily integrated with electronic circuits [1]. Among the different types antennas, the planar monopole antenna is a suitable candidate for wireless application. They provide attractive features like low profile, light weight, low cost, multi resonance behavior [2]. Numerous printed monopole antennas have been reported so far for multiband application. This multiband properties has been achieved by using different shapes like meandered T [3] , dual U [4], symmetrical L and U [5], G shaped[6] of monopole antennas. Previously reported different CPW fed monopole antenna [8-13] provides multiband characteristics. Different slot antennas [13-16] are proposed to provide multiband nature. But these all reported antennas are complex in design.
In this paper, a novel E shaped triband printed monopole antenna is proposed that provides triple resonant frequencies at 6.78 GHz, 7.84 GHz and 9.22 GHz which covers C band (4-8) GHz and X band (8-12) GHz wireless application. The antenna is simple in design and compact.

II. PROPOSED ANTENNA DESIGN

The detailed geometry of proposed E shaped printed monopole antenna is shown in Fig.1. The antenna is printed on FR4 substrate with relative permittivity of 4.4, thickness 1.6 mm and loss tangent .02. Overall dimension of the proposed antenna is 42mm×35mm×1.6mm. The proposed E shaped patch consists of three rectangular metallic strips each of dimension 18×3.06mm spaced 5.06mm apart is shown in Fig.1a (Top View). The E shaped patch is excited by 50Ω microstrip line of dimension 21.5 mm×3.06 mm. The bottom surface of the proposed antenna as shown in Fig.1b (Bottom View) consists of a partial ground plane of dimension 35mm×25mm with a thin metallic strip of dimension 20mm×3.06mm. The antenna is designed and simulated by Ansoft Simulation Software High Frequency Structure Simulator [17]. The optimal dimension of the proposed antenna is given in Table 1.The fabricated antenna is shown in Fig.2.

Table1: Antenna dimensions

W	W1	W2	W3	W4	Wg	L	L1	L2
35mm	14.94mm	0.5 mm	3.06mm	20.28 mm	3.06 mm	42 mm	3.06 mm	5.06 mm
L3	Lg	Ls						
22.7 mm	21.2 mm	20.8mm						

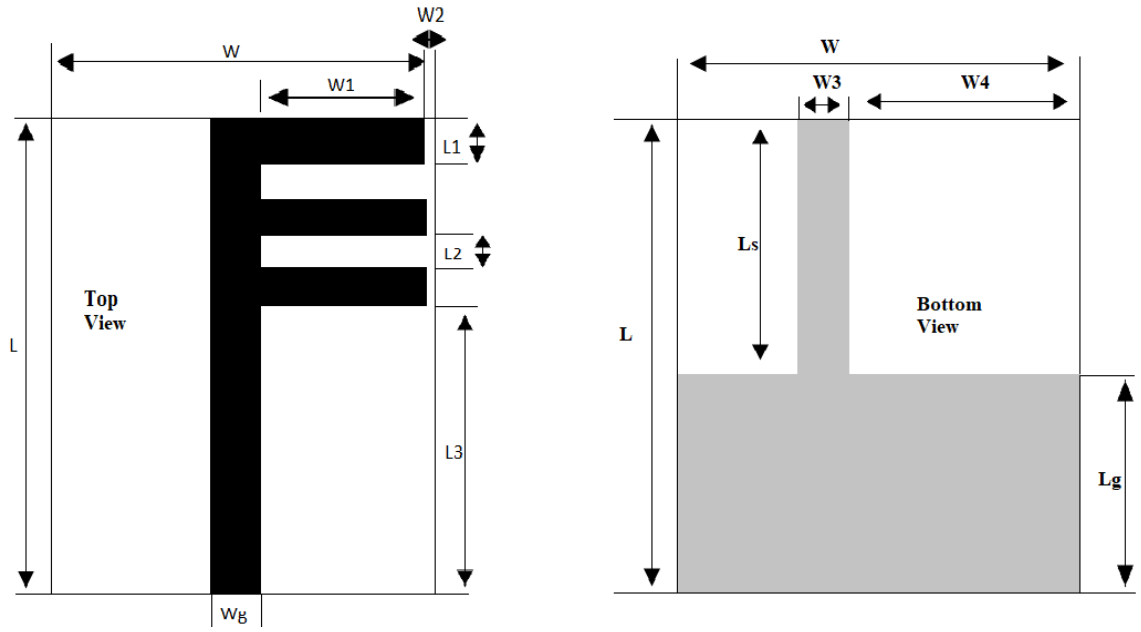

Fig.1 Geometry of the proposed antenna (a) Top View of the Proposed Antenna (b) Bottom View of the Proposed Antenna

Fig.2 Fabricated proposed antenna

III. RESULTS AND DISCUSSION

The simulated and measured reflection co-efficient, radiation pattern and gain of the proposed antenna are discussed here. The reflection co-efficient of the proposed antenna is measured by Vector Network Analyzer (mode no: ZVA 40). The simulated and measured reflection co-efficient versus frequency of the proposed antenna is shown in Fig.3.The proposed antenna provides triple resonances at 6.78 GHz,7.84 GHz and 9.22 GHz with measured impedance bandwidth of 250MHz,430 MHz and 580 MHz respectively.

The simulated E plane and H plane radiation patterns of the proposed antenna at 6.78 GHz are shown in Fig.4 (a) and Fig.4 (b) respectively. Fig.5 (a) and Fig.5 (b) show the simulated E plane and H plane radiation patterns at 7.84 GHz respectively. The simulated E plane and H plane radiation patterns of the proposed antenna at 9.22 GHz are shown in Fig.6 (a) and Fig.6 (b) respectively.

The peak gain versus frequency graph of the proposed antenna is given in Fig.7. Gains of 4 dBi, 2 dBi and 3 dBi at 6.78 GHz, 7.84 GHz and 9.22 GHz are obtained respectively.

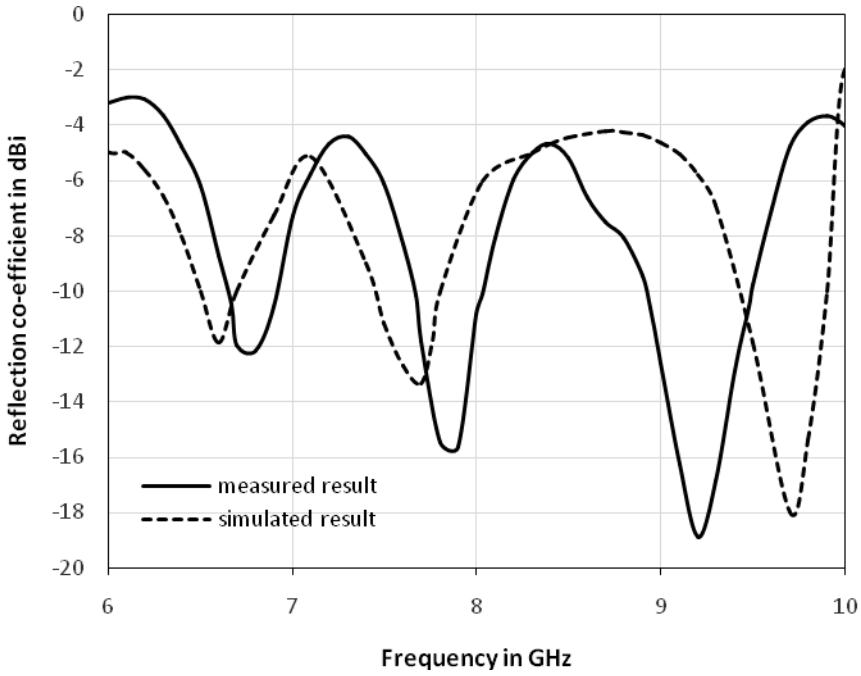

Fig.3 Reflection Co-efficient versus frequency curve

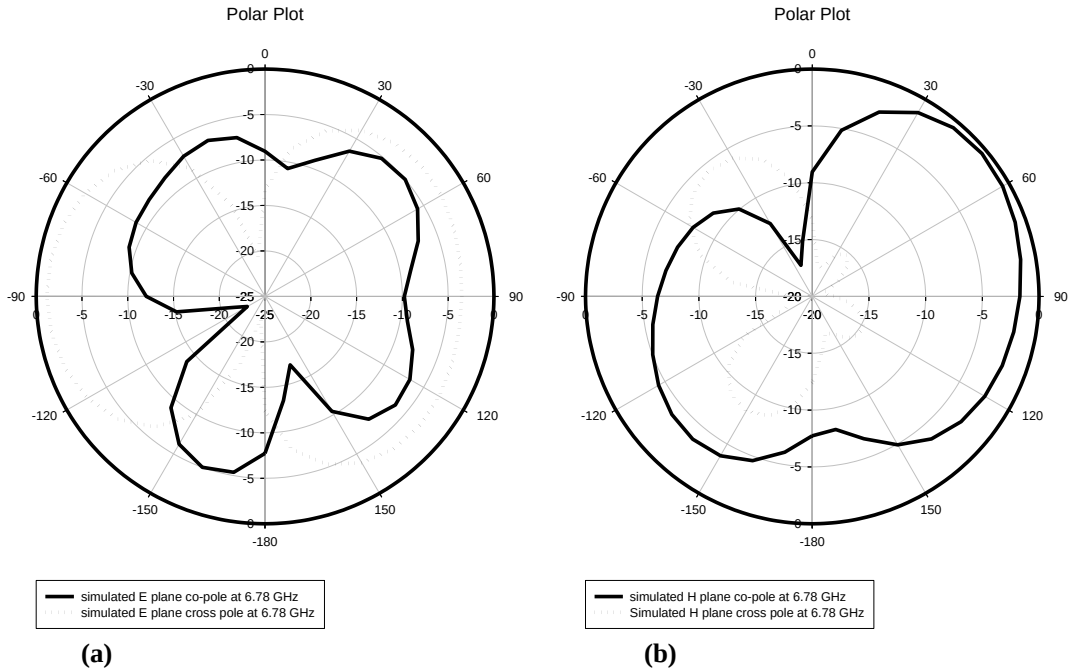

Fig.4 Radiation pattern at 6.78 GHz (a) E plane (b) H plane

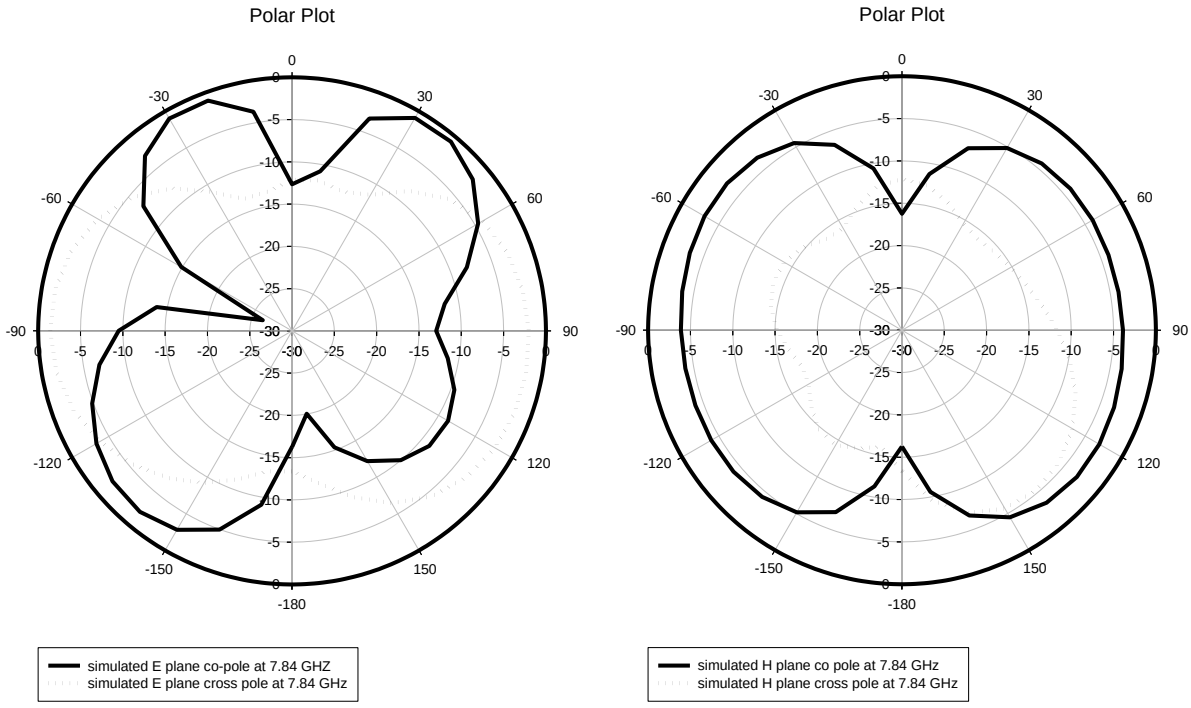

(a) **(b)**

Fig.5 Radiation pattern at 7.84 GHz (a) E plane (b) H plane

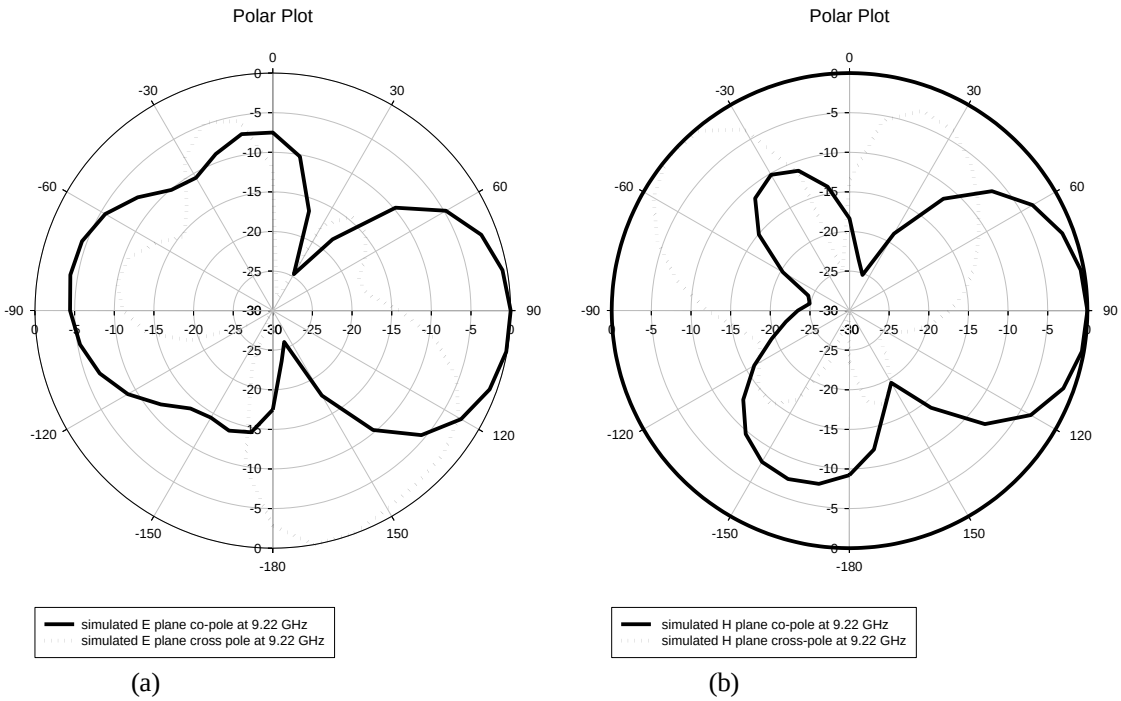

(a) (b)

Fig.6 Radiation pattern at 9.22 GHz (a) E plane (b) H plane

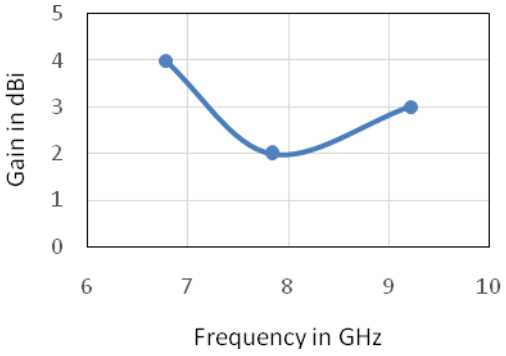

Fig.7 Frequency versus Gain at different resonant frequencies

IV. CONCLUSION

A simple, high gain, triband printed monopole antenna is presented in this paper. Three frequency bands with reflection co-efficient (S_{11}<-10dB) are obtained. Three resonant frequencies of 6.78 GHz,7.84 GHz and 9.22 GHz with measured impedance bandwidth of 250MHz,430 MHz and 580 MHz respectively are obtained. First two bands are useful for C band and last band covers X band of wireless application. Peak gain of 4 dBi at frequency 6.78 GHz is measured. The proposed antenna structure is simple and easy to design with high gain compared to previously reported monopole antenna of similar application.

REFERENCES

[1]Balanis, C.A., "Antenna Theory: Analysis and Design", John Wiley & Sons, Inc, 1997.
[2] Kumar, G. and Ray, K.P., "Broadband Microstrip Antennas", Artech House, Inc, 2003.
[3] Nan Chang and Jing-Hae Jiang, Meandered T-Shaped Monopole Antenna, IEEE Transactions on Antennas And Propagation57 (2009), 3976-3978.
[4] Jui-Han Lu and Wen-Chieh Chou, Planar Dual U-Shaped Monopole Antenna With Multiband Operation for IEEE 802.16e , IEEE Antennas and Wireless Propagation Letters 9 (2010), 1006-1009.
[5] Mahdi Moosazadeh and Sergey Kharkovsky, Compact and Small Planar Monopole Antenna With Symmetrical L- and U-Shaped Slots for WLAN/WiMAX Applications, IEEE Antennas and Wireless Propagation Letters 13 (2014), 388-391.
[6] Zhiya Zhang, Guang Fu, and ShaoliZuo, A Compact Printed Monopole Antenna for WLAN and WiMAX Applications, Key Laboratory of Antennas and Microwave Technology,52 (2010),857-860Vol.
[7] Xiaoliang Zhang, Xiaoli Yin, and Le Zhou, A Compact Triple-Band Printed Monopole Antenna for WLAN/WiMAX Applications, IEEE Antennas and Wireless Propagation Letters 15, 2016 (2016), 1853-1855.
[8] Hsien-Wen Liu, Chia-Hao Ku, and Chang-Fa Yang, Novel CPW-Fed Planar Monopole Antenna for WiMAX/WLAN Applications, IEEE Antennas and Wireless Propagation Letters 9(2010), 240-243
[9] Xin Sun, Gang Zeng, Hong-Chun Yang and Yang Li, A Compact Quadband CPW-Fed Slot Antenna for M-WiMAX/WLAN ApplicationsIEEE Antennas and Wireless Propagation Letters 11(2012) , 395-398.
[10] Naser-Moghadasi, R. Sadeghzadeh, L. Asadpor, and B. S. Virdee,Member, A Small Dual-Band CPW-Fed Monopole Antenna for GSM and WLAN Applications, IEEE Antennas and Wireless Propagation Letters 12 (2013), 508-511.
[11] Hong Chen, X. Yang, Y. Z. Yin, S. T. Fan, and J. J. Wu, Triband Planar Monopole Antenna With Compact Radiator for WLAN/WiMAX Applications, IEEE Antennas and Wireless Propagation Letters 12 (2013), 1440-1443.
[12] Haiwen Liu, Pin Wen, Shuangshuang Zhu, Baoping Ren, Xuehui Guan, Quad-BandCPW-FedMonopoleAntennaBasedon Flexible Pentangle-Loop Radiator, IEEE Antennas and Wireless Propagation Letters 14 (2015), 1373-1376
[13] Xiao Chuan Fang, Daniele Inserra, Yong Jun Huang, Guang Jun Wen and Wei Hu, Compact slotted CPW-fed Y-shape patch antenna for Wi-Fi and WiMAX applications, Microwave and Optical Technology Letters 60(2018),1929–1934.
[14] Tze-Hsuan Chang and Jean-Fu Kiang, Compact Multi-Band H-Shaped Slot Antenna, IEEE Transactions on Antennas And Propagation61 (2013), 4345-4349.
[15] Lin Guo, Yan Wang, Zhengwei Du, Yougang Gao, and Dan Shi, A Compact Uniplanar Printed Dual-Antenna Operating at the 2.4/5.2/5.8 GHz WLAN Bands for Laptop Computers, IEEE Antennas and Wireless Propagation Letters 13,(2014), 229-232
[16] Ali Mansoul, Switchable multiband slot antenna for 2.4, 3.5, and 5.2 GHz applications, Microwave and Optical Technology Letters 59(2017), 2898–2903
[17] https://www.ansys.com/en-in/products/electronics/ansys-hfss

Proceedings of National Conference on Device Modeling and Soft Computing for real time applications (DMSC-2019)
Organized by Dept. of ECE, MIT Bishnupur in collaboration with The Institution of Engineers India (IEI)

DESIGN AND ANALYSIS OF CHEBYSHEV AND BUTTERWORTH FILTERS USING MATLAB

Manira Khatun* and Debashree Patra Karmakar
Dept. of Electronics & Communication Engineering, Mallabhum Institute of Technology, Bishnupur, India
*mum_sekh85@rediffmail.com

Abstract: *In digital signal processing filter plays a very important role. The Butterworth filter is that kind of filter which having a very flat type frequency response in pass band. It is also known as a maximally flat magnitude response filter. Here the analysis of Butterworth filter is done regarding its magnitude response, phase response, pole-zero response and impulse response. Chebyshev filter is also analyzed in this paper. As we know Chebyshev filter is can be used for distinct frequencies of one band from another. The main feature of Chebyshev filter is their speed, normally faster than the windowed-sinc.*

Keywords: *Optimization, Chebyshev, Butterworth, Filter*

I. INTRODUCTION

Filter is a devise which allows a specific range of frequencies. The frequency response of the Butterworth filter is maximally flat or it has no ripples in the pass band and rolls off towards zero in the stop band. Compared with a Chebyshev filter the Butterworth filter has a slower roll-off, and thus will require a higher order to implement a particular stop band specification, but Butterworth filters have a more linear phase response in the pass-band than Chebyshev filters can achieve [1-4]. Now days filter designed and analysis is a very important issue. Two types of filter- Butterworth and Chebyshev have been designed in MATLAB and their response has been analyzed and discussed here.

II. CHEBYSHEV FILTER

Chebyshev filters are analog or digital filters having a steeper roll-off and more pass band ripple (type I) or stop band ripple (type II). Chebyshev filters able to reduce the error between actual filter and idealized filter characteristic. As the Chebyshev polynomials are used to derive the mathematical expression of Chebyshev filter, so it is named after Scientist Pafnuty Chebyshev . The type I Chebyshev filters are called usually as just "Chebyshev filters", the type II ones are usually called "inverse Chebyshev filters".Though Chebyshev filter has more smooth response in passband but stopband is not ripple free, so it is preferred for some applications. We have designed a Chebyshev and Butterworth filter whose design parameters are given below in Table-1.

Table-I

f_s (sampling frequency)	48000Hz
N (order of filter)	15

III. RESPONSE ANALYSIS OF CHEBYSHEV FILTER

Analysis of Chebyshev filter is done considering order number-15, whose characteristics are given in table above. Chebyshev filter is simulated using MATLAB. Fig.: 1 showing the magnitude response of a Chebyshev filter. Fig. 2 showing the phase response of a Chebyshev filter, whose characteristics are already maintained .

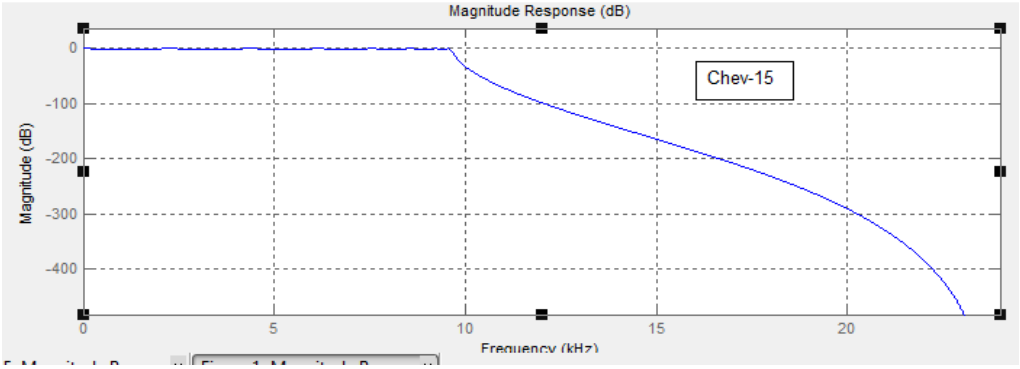

Fig.: 1 Magnitude response of a Chebyshev filter

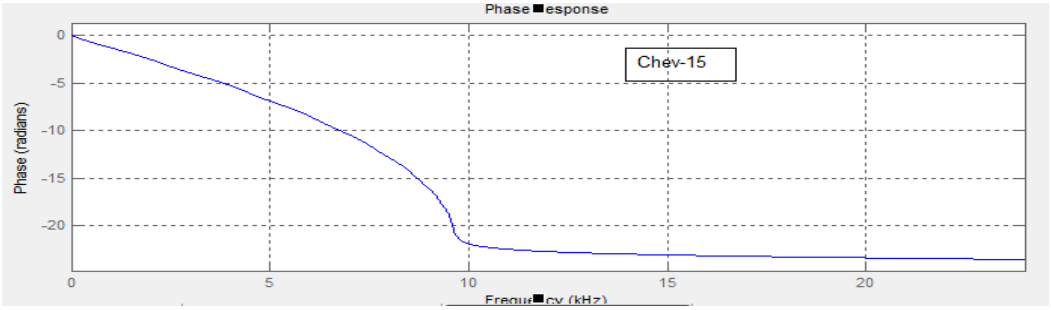

Fig.: 2 Phase response of a Chebyshev filter

Fig. 3 showing the impulse response of a Chebyshev filter, whose characteristics are given in table below.

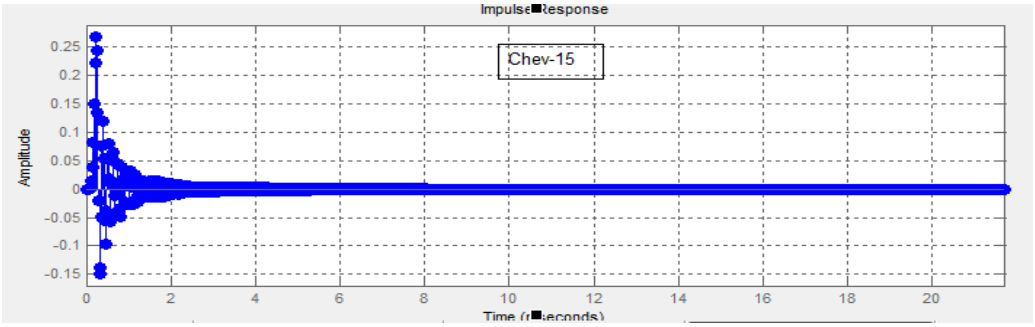

Fig.: 3 Impulse response of a Chebyshev filter

Fig. 4 showing the pole-zero response of a Chebyshev filter, whose characteristics are given in table below.

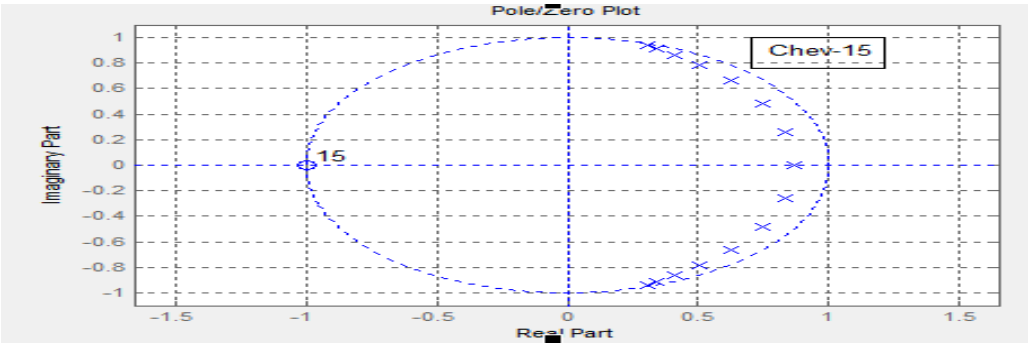

Fig.: 4 Pole-zero response of a Chebyshev filter

IV. BUTTERWORTH FILTER

The Butterworth is a type of filter which has comparatively flat response in pass-band and roll off factor is nearly zero in the stop-band. We find application of Butterworth filters in motion analysis and in audio circuits. Butterworth filters are also used in RF and general filters. Properties of the Butterworth filter are: monotonic amplitude response in both pass band and stop band.

V. RESPONSE ANALYSIS OF BUTTERWORTH FILTER

Analysis of Butterworth filter is done considering order number-15. Whose characteristics are already mentioned in TABLE-I. Analysis of filter is done considering order number-15. This filter is simulated using MATLAB. Butterworth filter is simulated using MATLAB. Fig.: 5 showing the magnitude response of a Butterworth filter. Fig.: 6 showing the phase response of a Butterworth filter, whose characteristics are already maintained. Fig.: 7 shows the impulse response of a Butterworth filter and Fig. 8 shows the pole-zero response of a Butterworth filter.

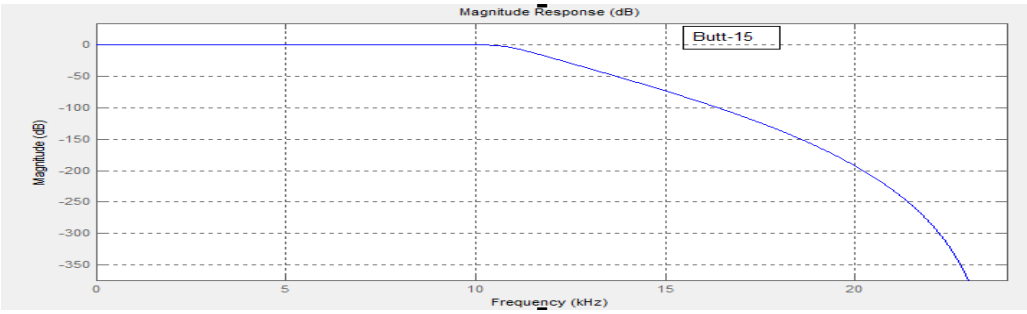

Fig.: 5 Magnitude response of a Butterworth filter.

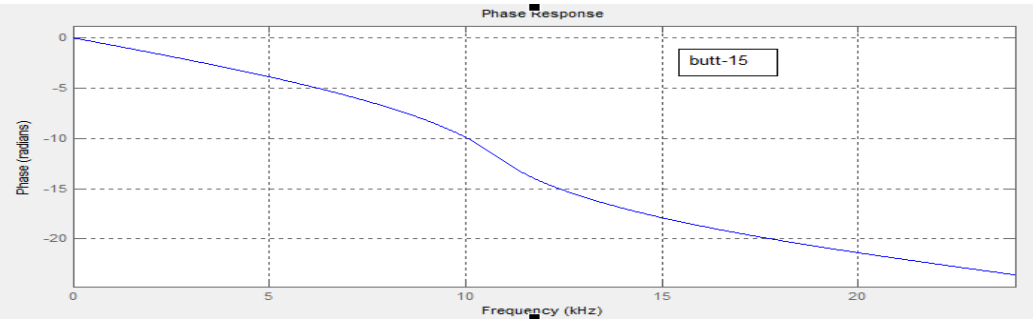

Fig.: 6 Phase response of a Butterworth filter

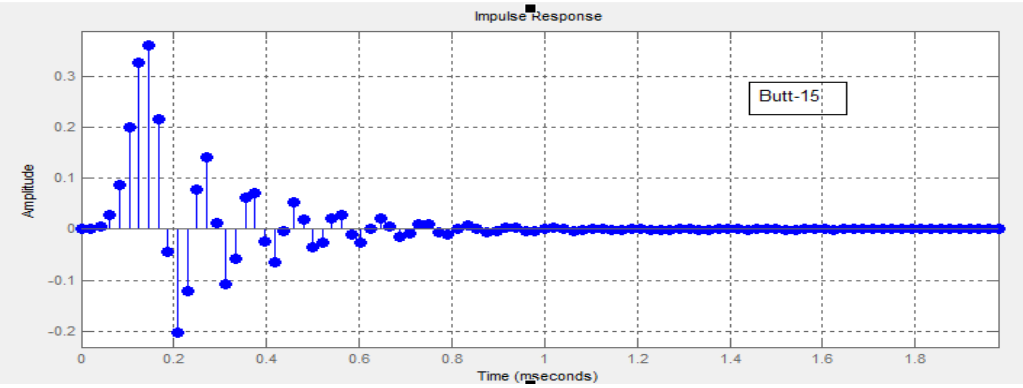

Fig.: 7 Impulse response of a Butterworth filter

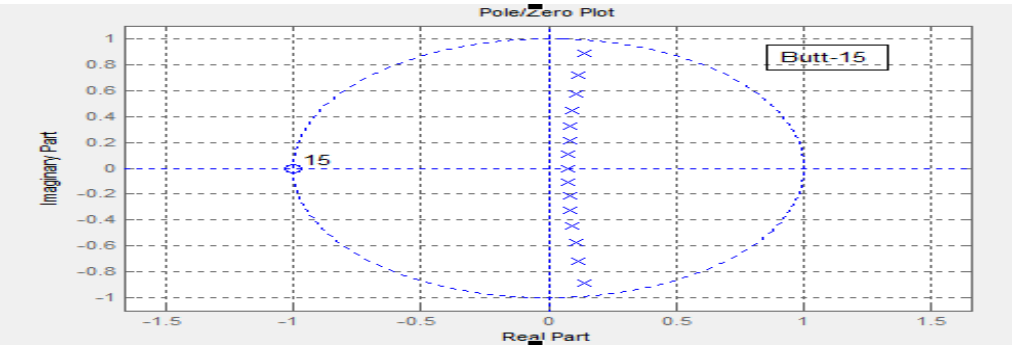

Fig.: 8 Pole-zero response of a Butterworth filter

VI. CONCLUSION

From the graph for magnitude response of Chebyshev filter and Butterworth filter, we can observe that the response of Butterworth filter having less ripple compare to Chebyshev filter and more smooth. The Chebyshev filter achieved a faster roll-off by allowing ripple in the frequency response. It has a good phase response. Butterworth filter has quick roll-off around the cut off frequency which improves with increasing order. Butterworth filter has slightly non linear phase response. From the figure of analysis using MATLAB software we can see the poles lies on a circle for Butterworth filter. In case of Chebyshev filter the poles lies on an ellipse.

REFERENCES

[1] M. Sandhu, S. Kaur, J. Kaur, "A study on design and implementation of Butterworth, Chebyshev and Elliptical filter with matlab"-IJETER,Vol-4,Issue-6,June-2016
[2] Tushal Malica,Singdha shekhar, Zakir Ali,"Design and comparison of burrerworth and Chebyshev type-1 lowpass filter using MATLAB" researchgate.net/publication/236058763, September 2011
[3] M. Singh Saini and K. Kaur," Design of IIR Filter Using Chebyshev",- IJARCET, Vol. 4(Issue 6), 2015
[4] A. Singhal," Filter Design: Analysis and Review," –IJERA,Vol. 4, Issue 1(Version 3), January-2014
[5] www.mathworks.com

Proceedings of National Conference on Device Modeling and Soft Computing for real time applications (DMSC-2019)
Organized by Dept. of ECE, MIT Bishnupur in collaboration with The Institution of Engineers India (IEI)

MODELING AND PERFORMANCE COMPARISON OF BRUSHLESS DC MOTOR WITH VARIOUS POLES/SLOTS COMBINATION

Soumitra Adak*[1], Mayumi Mukherjee[2] and Sudeshna Datta[3]
[1]*Electrical Engineering Dept., Mallabhum Institute of Technology, Bishnupur, India*
[2]*Electronics & Communication Engineering Dept. Mallabhum Institute of Technology, Bishnupur, India*
[2]*Electrical Engineering Dept., Kingston Polytechnic College, Kolkata, India*
*soumitraadakvsu@gmail.com

Abstract: *Now-a-days Brush less dc motors are rapidly used in many applications, such as electric and hybrid vehicles, electric scooter and bicycle, aerospace and household appliances etc. This paper describes how to design, construction features and efficiency improvement of BLDC motor. With help of the finite element method we determined the various parameters of motor. Different numbers of poles are simultaneously used for stator and it simulates in finite element method. All the results are comparing to find out the optimal model.*

Key Words*: BLDC motor, Finite Element, Motor Modeling.*

I. INTRODUCTION

Basically two types of dc motors are uses in industries, conventional DC motor and brushless DC motor. Conventional DC motors are bulky and heavy. It consists of yoke, salient field poles bolted in inner periphery of the yoke, bearing, brush-rigging carrying brush holders, end covers, commutator, rotor winding etc. [1-8] BLDC motors are potentially more efficient because permanent magnets give the necessary flux, so there is no electrical power required. BLDC motors have same torque speed characteristics as a conventional DC motor. But it has several advantages over conventional DC. Such as high power density, low rotor inertia, no brushes (brush drop is zero) and it operates very high-speed about 12,000 rpm under loaded and unloaded condition. The stationary part of brushless motor has several nos. of permanent magnets made by neodymium iron boron (NdFeB). It is also known as 'neo'. Today these types of permanent magnets are widely available. Rotor windings are properly connected to the ac source, so that electromagnetic flux generated in core. Again the electromagnetic flux links with the permanent magnet and results rotating torque.

II. DESIGN OF BRUSHLESS DC MOTOR

Stator slots and rotor pole: Here we designed the 12S16P, 12S14P and 12S8P BLDC motors. The nos. of slots should never be equal to nos. of poles but must be either larger or smaller. If it is equal motor will produce large cogging torque will refuse to self start. Again when slot per pole ratio less than 0.25 rotor pole arc cover less than half of the stator teeth, therefore several no of north and South Pole are under each stator teeth. Due to this configuration torque will be reduced. Generally slot per pole less than 0.25 is not taken. Unbalanced winding will produce higher order of harmonics. For balanced winding = $\frac{number\ \ of\ \ slots}{3\ GCD\ (no.of\ \ slots, pole\ \ pairs\ )}$

= integer number. Here for all three cases gives the integer, so that all are balance winding.

Table 1.Dimension of stator and rotor:

Rotor outer diameter	90mm
Rotor inner diameter	80mm
Depth of pole	20mm
Shaft diameter	20mm
Stator outer diameter	64.7mm
Length	30mm

Table2.Materials used:

Yoke	M22 steel
Shaft	Hot rolled carbon steel
Rotor core	M22 steel
Permanent magnet pole	NdFeB 40 MG oe
Field winding	0.34 mm wire

Table3. Pole position:

For 16 pole machine	For 14 pole machine	For 8 pole machine
90	-102.857	90
-112.5	51.428	-135
45	-154.85	360
-157.5	359.999	135
360	154.285	270
157.5	308.571	45
315	102.857	180
112.5	257.1428	-45
270	51.4285	
67.5	205.7142	
225	-2.84217	
22.5	154.2857	
180	-51.4285	
-22.5	102.857	
135		
-67.5		

Stator winding sequence:

Generally, integrated switch circuit are connected BLDC motor stator winding. Switches are operates in prescribe way so that it gives trapezoidal shape of waveform. Stator electromagnet produced uniform mmf in air gap. The electromagnetic force (= magnetic field x conductor length x current) produced between stator and permanent magnet rotor, rotor will continue to run. Table 4.Stator winding sequences:

R	1	+VE & -VE
	7	-VE & +VE
Y	3	-VE & +VE
	9	+VE & -VE
B	5	+VE & -VE
	11	-VE & +VE
R'	2	-VE & +VE
	8	+VE & -VE
Y'	4	+VE & -VE
	10	-VE & +VE
B'	6	-VE & +VE
	12	+VE & -VE

III. FEMM ANALYSIS OF BLDC MOTOR

Finite element method magnetic is open source software for solving electromagnetic problem. Maxwell equation is very useful to derive the magnetic field with the help of field intensity (E), current density (J), and flux density (B). The FEMM satisfies the equations are-

$$\nabla \cdot E = \frac{\rho}{\varepsilon} \quad (1)$$

$$\nabla \times E = -\frac{\partial B}{\partial t} \quad (2)$$

$$\nabla \cdot B = 0 \quad (3)$$

$$\nabla \times B = \mu\left(J + \varepsilon\frac{\partial E}{\partial t} \right) \quad (4)$$

$$J = \sigma E \quad (5)$$

Where ρ ,ε, σ, μ are charge density, electric permittivity, medium conductance and magnetic permeability [1]. For unique problem solution boundary condition must be needed. Finite element method magnetic (FEMM) analysis has five modes of operations,

operator on nodes, on segment, on arc segment, on block label and on group of object. First four are define problem of geometry. Node defines all corner of geometry, line and arc connected with the nodes creates the boundary and interface, block label used for putting the material that is particularly used the specified boundaries. When manipulate the entire part we used a group operator. Here we designed a planar magneto static problem and sets millimeter unit.

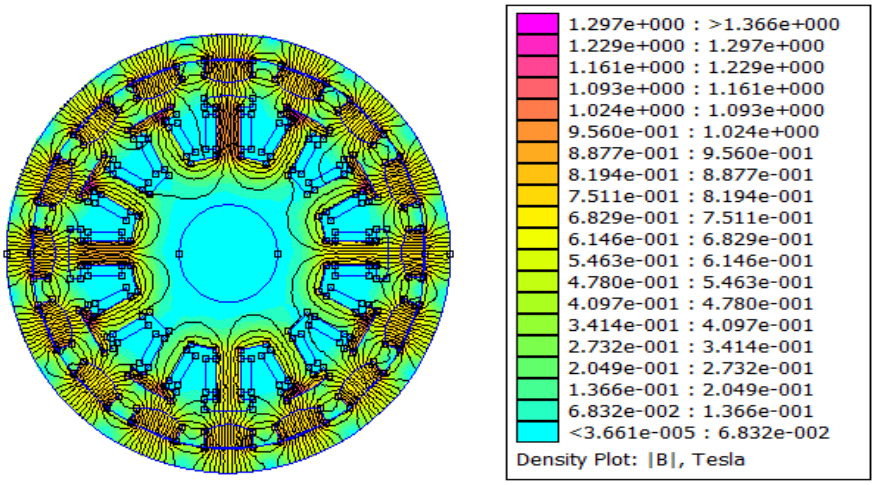

Fig 1 Density plot of 16 pole 12 slot machine

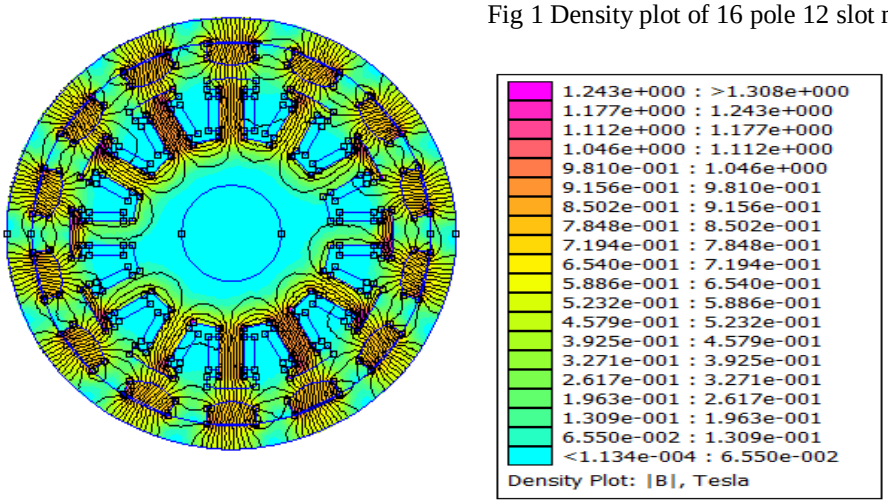

Fig 2 density plot of 14 pole 12 slot machine

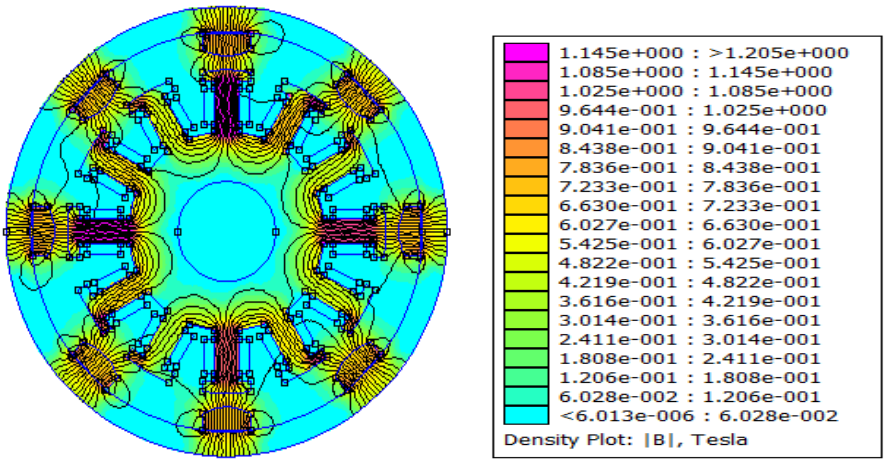

Fig 3 density plot of 8 pole 12 slot machine

IV. RESULTS

Table 5 gives us the various FEMM analysis result. If we compare the results, the 12S16P brush less motor gives the better torque value. The value of flux density determines the overload capacity. For normal design the value of flux density lies between 0.3 and 0.6 Tesla. The air gap of motor is made as small as possible. The shaft is made short and stiff, otherwise small deflection of rotor would create large magnetic pull.

Table 5: FEMM analysis

FEMM ANALYSIS	12S16P	12S14P	12S8P
Magnetic field Energy	10.4766 J	9.04415J	5.43953
Block cross sectional area	0.0074831 m^2	0.0074831 m^2	0.00885578m^2
Block volume	0 .000224505 m^3	0 .000224505 m^3	0.000265673m^3
Contour length	0.009 m	0.009 m	0.009m
Surface area	0.00027m^2	0.00027m^2	0.00027m^2
Force	X component 9.84 N, Y component -12.73N	X component 9.57 N, Y component -5.16N	X component 3.22982N, Y component 5.9952N
Torque	33.4429	19.10 Nm	14.38Nm
Normal flux	8.07 X 10^{-5}wb	7.38 X 10^{-5}wb	5.4355x10^{-5}wb
Average flux density	0.299 Tesla	0.272 Tesla	0.201 Tesla
MMF along contour	1563.28 amp-turn	916.091 amp-turn	1808.79 amp-turn

V. CONCLUSION

In this paper we deal with how to design the BLDC motor in FEMM software and check the various parameters of machine. For the same construction and equal volume, the mmf need of 16p12s and 8p12s is comparatively larger than the 14p12s motor. Large mmf would cause large value of magnetizing current. The value of flux density must be small as otherwise the machine will draw a large magnetizing current. We know that large magnetizing current gives significantly less efficient than which has low magnetizing current. Again the torque production of 8p12s motor is smaller than the others two. So, we can conclude that for same block volume the 14p12s BLDC motor is much efficient.

REFERENCES

[1] Gheorghe Baluta,Adrian Graur, Radu Pentiuc, C . Ciaconescu, Cezar Popa, "FEM Analysis of Brushless DC Servomotor with Fractional Number of Slot per Pole". Advances in Electrical and Computer Engineering in 2014, volume14.
[2] D. Hanselman , 'Brushless Permanent Magnet Motor Design', Second Edition, The writer collective, 2003.
[3] Jung-Moo Seo, Jung-Hwan Kim, Se-Hyun Rhyu, Jun-Hyuk, S. Jung, " A Study in Brushless DC Motor for High Toque Density, international Journal of Mechanical & Mechatronics Engineering, 2011.
[4] Rubai batham, Rameshwar Sing , "Speed Control of brushless DC Motor using Different Intelligence Scheme, IRJET, 2017.
[5] M. Pourjafari, E. Choolabi, M. Jafarboland, optimum DesigN of brushless DC Motor with Minimum Torque pulsation using FEM & PSO, American International Journal Of Science Research, 2012.
[6] Konstantinos B. Baltzis "The Finite Element Method Magnetics (FEMM) Freeware Package on 22nd may 2014.
[7] U.K Madawala and J.T Boys, "Magnetic Field Analysis of an Ironless Brushless DC Machine", IEEE transaction on magnetic", vol. 41, no 8, 2005.
[8] E.N.C Okafor, P.E Okon and C.C Okon " Magnetic Field Mapping of a Direct Current Electrical Machine Using Finite Element Method, Journal of Applied Science Research, vol 5, 2005.

DC MOTOR SPEED MONITORING SYSTEM USING PID CONTROLLER MODELED USING LABVIEW

Subham Singha[1], Santu Shit*[2] and Subhajit Bhattacharyya[2]
[1]*Department of Mechatronics Engineering, NITTTR, Kolkata, India*
[2]*Departmen ofElectrical Engineering, Mallabhum Institute of Technology, Bishnupur, India*
*santushit.ee@gmail.com

Abstract: *The LabVIEW-aided PID designed controller to monitor DC motor speed. This software are using a simulation to analysis its response. The design of motor generator coupling set, as the feedback signal through the generator sensor to produce voltage signal. The speed signal are getting from coupler using tachometer. To take out the analog voltage signal corresponding speed in rpm through D/A converter at same time acquire the signal via the NI DAQ card. The front panel will show the speed of DC motor on the screen. The behavior of PID controller to simulation results are quite match with the theoretical prediction. The performance of the proposed system is analyzed through several experiments.*

Keywords: *LabVIEW,DC Motor, PID controller*

I. INTRODUCTION

The DC motors are exceptionally well known in the business control territory for quite a while, on the grounds that they have numerous great qualities, for instance: high begin torque trademark, high reaction execution, simpler to be straight control. The distinctive control of the approach relies upon the diverse execution of engines. Since the fringe control gadgets are sufficient, there is a more broad application in the business control framework.

The speed control of dc motor using the PID controller in LabVIEW is an important aspect in any type of industry. Starting from the movement of robotic vehicles to paper mill, speed control of dc motor has wide application. In the motor-generator set, two motors are connected with a coupler, one is used as a motor and the other is used as a generator sensor. When a set point voltage is given to the motor, the motor rotates with this voltage and corresponding voltage information goes from the generator sensor to the PID controller in LabVIEW through the data acquisition card. There is a linear relationship of speed with dc voltage and required speed information by feedback is sent to the driver circuit through the DAQ card. Being change the value of proportional gain, integral gain and derivative gain in the PID controller set point error is removed. In a single line, one loop is consisted for regulating the speed of dc motor with the help of the PID controller in LabVIEW. The basic idea behind a PID controller is to examine a sensor, by then register the perfect actuator yield by learning comparing, irreplaceable, and backup responses and summing those three sections to process the yield. Before starting to portray the parameters of a PID controller, it is seen what a shut circle structure is and a bit of the wordings identified with it.

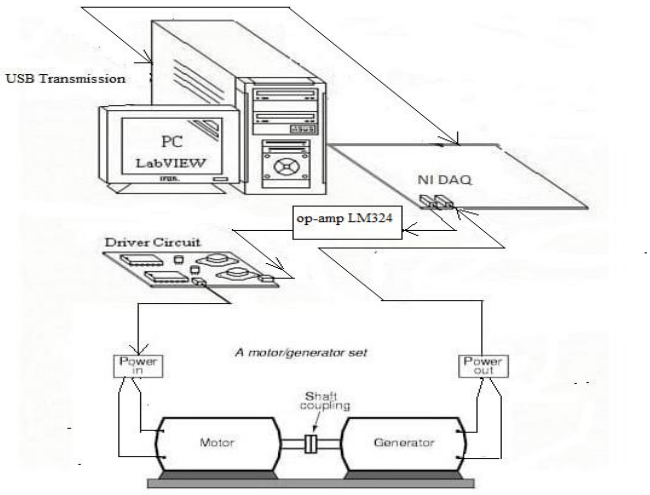

Figure 1: Schematic block diagram of the proposed model.

In Figure 1, connection of all parts of proposed paper work are shown briefly which gives a basic knowledge about speed control of DC motor using PID controller in LabVIEW. A closed loop is made with the help of a motor generator set, DAQ card, PID

controller in LabVIEW within pc, a small circuit of op-amp LM324, a driver circuit and DC voltage source.Power is given to the motor from the driver circuit which is connected to the DC voltage source.

The proposed objective was the generator sensor senses the voltage and this information is delivered to the LabVIEW block diagram through data acquisition controller card. The set point speed of the DC motor is specified by creating a Graphic User Interface for PID Controller in LabVIEW. From the generator sensor the output is sent back to the PID Controller in LabVIEW via a data acquisition controller card. To compare the DC Motor actual speed and set point speed with the help of PID controller. If its speed is not the same, PID Controller tries to minimize the error and bring the motor to the set point value.

II. MATHEMATICAL MODEL OF DC MOTOR AND CONTROL THEORY

DC motor system is a separately excited DC motor, which is often used to the velocity tuning and the position adjustment. The control equivalent circuit of the DC motor using the armature voltage control method [21] is shown in Fig 1.

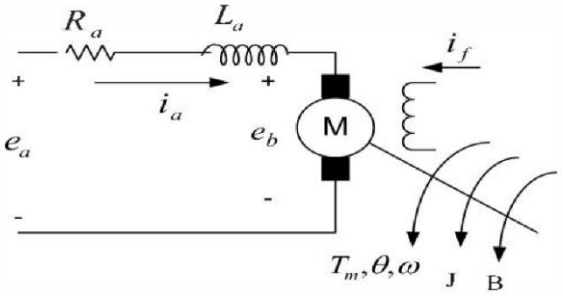

Figure2 : The Control Equivalent Circuit of the DC Motor

WhereR_a : Armature resistance
L_a: Armature inductance
i_a: Armature current
i_f: Field current
e_a: Input voltage
e_b : Back electromotive force (EMF)
T_m: Motor torque
ω: An angular velocity of rotor
J: rotating inertial measurement of motor bearing
B : a damping coefficient

The development of PID control theories has already 60 years so far, PID control has been one of the control system design method of the longest history. However, this method is still extensively used now [20].The structure of PID controller is simple, it is the most extensive control method to be used in industry so far. The PID controller is mainly to adjust an appropriate proportional gain (K_P), integral gain (K_I), and differential gain (K_D) to achieve the optimal control performance. The PID controller system block diagram of this paper is shown in Fig 3.

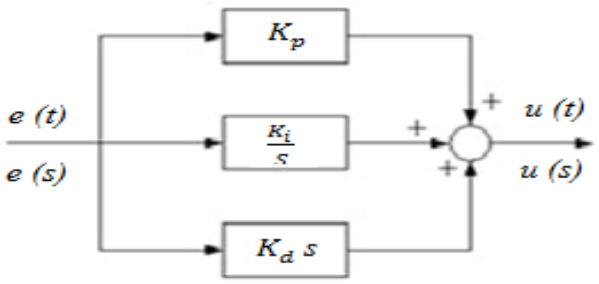

Figure 3. PID controller system block diagram
The connection between the info e (t) and yield u (t) can be planned by the equations (1) to (3),

$$u(t) = K_p . e(t) + K_i . \int_0^1 e(t)\, dt + K_d \frac{de(t)}{dt} \qquad (1)$$

The transfer function is communicated as pursues,

$$C(s) = \frac{U(S)}{E(S)} = K_p + \frac{K_i}{S} + K_d\, s \qquad (2)$$

The PID DC motor speed control framework square chart has appeared in Figure 4

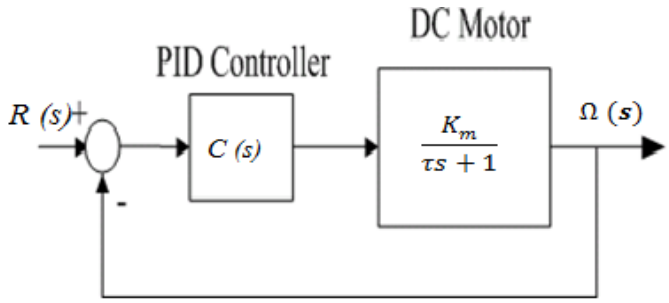

Figure 4: PID controller with DC motor speed control framework square chart

The shut circle exchange capacity of the DC motor speed control framework communicates as pursues,

$$G(s) = \frac{\Omega(s)}{R(S)} = \frac{(K_p + \frac{K_i}{S} + K_d\, S)\frac{K_m}{\tau s+1}}{1+(K_p + \frac{K_i}{S} + K_d\, S)\frac{K_m}{\tau s+1}}$$ (K_m = motor gain and τ= time constant) (3)

$$= \frac{(K_d S^2 + K_p S + K_i)\, K_m}{(K_d K_m + \tau)S^2 + (1+K_p K_m)S + K_i K_m}$$

III. FUNCTIONAL BLOCK DIAGRAM OF TOTAL SYSTEM STRUCTURE

The fundamental point is to interface the PC by means of a USB transmission line and information obtaining module (NI DAQ USB-6008), at that point control the engine framework to accomplish the speed control of the engine and investigate the reaction of the engine by programming. It allows communication between PC, embedded platform, sensors and other devices interconnected using USB. This system is used to generate a voltage signal through the generator sensor in the dc motor generator coupling set. Output voltage and coupler speed are varying with varying the input voltage. This technique is employed to get a voltage signal through the generator sensing element within the dc motor generator coupling set. Output voltage and mechanical device speed square measure varied with variedthe input voltage. From their data goes to LabVIEW in pc through USB at that point execute the parameter alteration of the PID controller through the planned program in the LabVIEW condition so as to diminish the yield error, as appeared in The outcomes from the closed loop framework demonstrate that the speed of the DC motor can be controlled successfully and keep up the steadiness of the framework.

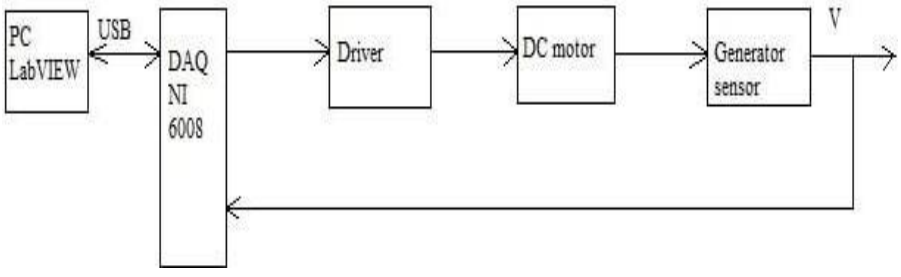

Figure 5: Block diagram of DC motor speed control using a PID controller

IV. RESULTS & DISCUSSION

In this experiment driver circuit (model no is L298) and small circuit of op-amp LM324 is used for regulating the speed of DC motor using the PID controller in LabVIEW by the feedback control process.If the set point rpm and measured rpm are not the

same, then the error is eliminated by changing the value of proportional gain, integral gain, and derivative gain. Various types of graphs (Fig. 6) are seen from the experiment data at different set points for a specific value ofK_p, K_i andK_d. Due to friction and small specification of DC motor tuning is not properly done by the regulating value of K_p, K_i andK_d.

Motor output rpm vs set point rpm	**Motor output rpm error(%) vs set point rpm**
K_p = 0.2, K_i = 0, K_d = 0	
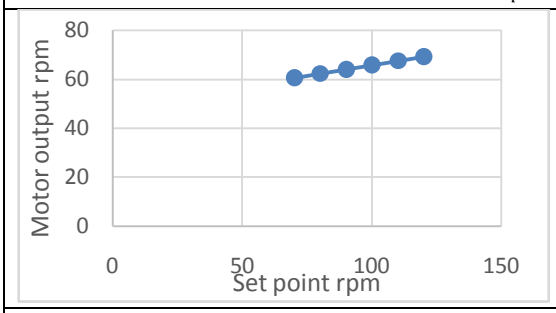	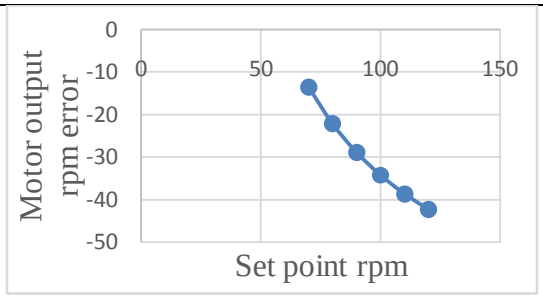
K_p = 0.3, K_i = 0, K_d = 0	
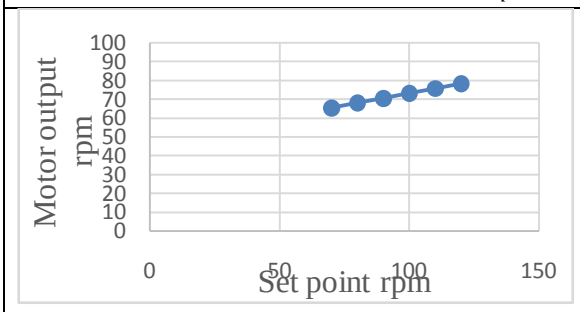	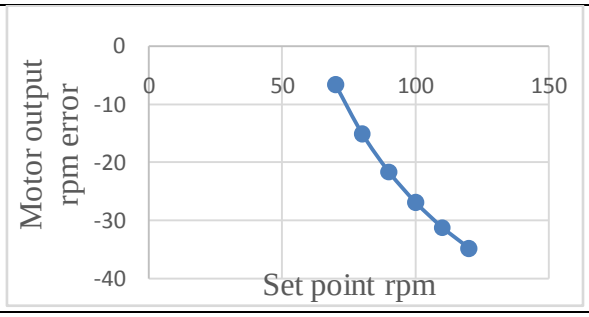
K_p = 0.4, K_i = 0, K_d = 0	
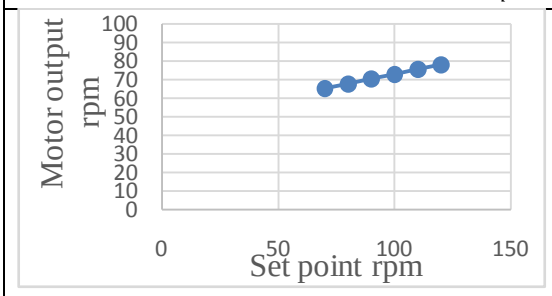	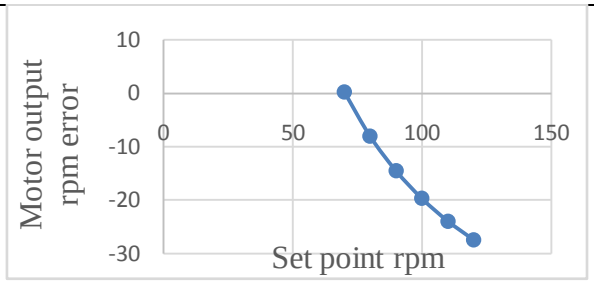
K_p = 0.2, K_i = 0.0007,K_d = 0	
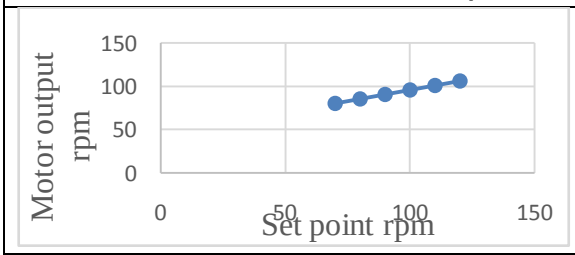	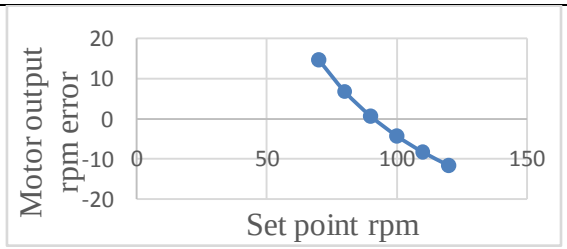
K_p = 0.3, K_i = 0.0008, K_d = 0	
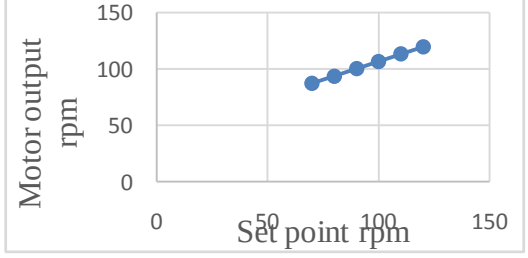	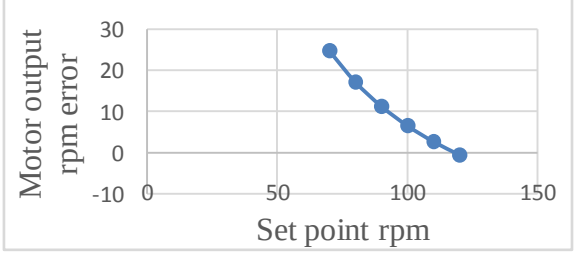

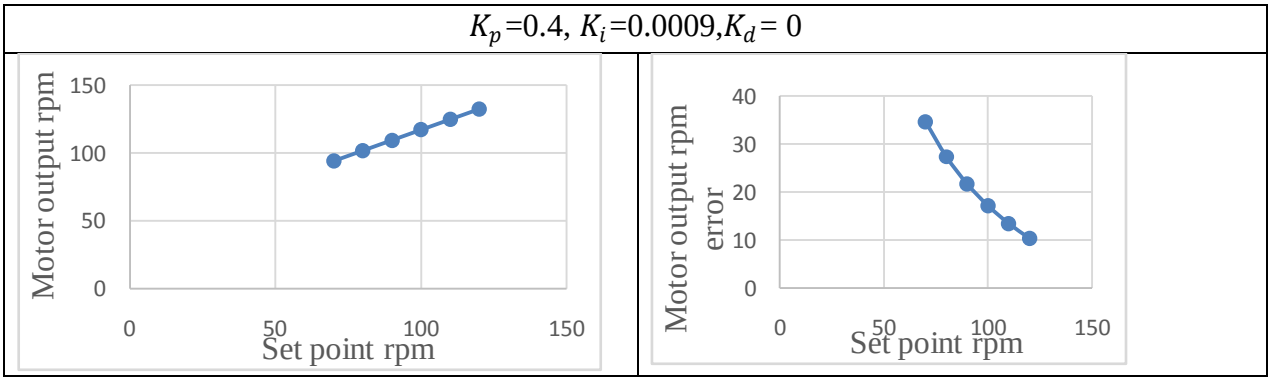

Figure 6: Motor output rpm vs set point rpm; Motor output rpm error (%) vs set point rpm

Table 1: Tabular chart of motor speed in rpm corresponding set point rpm

Set no.	Set point rpm	K_p	K_i	K_d	Motor speed in rpm	Error	Remarks about error
1	70	0.2	0	0	61	-12.86	Increasing
	80	0.2	0	0	62	-22.50	
	90	0.2	0	0	64	-28.89	
	100	0.2	0	0	66	-34.00	
	110	0.2	0	0	67	-39.09	
	120	0.2	0	0	69	-42.50	
2	70	0.3	0	0	65	-7.14	Increasing slowly from previous
	80	0.3	0	0	68	-15.00	
	90	0.3	0	0	71	-21.11	
	100	0.3	0	0	73	-27.00	
	110	0.3	0	0	76	-30.91	
	120	0.3	0	0	78	-35.00	
3	70	0.4	0	0	70	0	Increasing slowly from previous
	80	0.4	0	0	74	-7.50	
	90	0.4	0	0	77	-14.44	
	100	0.4	0	0	80	-20.00	
	110	0.4	0	0	84	-23.64	
	120	0.4	0	0	87	-27.50	
4	70	0.2	0.0007	0	80	14.29	Decreasing positive error and increasing negative error
	80	0.2	0.0007	0	85	6.25	
	90	0.2	0.0007	0	91	1.11	
	100	0.2	0.0007	0	96	-4.00	
	110	0.2	0.0007	0	101	-8.18	
	120	0.2	0.0007	0	106	-11.67	
5	70	0.3	0.0008	0	87	24.29	Decreasing positive error
	80	0.3	0.0008	0	94	17.50	
	90	0.3	0.0008	0	100	11.11	
	100	0.3	0.0008	0	107	7.00	
	110	0.3	0.0008	0	113	2.73	
	120	0.3	0.0008	0	119	-0.83	
6	70	0.4	0.0009	0	94	34.28	Decreasing high positive error
	80	0.4	0.0009	0	102	27.50	
	90	0.4	0.0009	0	110	22.22	
	100	0.4	0.0009	0	117	17.00	
	110	0.4	0.0009	0	125	13.64	
	120	0.4	0.0009	0	132	10.00	

Here it is demonstrated the utilization of the PC-Based to be a control the interface with the LabVIEW programming configuration program.With the PID controller, adjust the parameters. By changing the value of theK_p,K_i,$K_d$get the best reaction of the wonderful framework. Through the real modifyingK_p,K_i,$K_d$gains, the reactions of this framework can be gotten under various conditions. After all it is taken the real control parameters into LabVIEW to reenact, the outcomes with real reaction and speculations are somewhat close. It is noticed for the specific value ofK_p,K_i,K_d the error is eliminated between set point rpm and measured rpm at specific set point rpm.

REFERENCES

[1] Liau, J. C., A Study of LabVIEW Aided in DC Motor Speed Monitoring System. National Taiwan Ocean University Department of Mechanical & Mechatronic Engineering, 2000.
[2] Srinivasan, M.B., A.Shirkhodaie,andM.Malkani, "LabVIEWprogramdesignforon-linedataacquision and dpredictive maintenance", Proceedings of Thirtieth Southeastern Symposium on System Theory, 1998,pp.520-524.
[3] Li, K. Y., S. S. Huang and R. C. Chen, 8051/52 Application of Microcontroller. Skinfo Book co., Ltd, Taipei Taiwan, 1998.
[4] Deng, M. F., Application of ISP Single Chip Microcomputer. Knowledge and Execution Co., Ltd. Taichung, Taiwan, 2002.
[5] Huang, J. M., University Automatic Control, University City Books Enterprise Inc, Kaohsiung Taiwan, 2004.
[6] Wang, J. B., Control of Electric Machinery. GauLih Book co., Ltd, Taipei Taiwan,2001
[7] DAQ USB-6008 User Manual, National Instruments, 1999.

Proceedings of National Conference on Device Modeling and Soft Computing for real time applications (DMSC-2019)
Organized by Dept. of ECE, MIT Bishnupur in collaboration with The Institution of Engineers India (IEI)

DIFFERENT MODELS OF POWER AMPLIFIER USED IN D.C. CONTROL ELECTROMAGNETIC LEVITATION SYSTEM

Amit Kundu*
Department of Electrical Engineering, Mallabhum Institute of Technology, Bishnupur, India
*amitkundu32@gmail.com

Abstract: *The theme of the paper is to simulation of different types of power amplifier which are used in the electromagnetic levitation system. Out of many the most appropriate and stable power amplifier we used. To find the suitable power amplifier we are apply two processes they are time response and frequency response. Detail description and functioning of each power amplifier is explained along with the output waveform. In this paper we are used PSIM and MATLAB and PSPICE simulation for different power amplifier.*

Keywords: *Electromagnetic Levitation, D.C. to D.C. converter switch, Matrix Laboratory (MATLAB) software, Personal Computer Simulation Program with Integrated Circuit Emphasis (PSPICE) software, Persatuan Sepak Bola Indonesia Matarma (PSIM) software***.**

I. INTRODUCTION

The power amplifier is taking most important of control electromagnetic levitation system. Here power amplifier is used for D.C. to D.C. converter switch [1-5]. That means the power converter conversion of fixed dc voltage to an adjustable dc output voltage. Different kinds of power amplifiers have been proposed for electro-magnetic levitation. These include magnetic amplifiers (which are now obsolete) as well as the more modern type of solid-state amplifiers. For low power application both linear and solid state power has been proposed of their own advantage and disadvantage. The linear power supplies produce less switching noise and the overall electromagnetic interference is less when compared to the one produced by switching mode power amplifier(SMPS) circuit. But there is some limitation in linear power supply also, that are the transistor operates in its active region, incurring a significant amount of power loss. The overall efficiencies of linear power supply in a range of 30% to 60%. For high power electromagnet requires linear power amplifier will impractically large. . A combination of switched supply and linear amplifier circuit may be thought of to further improve the efficiency of linear amplifier circuits. Because of the switched mode DC to DC power supply circuits are energy efficient (70-90% range). This is used for mainly emergence of the switching power supply because it increase the switching speed, voltage rating and current rating is very high and also low cost. The coil current for the magnets used in levitation needs to be precisely controlled to meet the attractive force demand. This calls for a fast DC to DC switching power amplifier that can be controlled in a closed loop fashion. The switching mode DC to DC power supply (chopper) circuit is energy efficient but they generated electromagnetic noise which will affect the position signals. Once it has been decided to use the SMPS type circuit one must make a good layout of the power circuit to limit electromagnetic interference and some kind of electromagnetic shield may be provided between the power amplifier circuit and the position sensor. The other important consideration is the chopper switching frequency. The chopping frequency should be significantly higher than the frequency band of expected position signal to enable effective filtering of electromagnetic interference generated by chopper from the low frequency position signal. The low pass filter cut-off frequency should be kept significantly higher than the position signal frequency but much lower than the switching noise frequency. Due to high chopper frequency the resulting current in the magnet coil is almost continuous resulting in a linear transfer function for the chopper being used. High chopper frequency eliminates low order harmonics from the coil current resulting in smooth current variation and less humming noise. Depending upon the time response and frequency response we used four types of power amplifier they are buck converter, asymmetrical converter, half bridge converter and full bridge converter. By using of the PISM and MATLAB simulation we get time response and PSPICE simulation we get frequency response. Using by these two responses we get most appropriate and stable power amplifier which will use in the close loop electromagnetic system.

II. DEFINITION OF DIFFERENT TYPES OF SIMULATION SOFTWARE

Various types of simulation software available are*:*

A. PSPICE- PSPICE is an analog circuit and digital logic simulation software that runs on personal computers. It was developed by MicroSim and is used in electronic design automation. PSPICE, is more requirement in the complex industry, because it

intregrate the overall system design flow from OrCAD and Cadence Allegro. It has some additional feature like advance analysis with automatic circuit optimization, model editor, support for model optimization etc. In PSPICE, circuit simulation is the standard way to verify any circuit operation before manufacturing the circuit. These parasitic components can often be estimated more accurately using PSPICE simulation.

B. PSIM- PSIM is the leading simulation and design software for power electronics, motor drives, and dynamic system simulation. PSIM give faster, powerful and efficient nature for simulation. It is design for specially power electronics, analog and digital control and motor drives.

C. MATLAB SIMULINK- SIMULINK is the graphic user interface software from MATLAB which help us to prepare the model of the various power systems, power electronics and control system. The SIMULINK model gives us the exact static and dynamic response of the electrical and electronics circuit. Moreover it allows us to simulate exactly the same real time applications which are used in the various circuits.

III. SIMULATION OF DIFFERENT TYPES OF CONVERTORS USING PSPICE, PSIM AND MATLAB

A. Buck converter

1. ***Time response using PSIM and MATLAB simulation-***

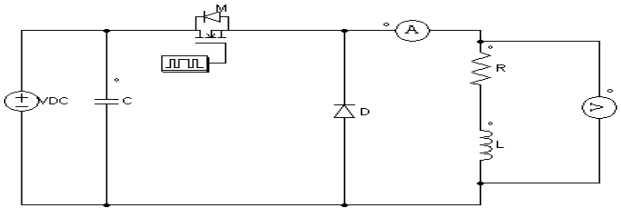

Fig.1. PISM circuit diagram for buck converter

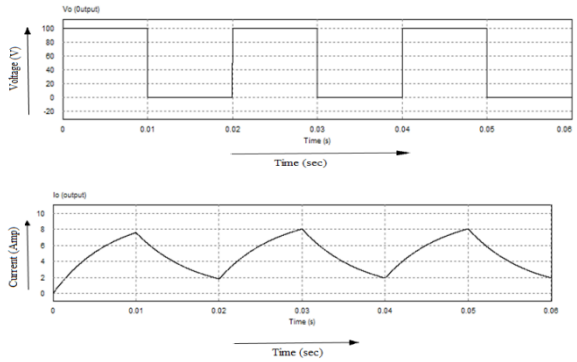

Fig.2. Voltage output and current output of PSIM circuit diagram

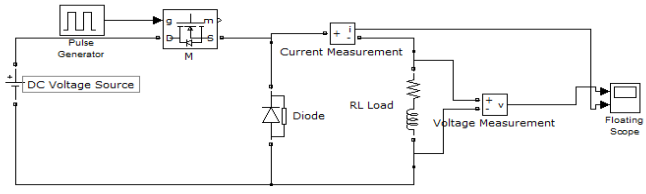

Fig.3. MATLAB circuit diagram for buck converter

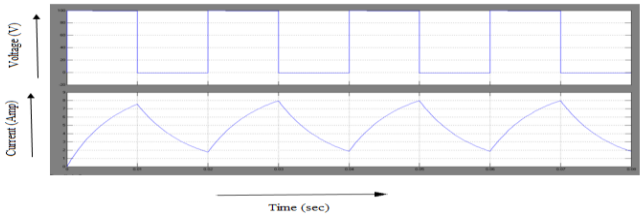

Fig.4. Voltage output and current output of MATLAB circuit diagram

In above two simulations we can see that the same output response is given. When the switch M is on and the diode D in this case become reversed biased, as its anode voltage is negative and cathode voltage is positive. So the diode terminals become open

circuited. The current will continue to flow from source to load. The voltage drop across the load, i.e. output voltage will be positive and is equal to the Supply D.C. voltage .i.e. $V_0 = V_s$ when the switch M is off. So in this case no current from the source is available for the load. Because the load terminal which is isolated from the source. Now inductor voltage will be reversed, due to its property and the anode of diode D becomes positive and the cathode of D becomes negative. So the diode becomes forward biased. The stored energy of the inductor will discharge through the freewheeling diode D [1-5]. The load voltage will be zero, as the load terminals, becomes short circuited. But in practical we may get a slight negative voltage due to a small voltage drop across the diode terminals. When the switch is on current rises through the inductor exponentially, when the switch is off the current falls through the inductor exponentially and the cycle repeats itself.

2. ***Frequency response using PSPICE simulation-***

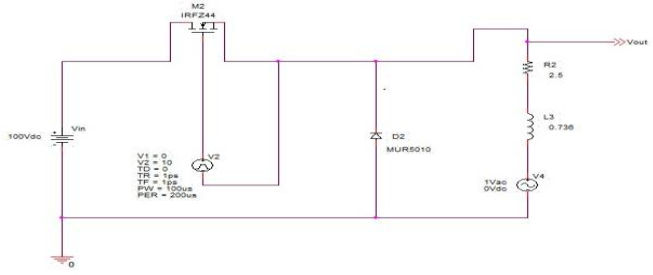

Fig.5. PSPICE circuit diagram for buck converter

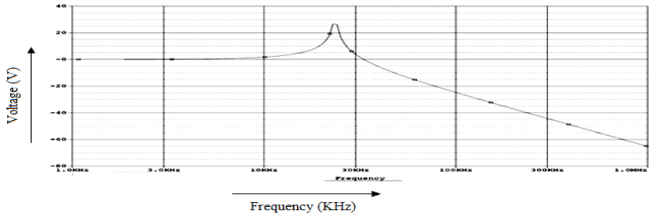

Fig.6. Frequency response of buck converter in PSPICE

The output of PSPICE circuit diagram gives the frequency response. In the circuit of buck converter the source voltage is 100V D.C. and the load inductance is 0.736H. In this case frequency response of buck converter gives the gain cross-over-frequency of 26.42 KHz. It gives a bandwidth of this frequency is quite small. Since the stability is directly proportional to bandwidth, hence the stability of the system is also less and has the slowest response.

B. ASYMMETRICAL CONVERTER

1. Time response using PSIM and MATLAB simulation-

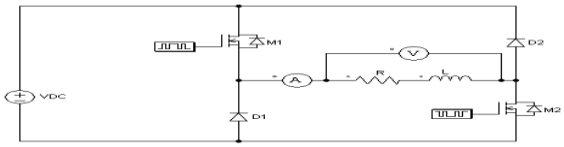

Fig.7. PISM circuit diagram for asymmetric converter

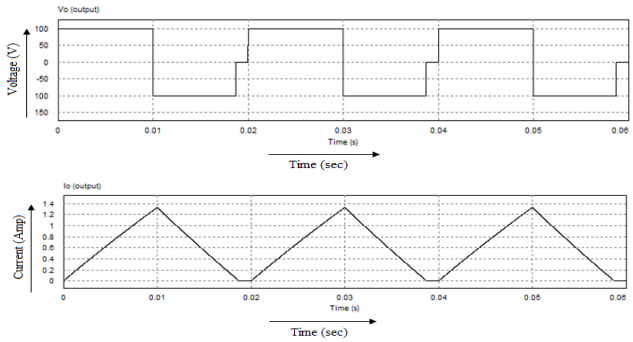

Fig.8. Voltage output and current output of PSIM circuit diagram

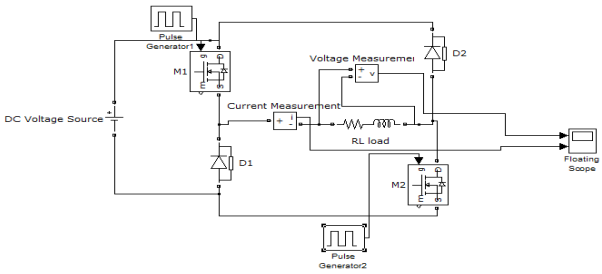

Fig.9. MATLAB circuit diagram for asymmetrical converter

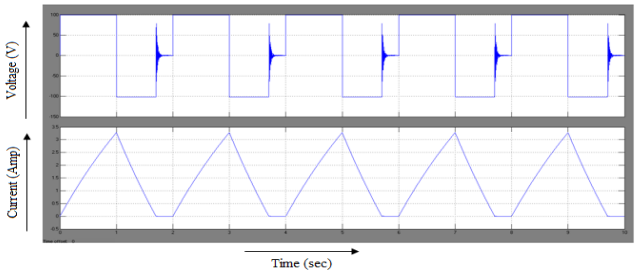

Fig.10. Voltage output and current output of MATLAB circuit diagram

In above two simulations we get same output response. When both the switches M1 and M2 are on, the cathode of diode D1 is more positive than its anode. So diode D1 becomes reverse biased. i.e. no current passes through the diode D1, i.e D1 becomes open circuited. Similarly, the cathode of diode D2 becomes more positive than its anode .i.e. no current passes through it. So the diode D2 becomes open circuited. So, in this case the voltage, which will appear across the load terminals, will be supply voltage. So, the load voltage becomes the supply voltage. i.e. $V_0 = V_s$.
When M1 and M2 are turned off, the energy stored in the coil will keep the current in the same direction until and unless it is depleted. Due to the property of inductor the coil voltage becomes reversed as soon as the supply voltage across coil are withdrawn M1, M2 are turned off. Here the anode of the diode D2 is more positive than its cathode. So diode D2 becomes forward biased. The cathode of the diode D1 is more negative than its anode. So the diode D1-becomes forward biased. i.e. in this case the output voltage Vo becomes negative and its magnitude is equal to the supply voltage Vs. i.e. $V_0 = -V_s$ [1-5].

2. ***Frequency response using PSPICE simulation-***

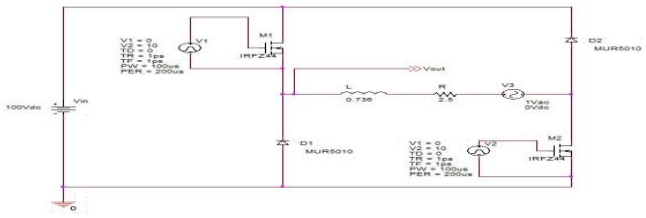

Fig.11. PSPICE circuit diagram for asymmetrical converter

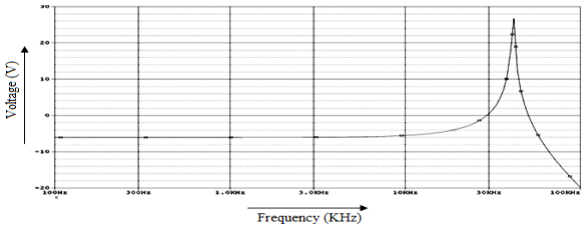

Fig.12. Frequency response of asymmetrical converter in PSPICE

Frequency response of asymmetrical converter gives the gain cross-over-frequency of 52.675 KHz. It gives a bandwidth of this frequency is high. Since the stability is directly proportional to bandwidth, hence the stability of the system is quite high and gives a faster response.

C. HALF BRIDGE CONVERTER

1. Time response using PSIM and MATLAB simulation-

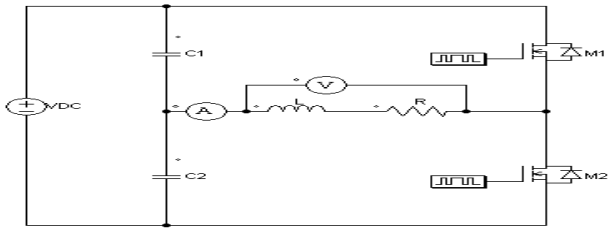

Fig.13. PISM circuit diagram for half bridge converter

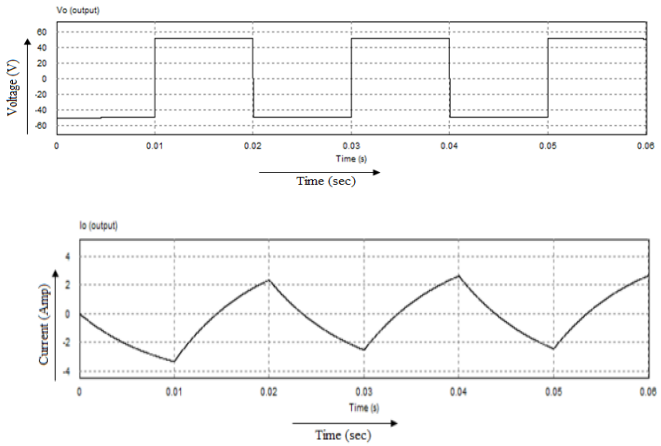

Fig.14. Voltage output and current output of PSIM circuit diagram

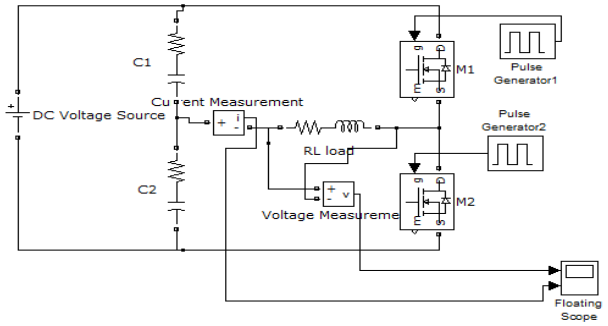

Fig.15. MATLAB circuit diagram for half bridge converter

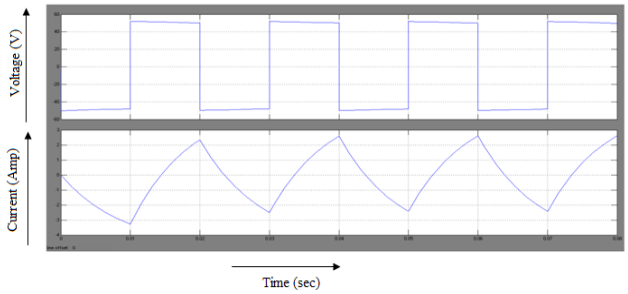

Fig.16. Voltage output and current output of MATLAB circuit diagram

Here two capacitor C1 and C2 work as voltage divider. Because the two capacitor is divided the source voltage into two part, that is C1=C2=Vs/2. When the switch M1 is on the capacitor C1 will discharge through the inductive load and in this case upper voltage source will act. And the Voltage across the load, $V_0 = -\frac{V_s}{2}$.

When M1 gets off, and M2 is on the voltage across the load is due to the second capacitor C2 only. Capacitor C2 will give supply to the load. Capacitor C1 Will store charge during this instant. Voltage across the load, $V_0 = \frac{V_s}{2}$ [1-5].

2. ***Frequency response using PSPICE simulation-***

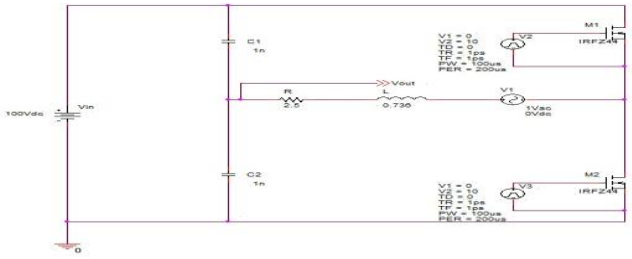

Fig.17. PSPICE circuit diagram for half bridge converter

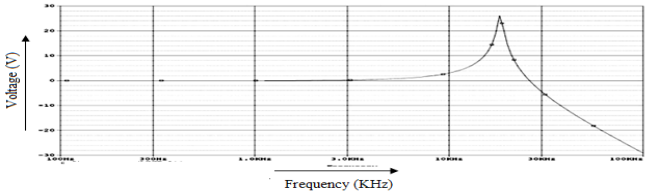

Fig.18. Frequency response of half bridge converter in PSPICE

Frequency response of half-bridge converter gives the gain cross-over-frequency of 19.582 KHz. It gives a bandwidth of this frequency is quite good. Since the stability is directly proportional to bandwidth, hence the stability of the system is also high but the response is slow.

D. FULL BRIDGE CONVERTER

1. Time response using PSIM and MATLAB simulation-

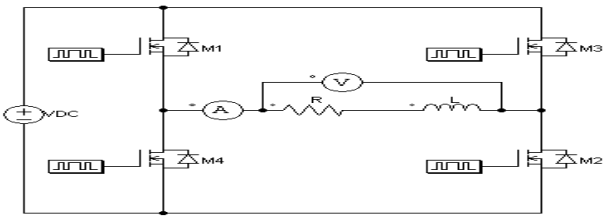

Fig.19. PISM circuit diagram for full bridge converter

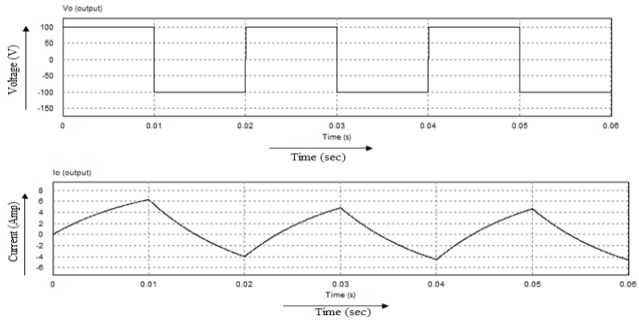

Fig.20. Voltage output and current output of PSIM circuit diagram

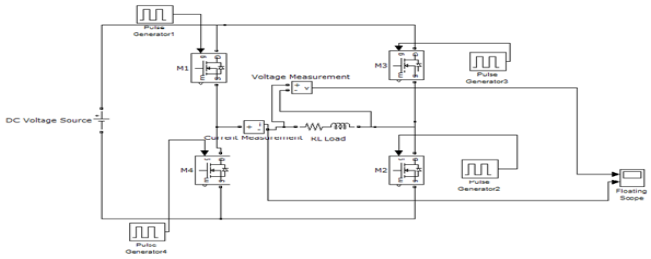

Fig.21. MATLAB circuit diagram for full bridge converter

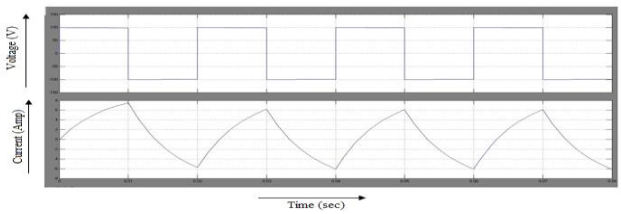

Fig.22. Voltage output and current output of MATLAB circuit diagram

When the switches M1and M2 are on (M3 and M4 are off). In this case the inductor charges and stores energy. Full supply voltage will come across the load, current rises exponentially. When the switches M3 and M4 are on (M1 and M2 are off).Here the voltage across the load reverses. But due to the property of the inductor, current does not change suddenly, but it decays exponentially. As current reaches to its minimum value, the switches M3, M4 become off and M1, M2 becomes on [1-5].

2. ***Frequency response using PSPICE simulation-***

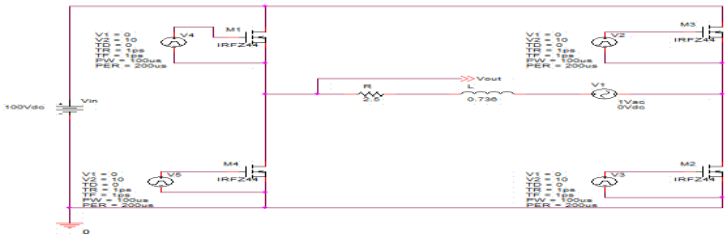

Fig.23. PSPICE circuit diagram for full bridge converter

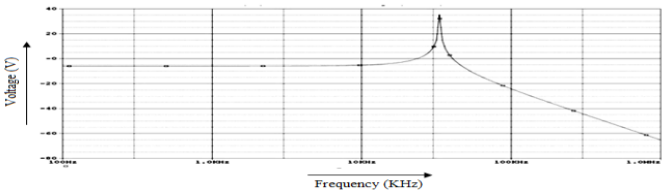

Fig.24. Frequency response of full bridge converter in PSPICE

Frequency response of full bridge converter gives the gain cross-over-frequency of 40.986 KHz. It gives a bandwidth of this frequency is small. Since the stability is directly proportional to bandwidth, hence the stability of the system is also low and gives a good response.

IV. CONCLUSION

In this paper an attempt to find out the power amplifier of the D.C. electromagnetic levitation system. From the output of the time response and frequency response we can find the appropriate and stable power amplifier. The stability and speed of response of the power amplifier is dependent upon the gain cross-over-frequency (GCF). That means which amplifier has given high gain cross-over-frequency that converter stability and speed of response is batter. In here we can see that the asymmetrical converter has high gain cross-over-frequency (GCF), i.e. 52.675 KHz. The giving load current of the asymmetrical converter is always positive. So the asymmetrical converter is selected as power amplifier of the D.C electromagnetic levitation.

REFERENCES

[1] P.C. Sen, 'Thyristorised DC Drive', New York : Wiley Interscience, 1981.
[2] P.S. Bimbhra, 'Power Electronics', Khanna Publication 5th Edition.
[3] Philip T. Krein, 'Elements of Power Electronics', Oxford University Press, 2003.
[4] Muhammad H. Rashid, 'Power Electronic', Wheeler Publishing, 1998.
[5] S. Banerjee, R. Bhaduri and D. Prasad, 'Some aspects of switching power amplifier used in electromagnetic levitation', Int. J. Power Electronics, Vol. 1, pp. 33-48, 2008.

AN AHP MCDM APPROACH FOR SELECTION OF WIND POWER PLANT LOCATION: A CASE STUDY FROM INDIA

Tilottama Chakraborty*[1] and Soumya Ghosh[2]
[1]*School of Hydro Informatics Engineering, National Institute of Technology, Agartala, India*
[2]*Department of Electrical Engineering, Mallabhum Institute of Technology, Bishnuur, India*
*tilottama86@gmail.com

Abstract: *The present study introduces a new way to identify location where maximum utilization of Wind Power Plant can be possible with minimum expenditure. In this aspect, AHP was used where cost and efficiency are used in an objective manner to compare the selected important parameters with respect to study objective. Results depict the importance of capacity factor in selection of locations for installation of wind power plants.*

Keywords*: Wind energy, Analytical Hierarchy Process, Location selection for wind power generation.*

I. INTRODUCTION

Electricity and energy production play an important role in modern life. During the last two decades energy production methods has been changed from fossil fuel to other environmental friendly methods, termed as Renewable Energy Methods and propose the usage of sustainable sources based on Wind, Water, Biomass, Solar Energy and Geothermal Energy for the production of electricity (Doukas et al., 2009). Due to the environmental issues renewable energy became more popular among the researcher (Rahman and Miah, 2017; Kaldellis et al., 2012; Giacomarra and Bono, 2015). It is found that more than 28 percent share of the world's total energy will be consumed in India and China by the year 2030 according to International Energy Agency. The total potential for renewable power generation in India as is estimated at 10, 01,132 MW (Energy statistics, 2018). Source wise estimated potential of renewable energy is shown in figure 1. With the more efficiency and less noisy in wind turbine, wind energy has became one of the major sources of renewable energy (Wolsink, 2007; Tampakis et al., 2013). A wind farm can be defined as a combination of wind turbines that acts as an electricity producing power station (Petersen and Madsen, 2015). India has 19,565 MW of total installed capacity of wind energy which leads to 5th rank in terms of wind energy producing country in the world. More than 95 percent of total nation's wind energy generates from the five states located in southern and western India i.e. Gujarat, Maharashtra, Karnataka, Tamil Nadu and Andhra Pradesh (Singh Madhu et al. 2014).

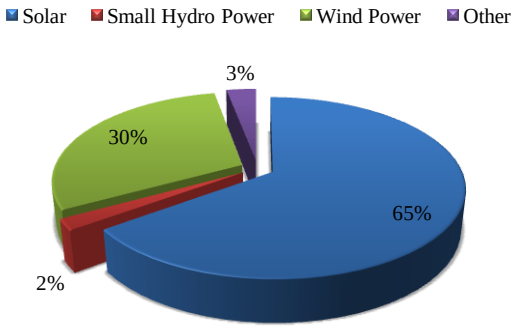

Fig. 1: Source wise estimated potential of renewable energy in India

The goal of the Wind Power Plant (WPP) location selection process is to maximize the efficiency of the power plant, reducing the cost and minimizing the adverse impact on environment. Hence, the purpose of this present study is to propose a novel methodology to select best locations for WPPs with least socio-economic, environmental and infrastructural development costs, and high return through power generation. This paper proposes a multicriteria decision making method (MCDM) based framework for evaluating and selecting optimal locations for wind power plants. The framework involves two stages. Firstly, the factors affecting the installation of WPP have been identified where social, technical, economical and environmental aspects were considered. Then, an AHP MCDM method is used to determine the weights of criteria, and to rank the alternative locations, respectively.

1.1 Analytic hierarchy process (AHP): This method was utilized by Saaty [Saty,1980] to determine the relative importance of a set of activities in a multi-criteria decision problem. The process enables the incorporation of judgments with respect to intangible

quantitative criteria [Badri. 2001]. The AHP method is based on three principles: first, the structure of the model; second, comparative judgment of the alternatives and the criteria; and third, synthesis of the priorities [Albayra et al,2004].

II. METHODOLOGY

The objective of the present study is to first identify the important decision criteria and sub-criteria relevant to the WPP location selection decision and then provides an effective integrated framework to evaluate and select the best locations. Two criteria and five alternatives have been identified through literature review and expert opinion.

2.1 Selection of Criteria and alternatives: Cost potential and efficiency potential have been considered as criteria in this present study objective.

Capacity factor, Elevation and slope, distance to fault line, distance to transmission line and distance to road have been considered as alternatives.

i) Capacity factor: It is defined as the efficiency of electricity production in a given location considering a standard turbine is installed.

ii) Elevation and slope: Elevation and slope can have impact on the cost of construction of WPP. The cost can differ between the two locations if the slope and elevations are different.

iii) Distance to transmission line: It is directly proportional to the efficiency of the WPP. The shorter route of a transmission line can minimizes the losses and maximizes the efficiency

iv) Distance to road: It can have impact on the cost of the construction and maintenances of WPP. Cost will be less if the location of installation of WPP is nearer to the main road.

v) Distance to fault line: In case of earthquake, if the location of installation of WPP is nearer to the fault line it became riskier.

2.2 Application of AHP MCDM: First step of the AHP method is to determine the weights of each of the criteria. A [2×2] matrix was developed to achieve this result.

In second step, alternatives were compared to each other with respect to each of the criteria and for this two [5x5] matrix were formed with respect to each of the criteria.

In the last step, with the determined values of two criteria and seven alternatives, a matrix multiplication has been done to find the priority value of each of the parameters. The procedure of the present study is shown in Fig.1.

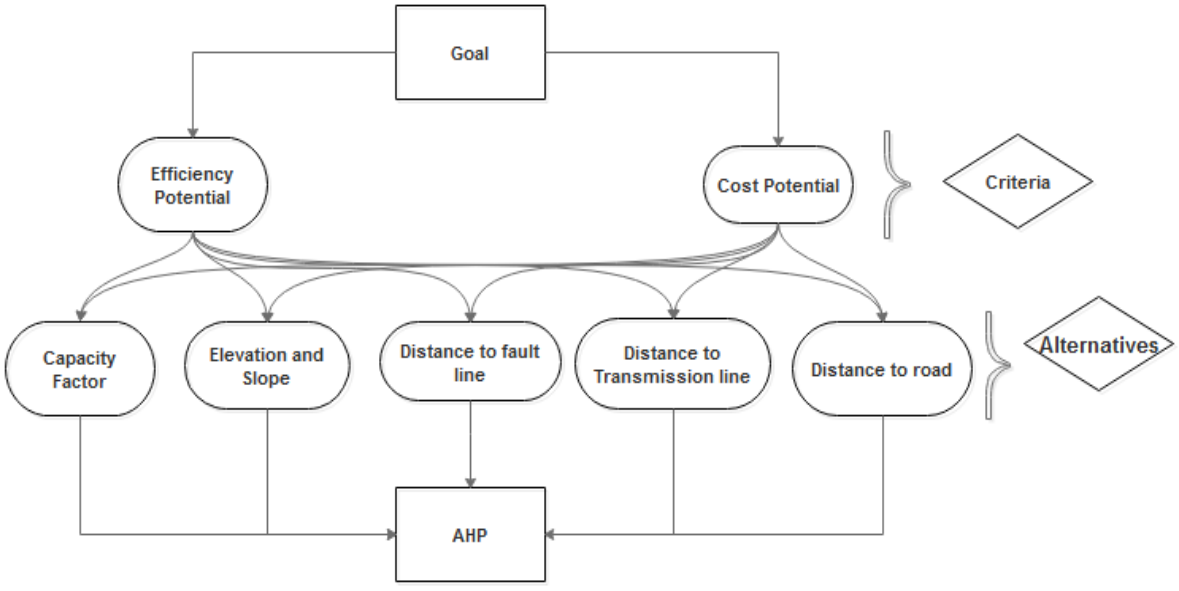

Fig.2: Decision Hierarchy Structure of AHP MCDM

III. STUDY AREA

Six locations (Fig.3) of India were selected for this study, namely Andhra Pradesh, Gujrat, Kerala, Karnataka Manipur and Assam.

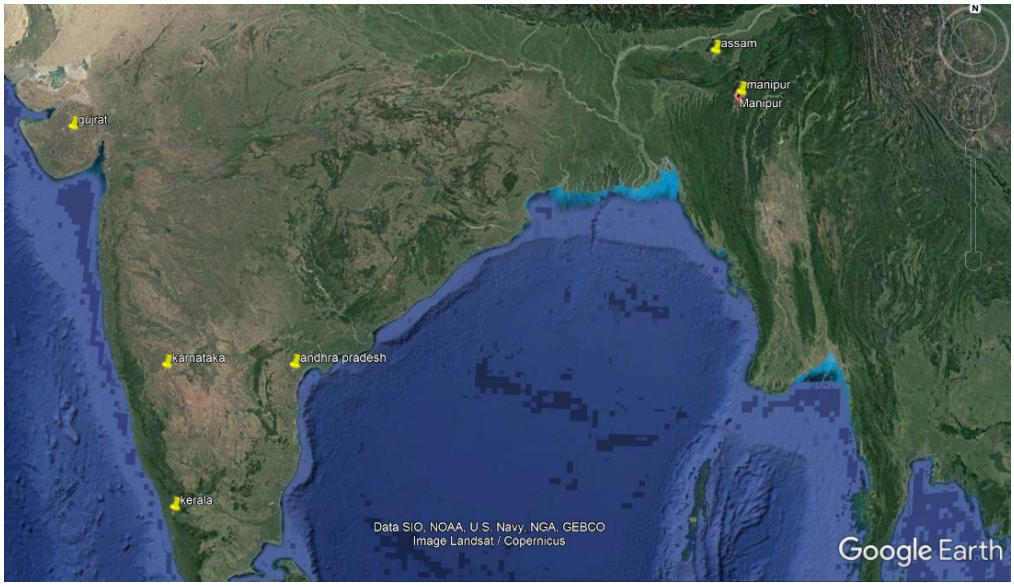

Fig.3: Schematic diagram of study area

IV. RESULTS AND DISCUSSION

Table 1 shows the rank of the criteria based on AHP method. The rank of the parameters with respect to each of the criteria is presented in Table 2. Literature survey and were found to be capacity factor the most important criteria and alternative respectively. Least important criteria were found to be data availability and alternative with lowest significance was found to be distance to fault line. Table 3 shows that the Gujarat has maximum potential among the six chosen locations whereas Manipur and Assam are showing least potential respectively.

Table 1: Rank of the Parameter

Criteria	Score	Rank
Literature Survey	0.240	1
Expert Survey	0.167	2
Data Availability	0.127	3

Table 2: Rank of the Parameter

Parameter	Rank
Capacity Factor	1
Elevation and Slope	4
Distance to fault line	5
Distance to transmission line	2
Distance to Road	3

Table 3: Weights Value of the Location according to the AHP MCDM Method

Location	Weights Value
Andhra Pradesh	0.28
Gujrat	0.60
Kerala	0.20
Karnataka	0.38
Manipur	0
Assam	0

V. CONCLUSION

The present study attempts to develop a new method to identify the ideal location for wind power generation plant. The methods applied MCDM to determine the weights of importance for the selected factors with respect to its influence on wind energy potential. The MCDM step also identified the most and least important parameters, which can help to identify suitable locations for optimal utilization of wind energy potential. To identify this, AHP method is applied in the locations of India where Gujrat was found to be the best location for wind power generation. Furthermore, a low number of criteria were used to estimate the weight of alternatives. As a future scope of the study, more criteria can be introduced. The temporal inconsistency of the parameters can be utilized instead of the magnitude peak or trough values of the parameters.

REFERENCES

[1] Doukas, Haris, Charikleia Karakosta, and John Psarras. "RES technology transfer within the new climate regime: a "helicopter" view under the CDM." Renewable and Sustainable Energy Reviews 13, no. 5 (2009): 1138-1143.

[2] Rahman, Syed Mahbubur, and Mohammad Dulal Miah. "The impact of sources of energy production on globalization: Evidence from panel data analysis." Renewable and Sustainable Energy Reviews 74 (2017): 110-115.

[3] Kaldellis, J. K., M. Kapsali, and Ev Katsanou. "Renewable energy applications in Greece—What is the public attitude?." Energy Policy 42 (2012): 37-48.

[4] Giacomarra, Marcella, and Filippa Bono. "European Union commitment towards RES market penetration: From the first legislative acts to the publication of the recent guidelines on State aid 2014/2020." Renewable and Sustainable Energy Reviews 47 (2015): 218-232.

[5] Tampakis, Stilianos, Garyfallos Arabatzis, Georgios Tsantopoulos, and Ioannis Rerras. "Citizens' views on electricity use, savings and production from renewable energy sources: A case study from a Greek island." Renewable and Sustainable Energy Reviews 79 (2017): 39-49.

[6] Wolsink, Maarten. "Wind power implementation: the nature of public attitudes: equity and fairness instead of 'backyard motives'." Renewable and sustainable energy reviews 11, no. 6 (2007): 1188-1207.

[7] Larsen, Torben J., Gunner Chr Larsen, Helge Aagaard Madsen, and Søren M. Petersen. "Wake effects above rated wind speed. An overlooked contributor to high loads in wind farms." In EWEA Annual Conference and Exhibition 2015, pp. 95-99. European Wind Energy Association (EWEA), 2015.

[8] Singh Madhu and Payal Singh. "A Review of Wind Energy Scenario in India". International Research Journal of Environment Sciences 3(2014): 87-92.

[9] Energy Statistics, Central Statistics Office Ministry of Statistics and Program Implementation Government Of India New Delhi, 2018.

[10] T.L. Saaty, The Analytic Hierarchy Process, McGrawHill, 1980.

[11] Badri, M. A. (2001). A combined AHP-GP model for quality control systems. International Journal of Production Economics, 72, 27–40.

[12] Albayrak, E., & Erensal, Y. C. (2004). Using analytic hierarchy process (AHP) to improve human performance: An application of multiple criteria decision making problem, Journal of Intelligent Manufacturing, 15, 491–503.

MODELING OF LAND AND AIR OPERATED ROBOTIC SURVEILLANCE VEHICLE

Arnav Banerjee, Kausik Chakraborty*, Debanjan Sarkar and Nibedan Pal
Department of Electronics and Communication Engineering, Mallabhum Institute of Technology, Bishnupur, India
*kausik.chakraborty@ymail.com

Abstract: *Environmental surveillance has become a trending issue these days. There are drones and wheeled unmanned vehicles(UAV) which does these jobs pretty efficiently and easily. However, despite of being so useful, these equipments are costly and the operation is not much user friendly and there isn't one single device which can be used both on land as well as air. Also noting that the price of such systems are much higher and the power consumption is a big factor. My idea here is to design a single vehicle which can be operated in both land and air and is both power efficient and cost effective.*

Keywords*: Surveillance, robotics, drone, Arduino, Land Robot, Land-Air vehicle, Voice Control, power Efficient, Cost effective.*

I. INTRODUCTION

Security, surveillance and survey are in an urgent need these days and the technology which tends to meet those needs instantly becomes important and comes in the trend immediately. Speaking of machines or equipments which act as a surveillance as well as an observing tool, we generally have two most common areas where these surveillance systems operate viz- land and Air. For example, land equipment maybe a camera operated robotic vehicle and a drone for an Ariel vehicle. Most of these machines are operated remotely via a wireless media and the control panel is a switching arrangement or perhaps a joystick simulator. In general, the cost of such a system is much higher and despite protection it's not much secure.

My aim here is to successfully design a single vehicle which can be operated in both air and land, which is both cost effective and power efficient. More additional features of the vehicle include various modes of communication, system lock and a dedicated emergency backup power. Once successfully designed, this vehicle maybe used as an observing and surveillance system with eases and can be operated in both land and air.

II. SYSTEM DESIGN

The proposed system is a microcontroller based system and is designed using cost effective equipments. The components and parts that can be used for the structure and circuit are discussed in the following section.

a. Arduino:

Arduino is a very common tool nowadays. An Arduino contains a microcontroller with CPU- Atmel AVR of 8-bit, can produce programmable 1s and 0s [1]. The programs can be written on the Arduino IDE software and can be transferred to the Arduino board via a USB cable [2]. Now we are not planning to use the mostly used Arduino UNO for this purpose. Keeping in mind, the need for cost minimization. The Arduino UNO is replaced with the Arduino NANO (Fig. 1), as it does the same job as the UNO, and is also available at a much lower cost.

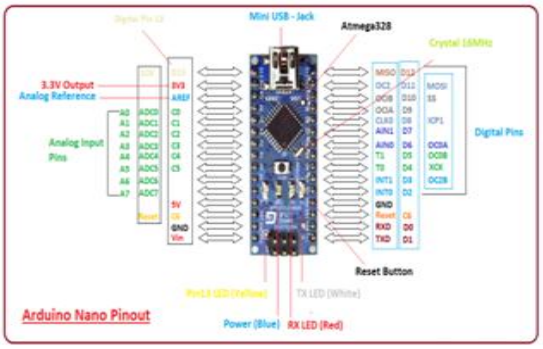

Fig 1- Arduino Nano

b. BT Module:

The Bluetooth module is commonly used to establish connection and communication between devices or a system and a control. It is supplied with 5 volts to power it up and the Arduino can be used to supply that power[4, 5]. It is available in the market easily at almost the same price as Arduino NANO. A HC-05 Bluetooth module is shown in Fig. 4 below

Fig 2:Bluetooth module

c. The L293D IC:

This is a bidirectional motor driver IC which uses a H-bridge inside it for its operation and will be responsible to drive our vehicle in the desired direction by controlling the combinations of 1's and 0's at its input. Now, the L293D operates on 5v which can be provided by the Arduino itself. However, separate power is supplied to power up the driving motors.[3]

d. Motors & propellers:

The choice of motors for our purpose is not anything specific. However I prefer a motor with a good and decent RPM. A simple and cheap toy motor can also be used for this purpose. We require four such similar motors with the same operating voltage and RPM. Speaking of propellers ,we need four such propellers used in a drone to establish flight.

e. Power Supply:

This is to power up the Arduino. For this purpose, batteries or power banks can be used to power it up. Also depending on the value of the voltage required for the motors, corresponding power maybe supplied at pin 16 of L293D. A 9 volts non-rechargeable dc power source is a perfect choice.

Besides all the above mentioned components we also need few wires and a Breadboard to build the circuit.

III. SYSTEM OPERATION

Now speaking of the operation in brief , the Arduino is powered up by a power source. The blue-tooth module as well the L293D motor driver IC are powered by the 5 volts output coming out from the Arduino nano. The four driving motors/propellers are connected to the L293D via wires and the motors are powered by a power source.

A general circuit involving two motors can be driven by L293D as shown in fig 3.

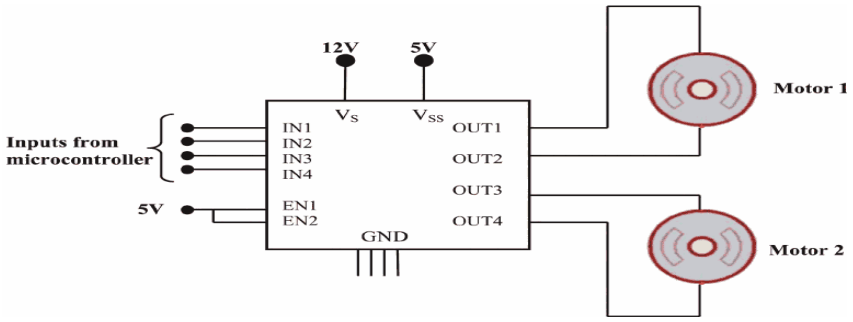

Fig 3: L293D driving two motors

The vehicle has two modes of operation

1. *The ground Vehicle*- operated in land using wheels
2. *The Drone*-operated in air using propellers.

The mainframe of the structure contains both wheels and the propellers. The wheels can be switched easily with the propeller which in turn transforms the four wheeled vehicle into a four winged drone.
The choice of the mode depends solely on the user. If the user wants to see or observe the surrounding through the camera from top, he may choose the drone mode and if he wants to stay on land he maybe continue with the Ground Vehicle mode. The weight of the structure are distributed and balanced in such a way that the flight becomes smooth and stable. After proper calibration it will be possible to allow easy mode switches, easy take off and landing. The L293D is solely responsible for moving the wheels and propellers when commanded by the user. Although, either the wheel set or the propeller set will work at a time and the power will be distributed equally among the four driving propellers and motors. A more improved version of this may contain a Ultrasonic sensor which will help the system to recognize sudden on-way obstruction and hence take proper measures accordingly[6]. The Arduino controlling the wheels maybe controlled by the Bluetooth using a Smartphone as shown in fig 4.

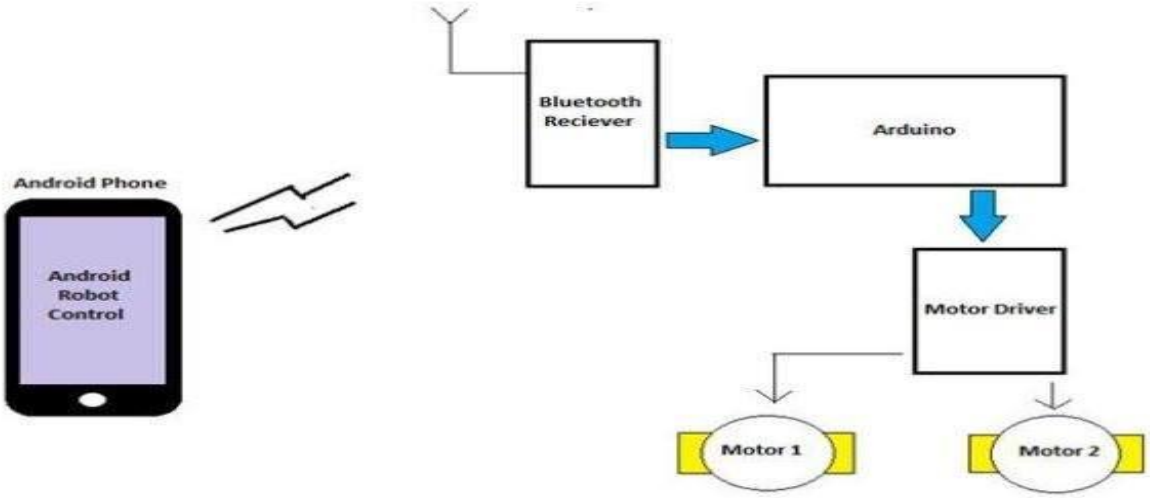

Fig 4: A simple version of Bluetooth controlled wheel –set

The entire circuitry is protected with insulated covers which is resists the effect of rain and lightning. However the propellers are exposed entirely so that is a minor drawback.

IV. SYSTEM POWER

The system has two power sources. One of them is a rechargeable cell, the other one is a pure dry cell, or a simple li-ion battery. The motion of the wheels induces current that charges the system when the vehicle is in motion. The recharged battery helps in powering up the system when it is in air. The dry cell is for the backup [9]. So in case all the other powers are depleted, the backup power maybe helpful in maintaining a smooth and continuous flight in the drone mode [8, 10].

V. OPERATION MODES

Basically here we talk about the control panel which is in direct control with the user.
My idea uses a Bluetooth module to establish the communication between the user and the vehicle. The various modes of operations for my vehicle are

1. Switches and buttons
2. Joypad/Joystick
3. Smartphone's Gyroscope sensor
4. Voice sensing

A rough model of my system is mainly governed by nine voice commands which I have mentioned below. The system can be controlled via the voice commands delivered by the authorized user. Any other voices will be practically rejected by the system, making the system more secured[7]. The voice input can be fed into a Smartphone and it can be analyzed and processed using an Application known as the "Arduino Voice Control" The screenshot of the voice sensing app is shown in Fig 5.

Fig 5: Snapshot of the voice app.

Voice Command	**Operation**
1. Forward	*Vehicle Moves Forward*
2. Backward	*Vehicle Moves Backward*
3. Turn Right	*Vehicle Turns Right*
4. Turn Left	*Vehicle Turns Left*
5. Rotate Right	*Vehicle Rotates Right*
6. Rotate Left	*Vehicle Rotates Left*
7. Lights On	*Turns The Headlights On*
8. Lights On	*Turns The Headlights Off*
9. Shutdown	*Turns of the entire system*

VI. CONCLUSION

The concept of a surveillance drone and a surveillance car is combined here to form a combination of both. Here a single device can travel in both land and air by switching the mode. And the choice of its modes of operation depends on the authorized user only. It is controlled by voice and is power efficient and the user has the option to choose the mode of operation. It is fully equipped with a backup power in case of an emergency. Such a system can be used in various applications and since it takes care of both power and cost, it would be a good choice for a surveillance system.

REFERENCES

[1] Leo Louis, "Working principle of Arduino and using it as a tool for study and research" by in International Journal Of Control, automation, Communications and systems.
[2] Manish Verma, "Working , operation and Types of Arduino Microcontroller", BUEST, Baddi , HP (India), international journal of Engineering Sciences & Research Technology
[3] Nikhil Tripathi, Rmeshwar Singh, Renu Yadav, "Analysis of Speed Control of DC motor-a review study", International Research journal of Engineering and Technology (IRJET)
[4] Jagjeet Kaur, Ramandeep Kaur , Manpreet Kaur, "Bluetooth Technology", International journal of Engineering and computer science
[5] Gypsy Nandi, "Bluetooth Technology: Security issues and its prevention", International journal of Computer Applications in Technology.
[6] Chun Fui Liew , Danielle DeLatte,Naoya Takeishi,Takehisa Yairi, Norzailawati mohd Noor, alias Abdullah and Mazlan Hashim "Recent Developments in Aerial Robotics: A Survey and Prototypes Overview, Remote Sensing UAV/drones and its applications for urban areas: a review", IOP Conference Series: Earth and Environmental Science
[7] Melissa Morris, "Comparison of Rechargeable battery technologies", Florida Polytechnic University
[8] Sid Megahed , Bruno Scrosati "Lithium-ion rechargeable batteries", Journal of power Sources
[9] Luiz Viera, Marcos Augusto M. Vieira, Alex Borges, "Efficient power management in real time embedded systems", in Emerging Technologies and Factory Automation,2003, proceedings: ETFA '03 IEEE Conference.

STUDY OF ROUGHNESS OF SURFACES MACHINED BY CNC AND CONVENTIONAL MACHINING

Swarnangshu Mukhopadhyay, Animesh Nandi*, Suman Mandal and Debasish Nandi
Department of Mechanical Engineering Mallabhum Institute of Technology, Bishnupur, India
*animech9@gmail.com

Abstract: *Now a day's surface roughness plays an important role in the field of manufacturing. Thus studies performed on the surface roughness of a wooden block machined by Computerized Numerical Control (CNC) machining as well as by a conventional machining. Radial depth of cut and axial depth of cut were employed in the different operations in the present study. The roughness of surface machined by CNC machining has been compared to surface machined by conventional machining. For measuring surface roughness Talysurf (Stylus probe) is used.*

Keywords: *Cutting speed, feed, depth of cut and surface roughness.*

I. INTRODUCTION

The challenge of contemporary machining industries is mainly focused on the accomplishment of high quality of product. The quality may be measured in terms of dimensional accuracy, surface finish, high production rate, less wear on the cutting tools, economy of machining. This also includes in terms of cost saving and increase of the performance of the product with reduced environmental impact. The ability to control the process for better quality of the final product is of paramount importance. In this study, the surface roughness taken into consideration keeping in views its importance on production [1]. The CNC machine will eliminate any human errors and will perform significantly quicker than any person could cut designs by hand [2, 3].

II. COMPARISON OF CNC AND CONVENTIONAL MACHINING

Selection of the parameters plays an important role in establishing and efficient machining. Thus it is a challenge for selecting parameters in better manufacturing for nearly a century and is still a subject of many studies. Optimum machining parameters are of great concern in manufacturing environments, where economics of machining operation plays a key role in the present competitive market. Besides the surface roughness value is dependent on parameters like depth of cut, cutting speed and feed rate [4].

The 'M-E' model specimen is displayed in Fig. 1. The surface roughness tester machine is displayed in Fig. 2. Table 1 and Table 2 represent details of cutting data and data collection chart. The objectives of the studies are shown below:

1. To predict the parameter that contributes to the optimum surface roughness value.
2. To study the relationship between the parameter that leading to the optimum surface roughness.

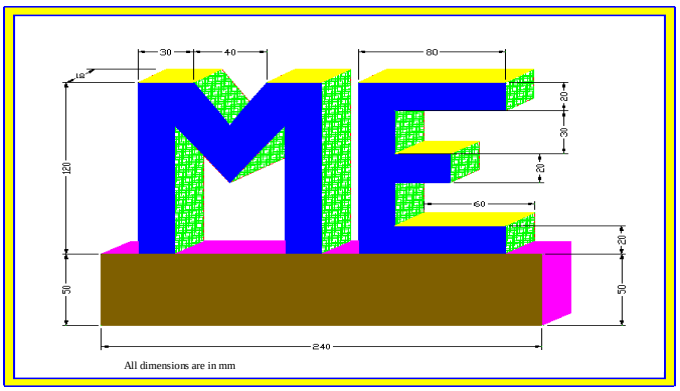

Fig. 1. Experimental design specimen

Table 1. details of Cutting data

Operation No.	Conventional machining				CNC machining			
	Radial depthof cut (RDC)mm	Axial depth of cut (ADC) mm	Cutting Speed (Vc) m/min	Feed (F) mm/min	Radial depth of cut (RDC) mm	Axial depth of cut (ADC) mm	Cutting Speed (Vc) m/min	Feed (F) m/min
1	3	1	200	50	1	3	600	60
2	4	1	200	60	1	4	1000	60
3	5	1	200	60	1	5	1500	60
4	6	1	200	50	1	6	1000	60

Fig. 2.Surface Roughness Tester Machine

Table 2: Data Collection

Operation No.	Conventional		CNC	
	Roughness, Ra µm(X)	Roughness, Ra µm(Y)	Roughness ,Ra µm(X)	Roughness, Ra µm(Y)
1.	19.31	18.60	6.648	5.659
2.	10.21	18.52	7.875	2.552
3.	13.53	9.696	4.788	6.914
4.	13.69	10.54	5.652	8.587

III. RESULT ANALYSIS

By analyzing roughness data , CNC machining method given better surface finish than that of Conventional method in any direction.

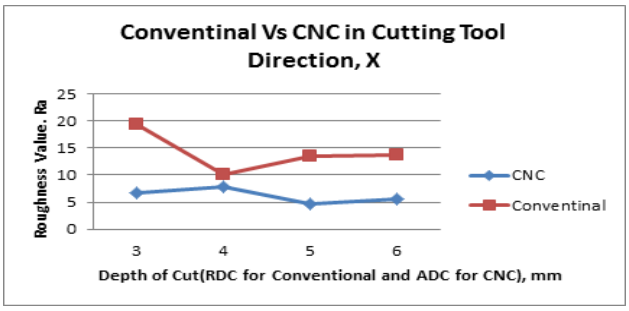

Fig. 3 (a) Surface roughness comparison of Conventional and CNC in cutting tool direction

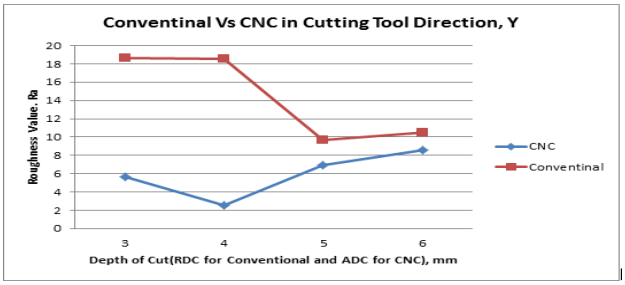

Fig. 3 (b) Surface roughness comparison of Conventional and CNC in transverse of cutting tool direction

From Figs. 3(a) and 3(b) it has been observed that with minimum depth of cut, there is a significant improvement in the surface roughness (both X and Y direction) by using CNC machining.

V. CONCLUSION

Significant advantages can be achieved by using CNC milling in manufacturing of the products made of advanced materials. CNC ensures high metal removal rates, boost productivity, improve surface finish and gives numerous benefits. It eliminates some treatment (e.g. manual finishing) besides simultaneously retaining the accuracy. These advantages are decisive for the use of CNC for machining the press dies. Even though CNC has been known for a long time, the research is still being developed for further improvement of surface quality.CNC machinery has more advantages than conventional machinery because it offers a more accurate result.

REFERENCES

[1] T.R. Thomas, "Characterizations of surface roughness", Precis. Eng., Vol. 3,1981
[2] Kadirgama et al. 2010. Response Ant Colony Optimization of End Milling Surface Roughness Sensors 2010. Vol.10,2054-2063
[3] Mohammad Reza, SoleymaniYazdi and Saeed Zare Chavoshi. 2010. Analysis and estimation of state variables in CNC facemilling of AL6061.,Prod. Eng. Res. Devel. Vol.4, pp. 535–543, doi: 10.1007/s11740-010-0232-7.
[4] P.G. Benardos, G.-C. Vosniakos, Predicting surface roughness in machining: a review, International Journal of Machine Tools & Manufacture 43 (2003)833–844

MODELING AND IMPLEMENTATION OF A PROJECT ENTITLED 'THIRD EYE FOR THE BLIND'

Subha Das*
Department of Electronics and Communication Engineering, Mallabhum Institute of Technology, Bishnupur, India
*subhaece55@gmail.com

Abstract: *There are many persons, whom God has given everything, but they can't see the light of the world; in one word they are known as 'Blind' people. Therefore we have come up with a project/system which will provide them support during walking. Whenever an object is in front or there is an obstacle, sound will be provided from this object or some form of vibration will occur with the help of this system blind people will be able to avoid accidents and take care of themselves."Third eye for people who are blind" is a project which will help of ultrasonic waves and they will also get notified by buzzer sound or vibration effect. They only need to wear this device as a band or like a cloth. The cost of this proposed system is very low and the poor people can easily afford it.*

Keywords: *Arduino, Ultrasonic sensor, Vibration motor.*

I. INTRODUCTION

We have come to know that God has the third eye, but at the moment it is not possible. I gave this project the name of "Third eye for the blind" because when a person can't see or they are blind in one word, this project will work as the third eye.

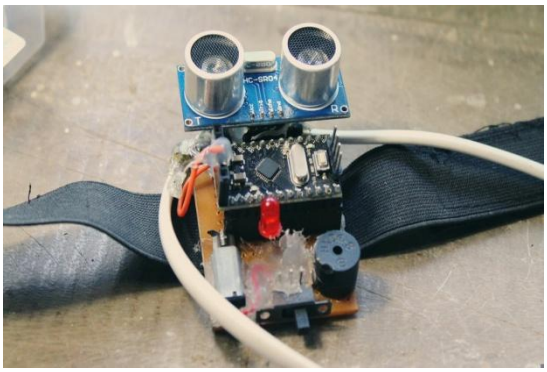

Fig. 1. A wearable project for people who are blind.

The blind people need to wear this device as a band or cloth. In our world there are 39 million people as blind worldwide. They suffer lot of problem in their daily life. So the goal of the project is to develop a cheaper and more efficient way to help the visually impaired to navigate with greater comfort, speed, and confidence. It solves all problems of existing technology. The total cost is less than 1000/-. As studied from literature [1,4], there are no device that are available in the market can be nourished like fabrics and they have low cost and simplicity. Fig. 1 shows the snapshot of the proposed project and Fig. 2 shows the position of one module and area of detection.

Fig. 2. Position of one module and area of detection

The device is equipped with five ultrasonic sensor, which are five modules that are connected to different parts of the body, two for both shoulders, two for the knees and one for the hands. Using five ultrasonic sensors, blind people can detect objects in five dimensional views around them and easily travel anywhere. The ultrasonic sensor detects an obstruction, the device will notify the user via vibration and sound beeps. With increasing distance the vibration and beam rate increase the intensity and it is a fully automatic device. The entire project can be made in the form of a jacket. The use of specially designed boards instead of Arduino and high quality ultrasonic sensors enables faster crowding which enable device crowds.

II. SYSTEM DESIGN

The system design is kept simple, more compact and cost effective compared to the complicated designs as in [1-4]. The system aims is to save the blind people to help of this system from accident.

- Arduino Pro Mini
- Ultrasonic Sensors
- Vibrating Motor
- Buzzer

2.1 Arduino Pro Mini: The Arduino pro mini (Fig. 3) comes with a microcontroller board developed by Arduino.cc and the Atmega328 microcontroller embedded inside the board. It has 14 digital input/output which 6 pins are used for providing PWM output. There are 8 analog pins are available on the board. It's lot a smaller than1/6 of the Arduino Uno's total size. There are only one voltage regulator included in 3.3 volt like a mobile battery. There is no USB port available and its lacks a built in programmer.

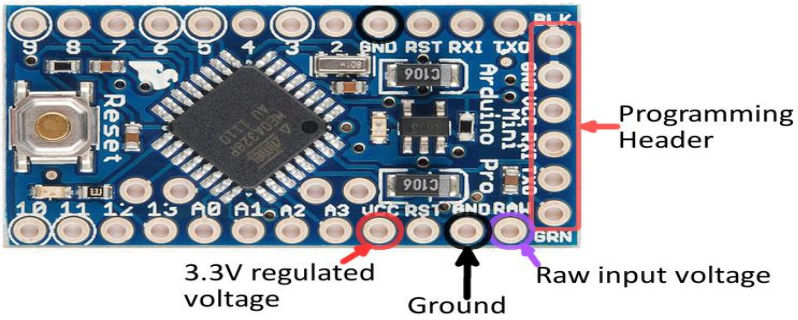

Fig. 3. Arduino Pro Mini

This board does not come with built in connectors that give you the flexible to sell the connector based on the requirements and space needed for any project. The Arduino pro mini is an open source tool that you can modify and use the board to suit your needs as all information and support regarding this board is readily available. SRAM is a static random access memory that is 2Kb. RAM memory is highly volatile in nature and mainly depends on the constant source of power supply. EPROM comes with a memory of 1Kb. This is a read only memory that can be deleted and reprogrammed. This memory can be erase using more than normal electrical signals. The code we write on the board is called a sketch. The Arduino pro mini comes with a built in LED that we will block and compile the relevant program on the board.

2.2 Ultrasonic sensor

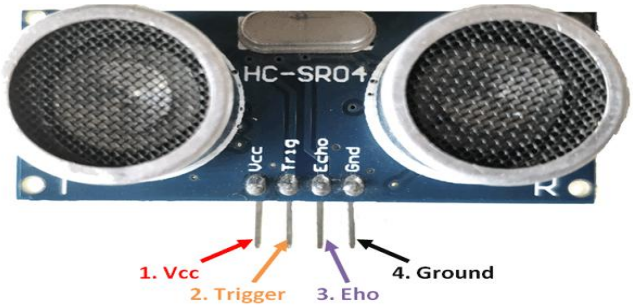

Fig. 4. Ultrasonic sensor

An Ultrasonic sensor (Fig. 4) is a device that can measure the distance of an object using sound waves. It sends a sound wave to a certain frequency and measures the distance by returning that sound wave back. By recording the latency time between the sound wave bouncing back, it is possible to calculate the distance between the sensor and object (Fig. 5).

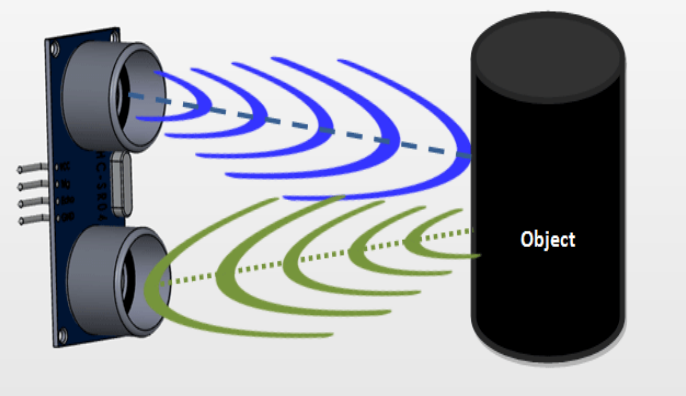

Fig. 5 Working procedure of an ultrasonic sensor

Since it is known that the noise travels through the air at about 344 m/s, you may take time to go back to the sound wave and multiply by 344 m total round trip the sound wave. Round trip means that the sound wave travels 2 times the distance of the object before is detected by the sensor; It includes the trip from the objects gold sensor. To find the object distance, simply divide the round trip distance in half.

2.3 Vibration Motor:

A vibrator is a mechanical device for generating vibrations (Fig. 6). The vibration is often produced by an electric motor with an unbalanced mass on its driveshaft. There are several different types of vibrators, they are associated with the Rumble feature of elements of larger products such as smart phones, puzzles, vibrant toys, or video game controllers.

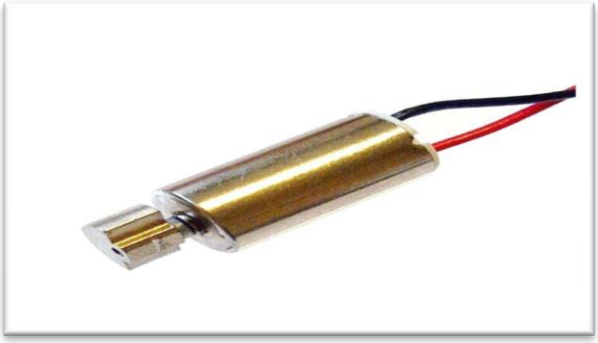

Fig. 6 Vibration motor

When smart phones and pagers vibrate, the vibrating alert is produced by a small element that is built into the phone or pager. Many older, non electronic instruments and doorbells have an element that vibrates for the purpose of producing a sound. Tattoo machines and some types of electrical engraving equipment have a mechanism that vibrates a needle or cutter tool.

III. WORKING PRINCIPLE

The ground of LED, buzzer, and vibration motor connected to the ground of Arduino. Then +ve of LED and middle leg of switch to Arduino pin 5. Then + ve of Buzzer to first leg of Switch. Then + ve of Vibration motor to third leg of switch. Then Ultrasonic sensors pin vcc is connected to the pin of Vcc of Arduino. Ultrasonic sensor pin ground connected to the Arduino pin ground. Then Ultrasonic sensor pin Trig is connect to pin 12 of Arduino. Then Ultrasonic sensor pin Echo is connect to pin 12 of Arduino. The switch is used here is for selecting the mode buzzer or vibration motor mode (Fig. 6).

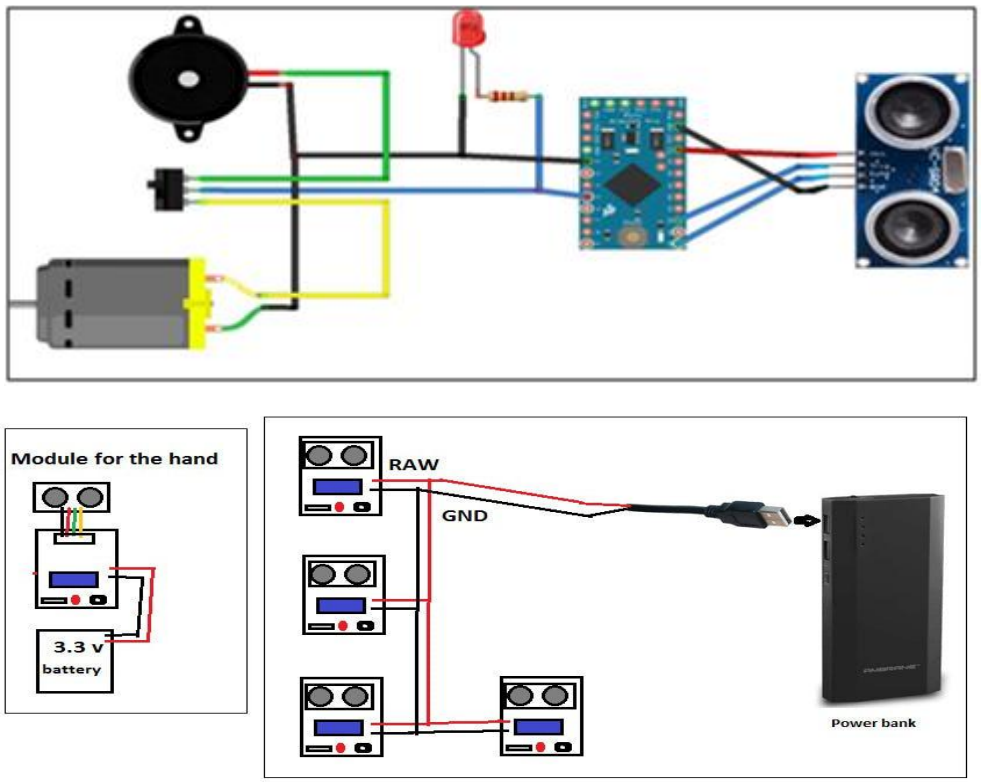

Fig. 6. Circuit/Module interconnections.

The Ultrasonic sensor is used a transducer, and harness transceiver. The transmitter emits a ultrasonic wave and if obstacle appear on the way, hits the ultrasonic wave. The impedance is reflected back, the reflection is the wave taken by the receiver. The combination of ultrasonic sensors transmitter and receiver. The sending and receiving of Ultrasonic signals is calculated, this time spacing is used to calculated the distance between the sensor and it barrier. The distance calculation equation for the sensor Distance from(cm)=[High time pulse width*Sound velocity(cm/sec)]/2. The sensors are placed on the waist belt. The sensors have a field of view over each other for distance of 4 feet about 60 degrees. Increasing the distance from the sensor, the coverage angle decreases. So the purpose is to cover a wide angle for identification, interrupts with ultrasonic sensors to help the blind people, and makes it easy for them to around no problem. That's why we used this system to help the people who are totally blind.

IV. CONCLUSION

Overall project succeeded in developing a more sustainable navigation strategy, excluding the existing ones. This is a key counterpart to the original concept that had to be presented here. If the project is used on a larger scale and distributed among the blind, it can truly have an impact on the community. The best part is that the cost of the parts does no exceed Rs/-1000 so it is affordable for everyone. This device cannot be used in crowds. The current technology of this project does not allow it to be used in places where it may require very fast response. The entire project can also be made in the form of a jacket, so that the device does not have to be worn at all. The use of specially designed boards instead of Arduino is quick to response.

REFERENCES

[1] G. Prasanthi, P. Tejaswidho Sensor assisted Stick for the Blind People-Transmission on Engineering and Sciences, vol:3, pp-12-16, 2015.
[2] I .Ulrich, J. Borenstein, The GuideCane, Mobile Robot Technologies to Assist the visually impaired, IEEE Tr.SMC, Vol:31, No.2, March 2001.
[3] S. Shovel et al. A travel aid for the blind, IEEE Tr. SMC, Vol.28, Aug. 1998.
[4] https://creat.arduino.cc/projecthub/third eye for the blind.

ABOUT THE INSTITUTE

With the mission, to develop the scenario of technical education in the backward region of West Bengal, a graduate engineering college namely Mallabhum Institute of Technology was setup in 2002 at Bishnupur. MIT has different streams (CSE, EE, ECE, ME & CE). The institute approved by AICTE and affiliated to MAKAUT.

ABOUT THE DEPARTMENT

The department of ECE started its journey since 2002 with a present intake of 60 students. There are well experienced & highly qualified faculty members in the department. The students of the department are well placed in various MNCs every year like TCS, LG, Erricson, Wipro etc. Some students have also qualified in GATE, MAT, CAT etc. and are pursuing higher studies.



BISHNUPUR, A PLACE OF HISTORICAL INTEREST

The historical town, Bishnupur, a subdivisional headquarter in the district of Bankura is accalaimed for its rich crafts and culture. The place is known for its mesmerizing fragrance of tradition and cultural heritage. It has eminence and popularity as a tourist spot.